Vilde S. Haslund

Wetting Testing of Cathodes for Aluminium Production

Supervisor: Espen Sandnes (NTNU, DMSE)
Co-supervisor: Camilla Sommerseth (SINTEF, Materials and Chemistry)

TMT4500 Materials Technology, Master thesis
for the degree of MSc Chemical Engineering,
Main profile: Materials Chemistry and Energy Technology

Trondheim, Spring 2017

The Norwegian University of Science and Technology
Faculty of Natural Sciences and Technology
Department of Materials Science and Engineering

NTNU

NTNU

The Norwegian University of Science and Technology

TMT4900 Materials Technology, Master thesis
for the degree of MSc Chemical Engineering,
Main profile: Materials Chemistry and Energy Technology

Faculty of Natural Sciences and Technology
Department of Materials Science and Engineering

Abstract

The aim of this work has been to assess the wettability of a set of carbon-TiB_2 composites towards aluminium. In order to do so, further improvements to the immersion-emersion method, a method used to assess the wetting properties of electrodes during aluminium electrolysis, was made. The method was tested for its validity and compared to the sessile drop test. Samples of composite cathode materials were supplied by an external manufacturer and tested. Pure graphite and TiB_2 were used as benchmarks. Furthermore, the tested TiB_2-samples were characterised in SEM and EDS.

It was found that results from the immersion-emersion varies greatly across parallels and are not consistent with those from sessile drop testing. None of the tested composites show significant wetting, but the particle size of TiB_2 has an influence on the properties of the material. Polarisation increases wetting for the materials, but the improvement is not sustained after polarisation is removed. The alumina concentration in the electrolyte was found to influence the wetting of the cathode, also after compensation for the electrolyte meniscus. Carbide formation was observed on most sample to a larger extent than previously seen, and was attributed to the increased duration of the immersion-emersion testing.

Further work should include a more detailed investigation of this carbide formation and the processes occurring on the surface of the samples during polarisation. Additionally, a modification to the apparatus, involving an inner, insulating crucible, has been suggested in order to eliminate polarisation of the metal bath. Minor changes to the immersion-emersion procedure has also been suggested. These should be incorporated and applied to a larger number of parallels in the next stage of the project.

Sammendrag

Formålet med dette arbeidet har vært å vurdere fukteegenskapene til en rekke karbon-TiB_2-kompositter mot aluminium. For å gjøre dette har neddykkings-oppdykkings-metoden (immersion-emersion method), som brukes for å måle fukteegenskapene til elektroder under aluminiumselektrolyse, blitt ytterligere bearbeidet og forbedret. Gyldigheten av metodens resultater ble testet, og sammenlignet med resultater fra sessile drop"-metoden. En ekstern leverandør har bidratt med prøver av kompositttmaterialer, som ble testet. Ren grafitt og ren TiB_2 ble brukt som standarder. De testede TiB_2-prøvene ble undersøkt med SEM og EDS.

Resultatene fra neddykkings-oppdykkings-metoden ble funnet til å variere betydelig mellom paralleller og avviket dessuten fra resultater fra "sessile drop"-metoden. Ingen av de testede kompositten viste god fukting, men størrelsen på TiB_2-partiklene ser ut til å være viktig for materialets fukteegenskaper. Polarisering øker fuktingen for de fleste materialer, men forbedringen vedvarer ikke når polariseringen skrus av. Aluminakonsentrasjonen i elektrolytten ble vist å påvirke fuktingen av katodematerialene, også etter at resultatene var justert for elektrolyttmenisken. Et belegg av aluminiumkarbid ble observert på majoriteten av prøvene - mer enn i tidligere faser av prosjektet. En mulig årsak til dette er den forlengede eksperimentelle prosedyren, og dermed forsøkstiden.

Videre arbeid bør involvere mer detaljerte undersøkelser av karbiddannelsen og andre overflateprosesser som foregår under polarisering. En modifikasjon av apparaturen med en indre, isolerende digel har blitt skissert, for å unngå polarisering av aluminiumsbadet. Mindre justeringer av prosedyren har også blitt foreslått. Disse bør inkorporeres og testes på flere paralleller av prøver i prosjektets neste fase.

Acknowledgements

I wish to thank all those who have contributed to this work. In particular, but not limited to, my supervisors Espen Sandnes (NTNU, DMSE) and Camilla Sommerseth (SINTEF) for their guidance, Henrik Gudbrandsen (SINTEF) for his immense help with the practical side of the experiments, and the external supplier for facilitating the work and providing the materials used. The supplier in question wished to be anonymous and will therefore not be disclosed in this work, but I am thankful for the contribution and cooperation. Also thanks to Tone Anzjøn and Sergey Khromov for their help with the supporting ananlyses of the materials.

Contents

List of Figures

List of Tables

Chapter 1

Introduction

Since the invention of the Hall-Héroult process in the late 19th century, the power consumption per kilogram aluminium produced has been significantly reduced [1]. Still, a significant discrepancy between the theoretical amount of power necessary and the actual amount consumed remains. As such, the aluminium industry is still trying to reduce its power consumption and improve the efficiency of primary aluminium production.

One of the major improvements made was the transition from Söderberg anodes to pre-baked anodes, allowing for a closed cell design. A sketch of this type of cell is shown in Figure 1.1. Today's design requires a certain amount of aluminium to be kept in the bottom of the cell for a continuous, stable and conductive pad to be maintained on the poorly wet cathode. With the presence of strong electrical currents in the electrolysis cell, movements arise in this metal pad. Hence, additional distance between the electrodes is required to prevent short-circuiting of the cell, leading to a considerable ohmic drop and dissipation of energy. An alternative design is that of the drained cell, illustrated in Figure 1.2. Such a drained cell would be able to accommodate a shorter distance between the electrodes.

A key issue to be resolved to realise this shift in design towards a drained cell, is to develop a suitable cathode material. The drained cathode should be an industrially applicable material with improved wettability towards aluminium. This would enable the formation of a continuous film rather than droplets at with amounts of aluminium, and the pad would no longer be needed [1]. Titanium diboride (TiB_2) exhibits several desirable properties for the application, and has therefore been considered the most promising candidate material for a long time [1]. However, due to its high price and poor machining properties, its use is still limited [2]. Recent research activities have focused on mediating these shortcomings through a composite material, combining the chemical properties of TiB_2 with the economic and mechanical properties of carbon [1].

The aim of this work has been to further develop the experimental procedure of the immersion-emersion method used to assess wetting properties of electrode materials during electrolysis. The updated method has been tested for its validity and applied to a series of composite materials. These materials have been prepared with different microstructure and various fractions of TiB_2 to carbon. This thesis aims to determine the role of the microstructure on the wetting properties of the cathode block towards aluminium metal. The work has been undertaken for the degree of MSc in Chemical Engineering.

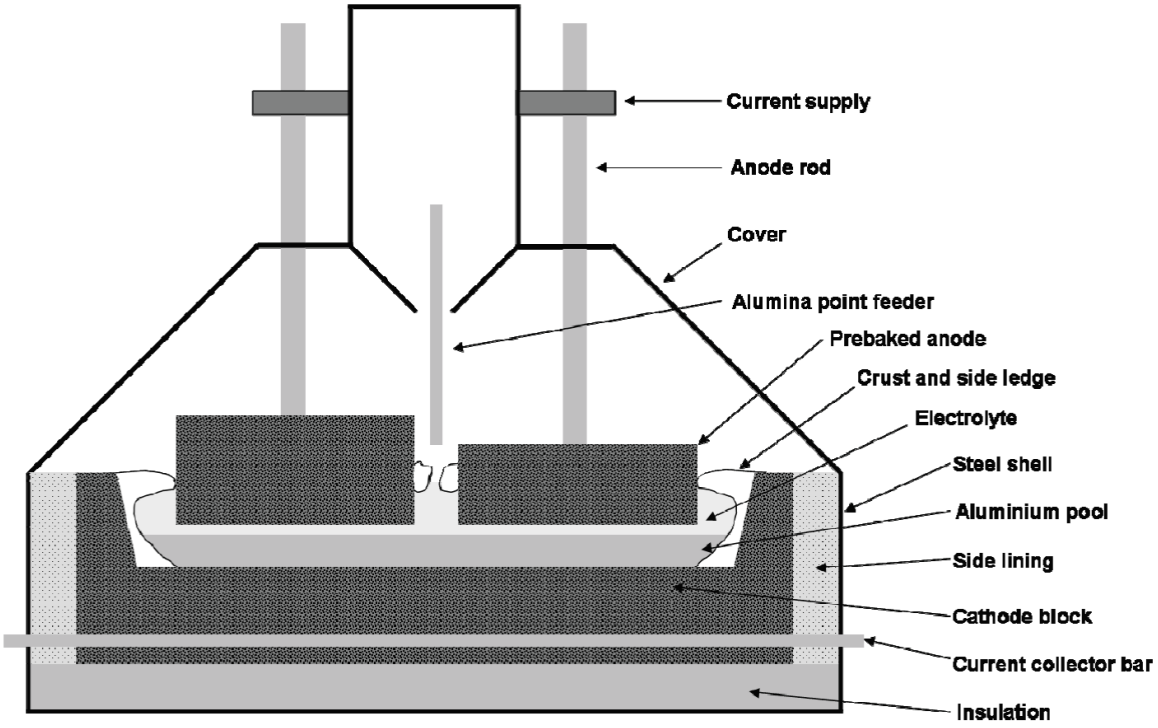

Figure 1.1: Sketch of the conventional design of a closed cell with pre-baked anodes used in the Hall-Héroult process for aluminium production. Figure is extracted from [1].

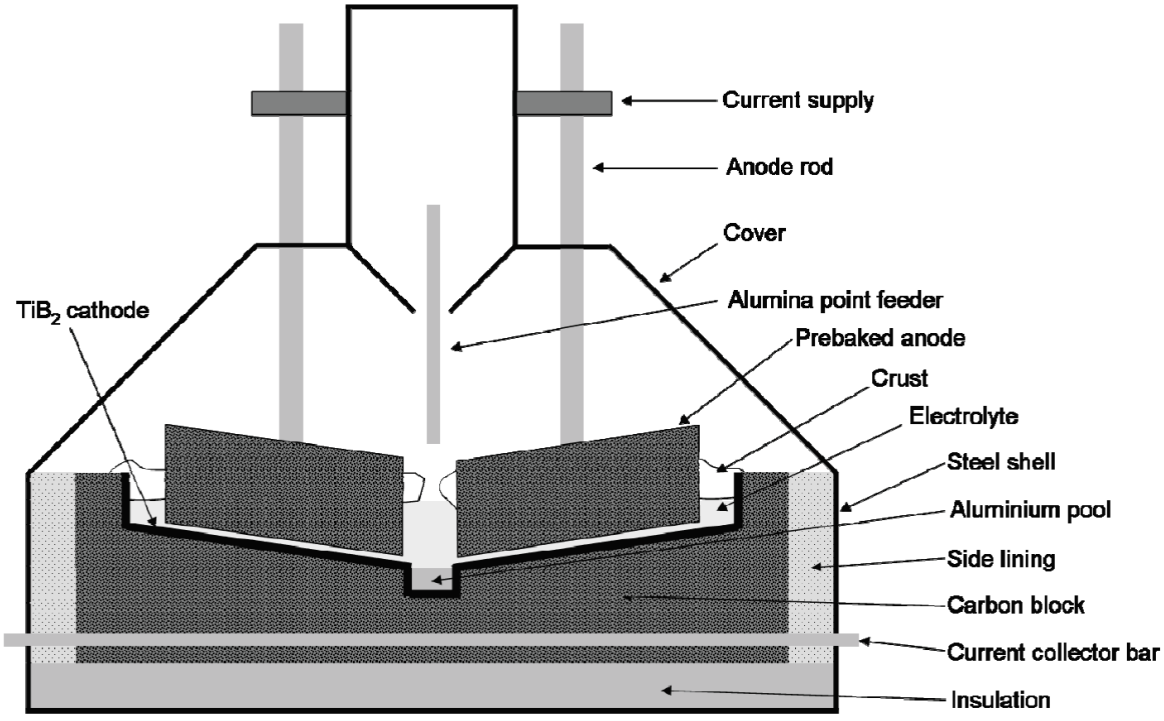

Figure 1.2: Sketch of suggested drained cell. Electrodes are placed closer together and the aluminium formed is continuously drained. Figure is extracted from [1].

About the Report

Since this work consists of several parts that can be interpreted on its own and as the method employed relies heavily on the interpretation of the results, minor deviations from the standard thesis structure was considered to be advantageous. Therefore, some results will be presented and immediately discussed, before more results are presented in the following chapter. A general discussion will be given towards the end, as well as a final conclusion, in order to make up the larger picture of all the individual parts of the thesis.

Chapter 2

Theory

2.1 Aluminium Electrolysis

Industrial production of aluminium today is done by the Hall-Héroult-process. The process was invented by Charles Martin Hall and Paul Héroult independently, hence the shared name. It is electrochemical in nature whereby alumina (Al_2O_3) is reduced to elemental aluminium in an electrolysis cell, as shown in Figure 1.1. The electrolyte mainly consists of cryolite (Na_3AlF_6) which also aids the dissolution of alumina. The process takes place at approximately 970°C [1]. Due to the elevated temperature and the corrosive electrolyte, the lifetime of the carbon cathode material is limited. The typical lifetime for the cathode is 2000-2500 days, depending on operational factors such as current density. Relining of the cell represents a great economic impairment to the industry [3].

A pad of aluminium forms on the carbon lining and effectively acts as the cathode in the circuit. However, the term 'cathode' refers to the carbon cathode, not the aluminium pad. Modern cathodes are made of graphitised carbon, which offers high thermal and electrical conductivity. Graphite also exhibits less sodium swelling than the formerly used anthracite material. This has contributed to more energy efficient aluminium production [3]. The anode also consists of carbon, but is consumed in the process and converted to CO_2. The overall reaction for the electrolysis is:

$$Al_2O_3(\text{dissolved}) + \frac{3}{2}\,C(s) \quad = \quad 2\,Al(l) + \frac{3}{2}\,CO_2(g) \tag{2.1}$$

The theoretical energy consumption for the reaction is 6.34 kWh/kg aluminium [1]. The latest figures from Norsk Hydro put the actual power consumption from the latest generation of electrolysis technology at approximately 11.8 kWh/kg, while the global industry average is close to 14 kWh/kg [4]. This indicates that there is still significant room for improvement of the production.

2.2 Titanium Diboride

A suitable inert cathode material should, among other characteristics, be both thermally and chemically stable, conduct electricity, have an acceptable cost and of course be well wetted by aluminium [1]. The chemically aggressive nature of the melt used in aluminium electrolysis rules out most materials for the application. The ceramic material titanium diboride, TiB_2, fulfils several of these requirements – especially its wetting properties and inertness towards cryolite are desirable. Further it is highly electrically conducting and has low solubility in aluminium [1].

Less feasible is the cost of the material and rapid degradation of the bulk material. The latter is mainly due to penetration of aluminium along grain boundaries [2]. Hence, the material is not an economically viable solution for inert industrial cathodes on its own, but still has a promising outlook for use in carbon composites [5]. The resulting composite could be expected to have enhanced resistance to electrolyte penetration, while still maintaining satisfactory levels of wetting. Other properties of the composites, such as decreased electrical resistance, may also be improved. However, these are not investigated at this point.

2.3 Wetting

Wettability refers to a fluid's tendency to spread out on a solid surface in the presence of two immiscible fluids [6]. In the system of interest, the solid is the cathode and the immiscible fluids are molten aluminium and electrolyte.

2.3.1 Contact Angles and Interfacial Tension

A contact angle always arises at a point of contact between three phases. The value of the equilibrium contact angle is determined by the relative values of the surface tensions associated with each of the interfaces, σ_{ij}, as illustrated in Figure 2.1 [6].

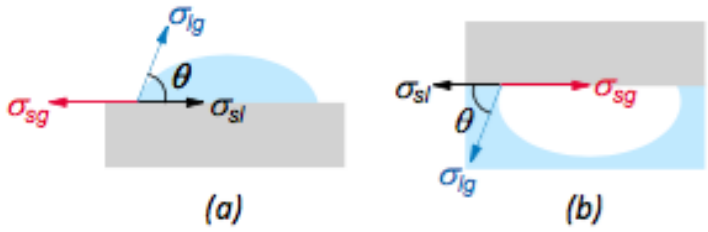

Figure 2.1: The equilibrium wetting angle at the three-phase contact point as a result of the force balance between interfacial tensions for a) liquid droplet and b) gas bubble. The figure is extracted from [6].

Surface tension depends on the chemical nature of the phases and is the amount of work required to create one unit of surface area . It is commonly given in the unit of Nm^{-1}. The theoretical relation between the contact angle, θ, and the three surface tensions, is described by Young's equation as shown in Equation 2.2: [7]

$$cos\theta = \frac{\sigma_{sg} - \sigma_{sl}}{\sigma_{lg}} \tag{2.2}$$

The contact angle is by convention always measured through the liquid. One distinguishes between three cases of wetting, all illustrated in Figure 2.2: [6]

- **Wetting:** When $\sigma_{sg} > \sigma_{sl}$ it means that the interface between the solid and the liquid is preferred to that between the solid and the gas. The resulting equilibrium contact angle is *smaller* than 90° and the liquid will wet the surface.
- **Neutral wetting:** When the two interfaces are energetically equal, i.e. $\sigma_{sg} = \sigma_{sl}$, the resulting contact angle will be $\theta = 90°$.

- **Dewetting or non-wetting:** The interface between the solid and the gas is energetically preferred to the interface between the liquid and the solid, i.e. $\sigma_{sg} < \sigma_{sl}$, thus the system will minimise its energy at a contact angle *larger* than 90°.

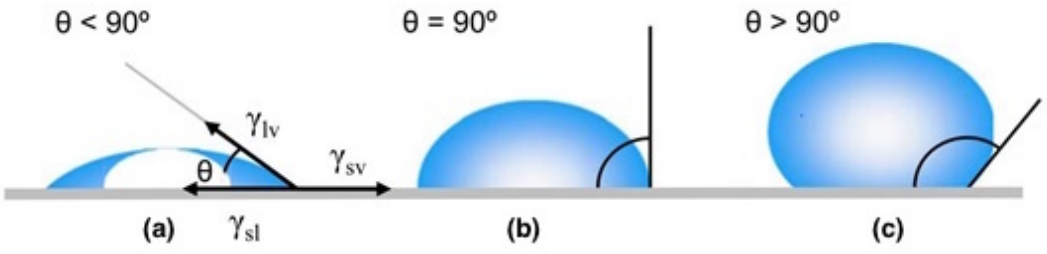

Figure 2.2: Three cases of equilibrium contact angles a) wetting, b) neutral wetting and c) non-wetting. The figure is extracted from [8].

It should however be noted that the above description only applies to the equilibrium situation – which is not often achieved. Surface roughness, insufficient time scale, chemical heterogeneities on the substrate surface are all factors preventing a system from achieving its equilibrium value. [6]

2.3.2 Wetting Hysteresis

Wetting hysteresis is an example of such non-equilibrium behaviour and can be defined as a change in wetting angle due to movement of the three-phase contact point along the surface of the solid [7]. This gives rise to two contact angles; one advancing angle in front of the droplet and one receding angle trailing the droplet, as illustrated in Figure 2.3. Note that since the angle is measured through the liquid, the angles are interchanged for bubbles and droplets.

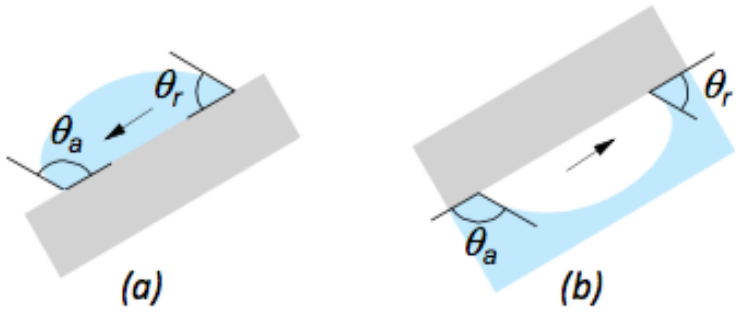

Figure 2.3: Advancing and receding contact angle for a) liquid droplet and b) gas bubble. The figure is extracted from [7].

For some time, hysteresis was attributed to surface roughness, but according to newer literature this is not the only contributing factor. Mechanical hysteresis from adhesion/de-cohesion processes can contribute to hysteresis, as well as intrinsic chemical irreversibility. The latter occurs during contact between the substrate and the liquid when the liquid alters the solid surface.

2.4 Wetting Results From External Supplier

The external supplier providing the composite samples has tested the wettability of the materials, in a system involving electrolyte. A sessile drop method was used, and the metal drop formed was observed using X-rays. This method allows for polarisation of the sample. The results are proprietary and can therefore not be disclosed in full detail, but the supplier has agreed to share the main findings. These are summarised in Table 2.1. The average contact angle is calculated from ten measurements, all of which are collected at the same drop on the sample surface, but observed from different incident angles. The preparation of the composites and their composition can be found in Section 4.2.3. In Figure 2.4 the measured contact angles have been plotted against the weight fraction of TiB_2 in the materials.

Table 2.1: Average contact angles between cathode sample and aluminium in the presence of electrolyte, with and without polarisation. Angles were observed using X-ray during electrolysis.

	Non-polarised		Polarised	
Sample	**Avg. contact angle [°]**	**Std. dev.**	**Avg. contact angle [°]**	**Std. dev.**
3112g	91	1	81	1
5002g	91	2	84	1
5020g	107	4	91	2
5036g	90	2	81	2
6004g	116	2	106	4

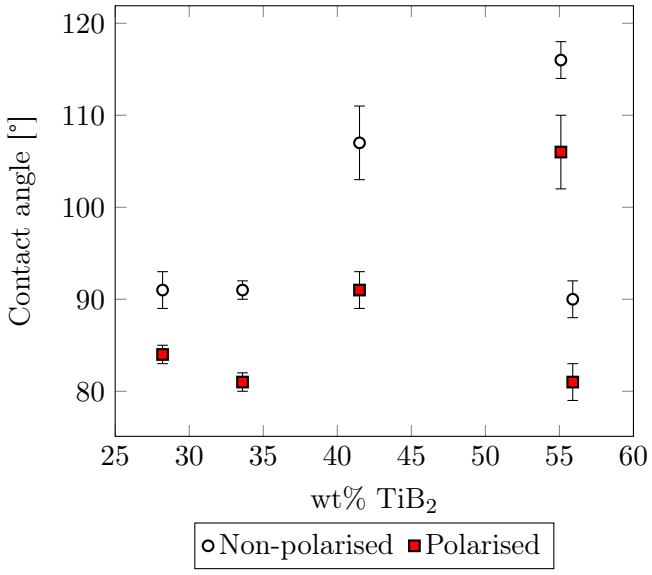

Figure 2.4: Contact angles measured by the external supplier for the provided composites, measured in a sessile drop set-up with electrolyte and polarisation. The angles are plotted against the TiB_2-content in the materials.

In Figure 2.4 there is no strong apparent trend between the TiB_2-content and the measured contact angle, but all materials have improved wettability during polarisation. Furthermore, materials of similar composition exhibit very different contact angles; The two materials with the highest fraction of TiB_2 have almost identical compositions, but the measured contact angles differ by almost 25°. These results will be compared with the results obtained by the author in this work. A full discussion of the results can be found in Chapter 8.

Chapter 3

Method

3.1 Immersion-Emersion Method

The immersion-emersion method is just one out of several methods available for determining the degree of wetting in a system. It is the chosen technique for this work as it is the only method considered to provide measurements under all of the following conditions [6]:

- High temperatures
- In the presence of fluoride vapour
- Dynamic conditions
- No restrictions imposed on the state of the solid surface (e.g. smoothness)
- Measurement both with and without polarisation

The underlying principle of the method is wetting forces acting on the sample and thereby changing the weight recorded. During the experiment, the weight of a suspended sample is continuously measured as the sample is first immersed in a fluid and subsequently pulled out. The weight of the sample will change due to i) a buoyancy force, F_b, and ii) wetting of the sample, F_σ [6]. In addition, there is a constant gravitational force, F_g, acting on the sample. The total resulting force can be expressed as:

$$F = F_\sigma + F_b - F_g = \sigma_{lg} cos\theta \times l + V\Delta\rho g - mg \tag{3.1}$$

In Equation 3.1, σ_{lg} is the surface tension of the gas-liquid interface and l is the wetted perimeter on the solid sample. V is the volume of the displaced liquid, $\Delta\rho$ is the difference in density between liquid and gas, whereas g is the gravitational constant. As before, θ is the contact angle. Immersion and emersion give rise to the advancing, θ_a, and the receding contact angle, θ_r, respectively. This is illustrated in Figure 3.1. Usually, some hysteresis will occur, giving rise to two different contact angles [6].

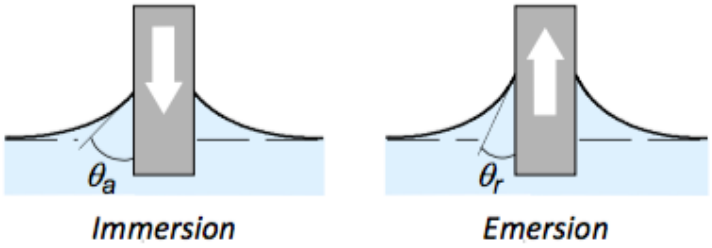

Figure 3.1: The immersion part of the cycle measures the advancing contact angle, and the emersion part the receding one. Here shown for a wetting system. Arrows indicate sample movement, not forces. The figure is extracted from [7].

3.1.1 Surface Tension and Curvature of the Liquid

Because of the limited size of the crucible used (10 cm in diameter) and poor wetting between aluminium and graphite, the liquid metal surface will unfortunately not be perfectly flat during the experiment, but somewhat curved as the sample encounters it. Hence, the curvature of the surface will exert an additional force on the sample and affect the measurement. This has been identified as a substantial source of error in previous experiments performed by SINTEF [7].

To mitigate the issue with curvature of the metal surface, the aluminium is alloyed with copper, in order to increase the density difference between the molten metal and the electrolyte. Previous work on the subject done by the same group suggested that ∼30 wt% copper would reduce the issue of curvature sufficiently [9], while keeping the change in surface energy within an acceptable range [10]. The latter is important for obtaining representative results for wetting in the cathode-aluminium system. The modelled curvature as a function of amount of copper is illustrated in Figure 3.2. Figure 3.3 shows how the surface tension for Al-Cu alloys changes as a function of the molar fraction of aluminium.

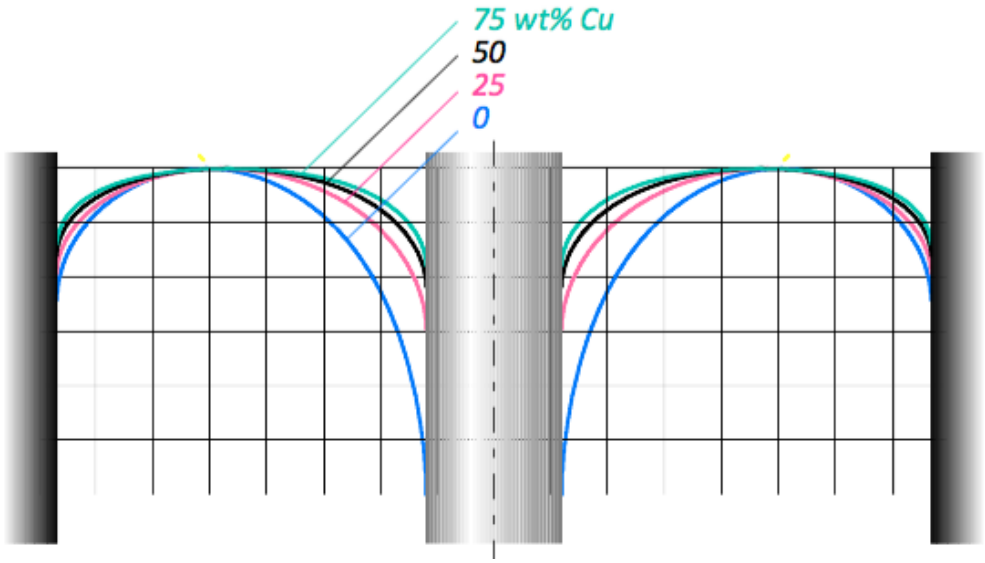

Figure 3.2: Curvature of the liquid metal surface as a function of copper weight fraction in a binary AL-Cu alloy. The grid in the figure is 5x5 mm. The figure is extracted from [9].

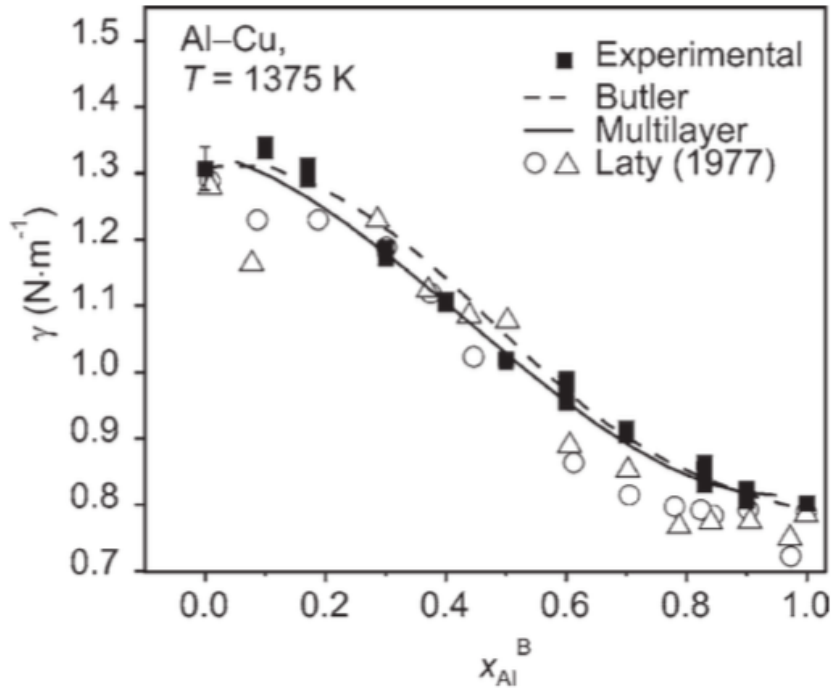

Figure 3.3: The surface tension of a liquid Al-Cu binary alloy, as a function of aluminium fraction. The figure shows experimental values together with theoretcal models. The figure is extracted from [10].

3.1.2 System of Two Menisci

In most wetting tests, there is only one three-phase interface, and the contact angle here is the one of interest. Such an interface does exist in this setup too, but it is not the only one; The contact angle of interest is the one where the solid sample meets the interface between the electrolyte and the metal. This will be referred to as the metal meniscus. However, the setup used for this work, which is described in detail in Section 4.1, will introduce a second contact angle [11]. This second three-phase interface is located between the electrolyte bath, the solid sample and the inert gas in the chamber, and will be referred to as the bath meniscus. The two menisci are indicated in Figure 3.4.

Previous work has shown that the effect of the bath meniscus is not negligible, especially during and after sample polarisation [11]. How to accommodate this finding is further discussed in Section 4.6.2 and 4.7.

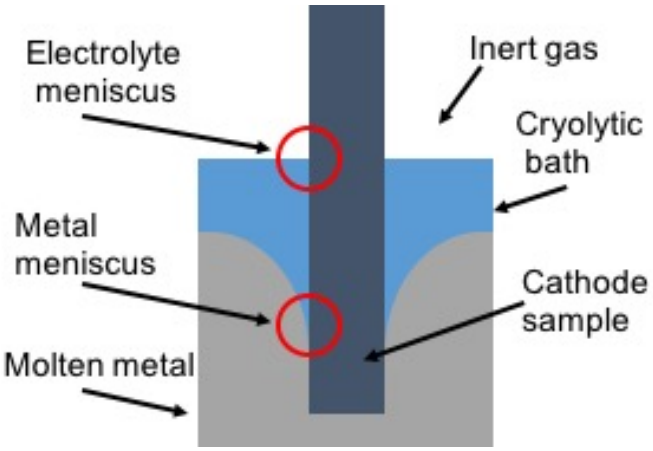

Figure 3.4: The setup used for this work gives rise to two contact angles, both indicated in red circles - one at the gas-electrolyte-sample interface and one at the electrolyte-metal-sample interface. The illustration shows a case of neutral wetting bath meniscus and non-wetting metal meniscus.

3.2 Sessile Drop Method

The sessile drop method is an alternative technique for assessing the wettability of a material. The method is based on visual observation of the contact angle formed when the material of interest is melted on the substrate upon heating [12].

The advantage of the sessile drop method is the simplicity of it. The test in its simplest form does not involve any moving parts, nor complex data processing, and can be conducted without the electrolyte phase. The contact angle is directly, visually observable [12] when the experiment is performed in high vacuum or in the presence of a gas. Some setups also allow for filling or draining the liquid droplet, which allows for measurement of the advancing and receding contact angle [12].

The weakness of the method also lies in its simplicity. A contact angle is always formed at a point of intersection between three phases. Since the electrolyte is not present in this setup, the results are not directly transferable to a system with electrolyte. However, the role of the sessile drop tests conducted in this work will be as a supporting analysis to the results from the immersion-emersion method, and it is the overall trend rather than the absolute value of the contact angle which is the desired outcome.

The method can be modified to include a liquid, third phase as well. Since the electrolyte is not transparent, the angle formed can no longer be observed by the naked eye. X-rays can however be used for the observation. This set-up was used by the external supplier when measuring the contact angles, as described in Section 2.4.

The final contact angle between the liquid and the substrate will depend on the time the system is given to relax. Literature contact angles for molten aluminium on graphite and TiB_2, measured with sessile drop test, are given in Figure 3.5. These results show that the wettability of all materials greatly improve over the course of the experiment. It is also evident that there is a significant and detectable difference between the contact angle observed on TiB_2 and graphite. The latter is important for the method to be applicable to the relevant system. As contact angles are visually observed in this method, a certain error of measurement is to be expected. If the expected difference was only a few degrees, this would be within the margin of error and the technique would not be suitable.

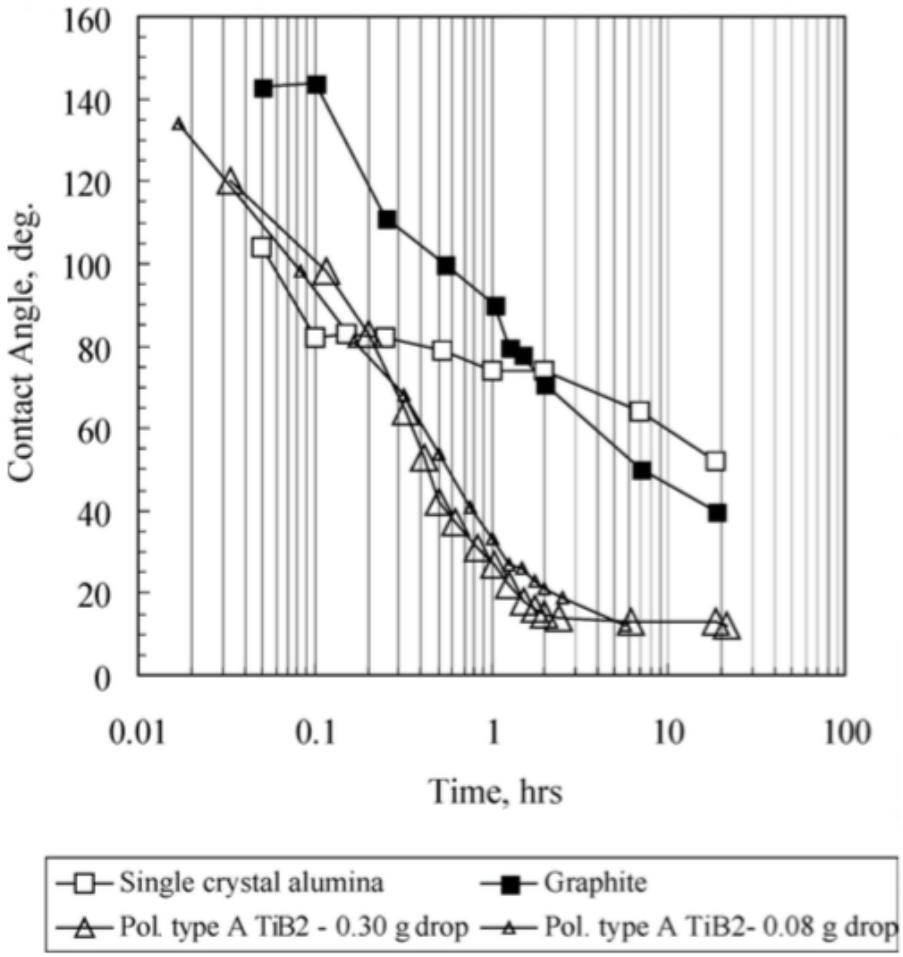

Figure 3.5: Literature contact angles for aluminium on different qualities of TiB_2 and graphite, from sessile drop testing. The figure is extracted from [13]

.

3.3 Scanning Electron Microscopy and Energy Dispersive X-ray Spectroscopy

A scanning electron microscope is used to image samples at a high resolution and magnification. Images are produced by electrons instead of visible light, which optical microscopes uses. It is suitable for investigating surfaces of conducting samples, that does not require any coating - in contrast to non-conducting samples [14]. An overview of the working components in a SEM is shown in Figure 3.6

SEM can be used for basic imaging of the surface, but also offer other types of surface characterisation; When the sample is bombarded with electrons, multiple signals are generated from the material, as illustrated in Figure 3.7. Normally, the secondary electrons are used for imaging. X-ray signals are produced when excited electrons returns to a lower energy state, and its wavelength is characteristic for the atom producing the signal [14]. Thus, these signals can be used to determine the elemental composition of the sample. This technique is called electron energy-dispersive X-ray spectroscopy (EDS) [16]. Spectra can be collected in spot mode, or as full maps.

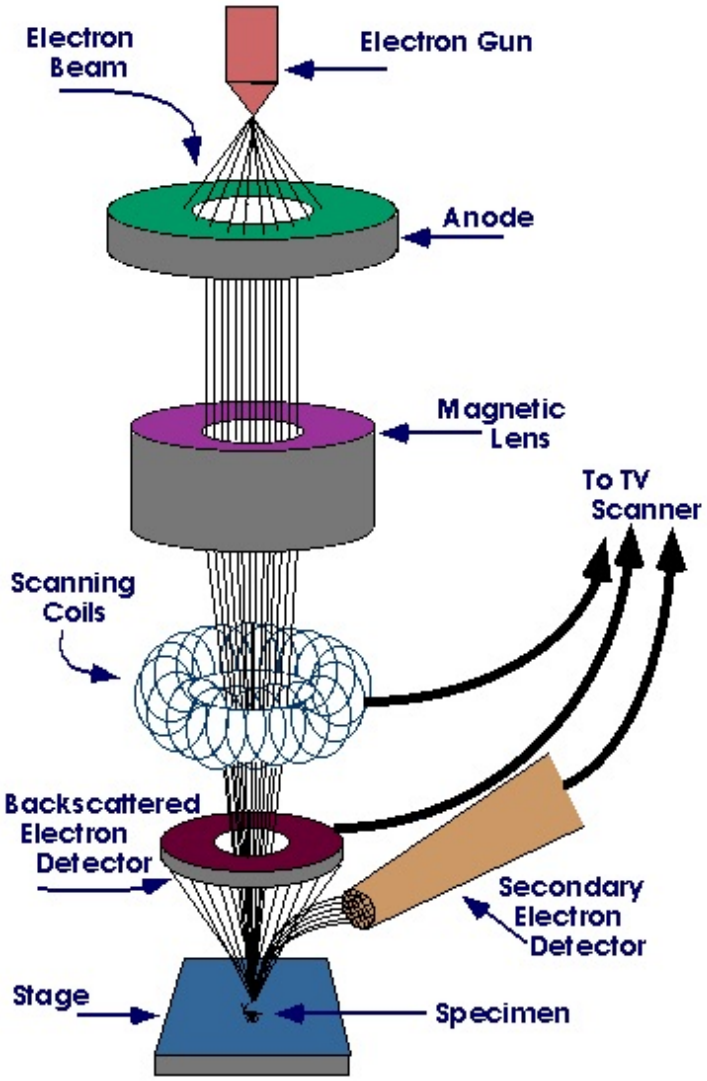

Figure 3.6: The working components in a scanning electron microscope (SEM). The electrons are fired from the gun, focused by the magnetic lens and projected onto the sample, after which it is detected and the signal is transferred to a monitor. Figure is extracted from [15].

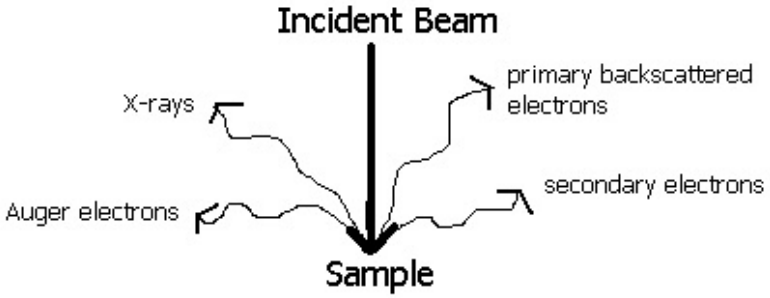

Figure 3.7: The incoming electron beam generates multiple emitted signals in the material examined. Figure is extracted from [15].

Chapter 4

Experimental

4.1 Description of Immersion-Emersion Apparatus

The equipment used for the immersion-emersion technique was built by SINTEF [6]. A cross-section of the water-cooled furnace is shown in Figure 4.1. A load cell (FUTEK LSB210) is mounted on top of the furnace, from which the sample is suspended by a rod. The sample's position remains fixed throughout the experiment while the crucible is moved up and down by a computer controlled stepping motor (ROBO Cylinder RCP2W-RA4C-I-42-P-5-150-P1-M-B). The position of the crucible is collected by the software developed by SINTEF for this specific application, which also collects the temperature, current and voltage. The apparatus also includes a power supply for polarisation of the sample. The current and cell voltage is logged by data logger (NI cDAQ 9174 with a NI9205 module). The signal from the load cell is registered by a micro-controller (FUTEK IMP650).

4.2 Preparation of Samples

The wetting testing can and has been performed with both quadratic and cylindrical samples [11]. The cylindrical geometry is preferred from a testing perspective; this geometry is better for minimising the unwanted curvature effects discussed in Section 3.1.1 [9]. Unfortunately, not all materials used in this work could be machined into cylinders and hence quadratic rods became the chosen geometry. The length varied between the samples, but was commonly between seven and nine cm. However, the immersed length of material was the same regardless of sample length.

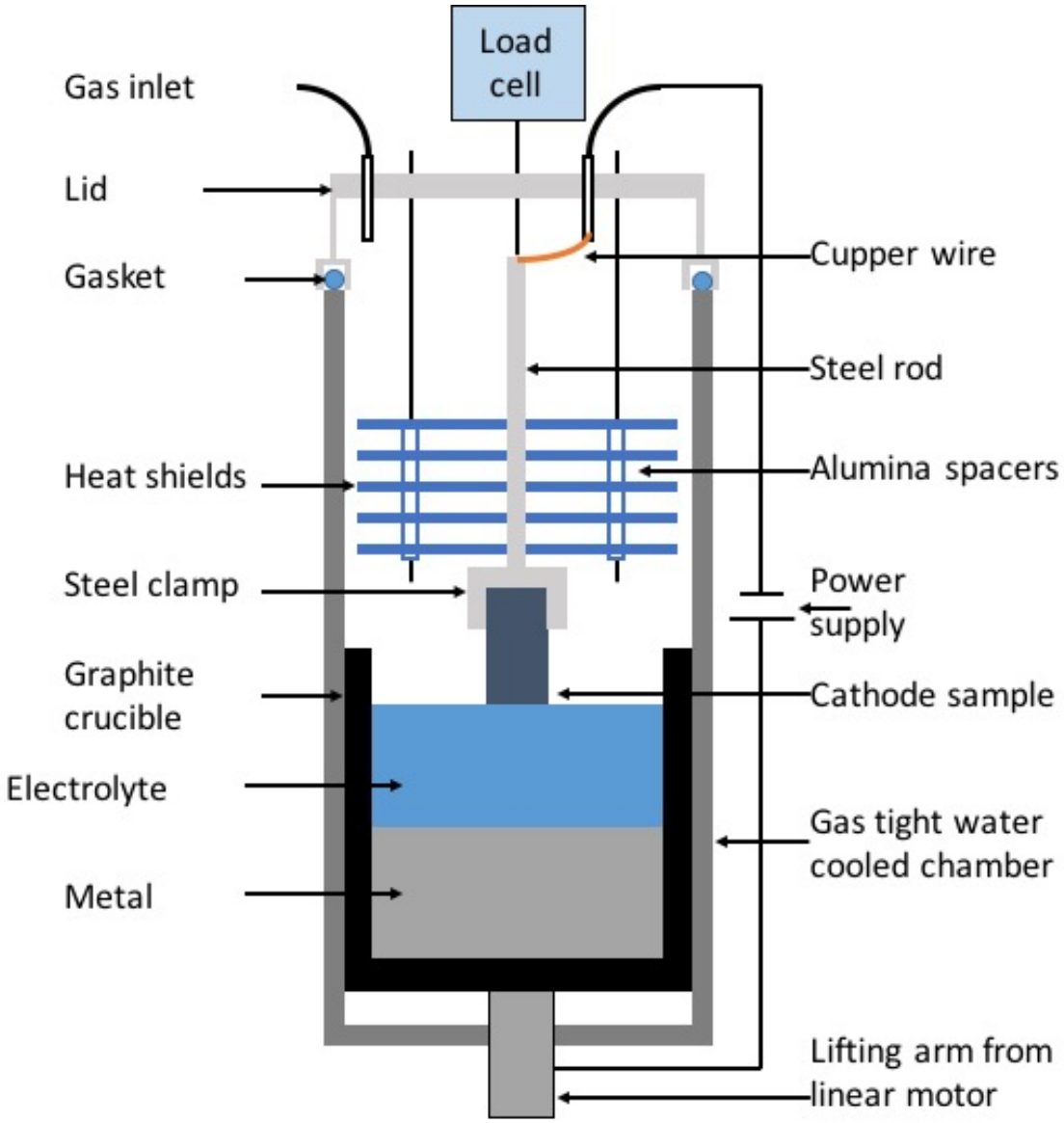

Figure 4.1: Cross section of the furnace used for immersion-emersion tests.

4.2.1 Preparation of Graphite Samples

The pure graphite samples were of commercially available quality, bought off the shelf from the SGL Group, a manufacturer of carbon products. Carbon cathodes used in the industry mainly come in three different qualities; graphitic, anthracitic and graphitised blocks [3]. The graphite from SGL used in this work belongs to the latter category. The material is graphitised by direct graphitisation at 2400 °C. After graphitisation, it is impregnated with pitch and subsequently baked. The bulk material was cut with a circular diamond saw into rods with quadratic cross sections of $\sim 1.5 \times 1.5\,\mathrm{cm}$. A part of the original block and the cut samples are shown in Figure 4.2.

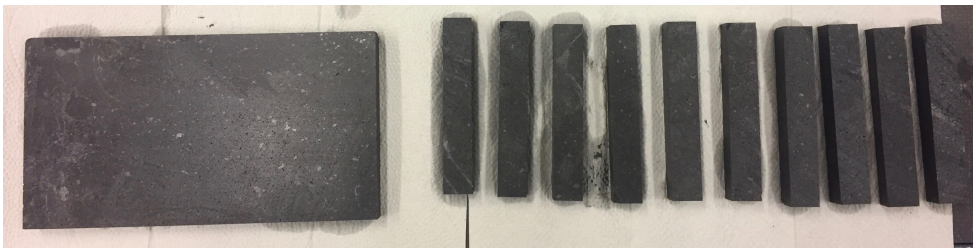

Figure 4.2: Block of graphite before (left) and after (right) cutting.

4.2.2 Preparation of TiB_2 Samples

The TiB_2 samples were prepared by the external supplier. TiB_2 is an extremely hard material and was cut by electrical discharge machining. The finished rods had the dimensions $1 \times 1 \times 8$ cm. Both pure carbon and TiB_2 samples are included in the work for the purpose of having standards to compare the composite materials to, as a form of benchmarking.

4.2.3 Preparation of Composite Samples

The materials of main interest are the carbon-TiB_2-composite materials. The composites have been provided by the external supplier, and is part of the supplier's ongoing research activity on wettable inert cathodes. A description of the samples' composition is given in Table 4.1. SEM images of the composites are shown in Figure 4.3.

Table 4.1: Composition of carbon-TiB_2 composites

Sample name	TiB_2-content [%]	Coke particle size [μm]	TiB_2-particle size [μm]
3018g	34.3	<63	<37
3112g	33.6	<25	<5
5002g	28.2	-	<37
5020g	41.5	-	<37
5036g	55.9	-	<37
6004g	55.1	-	<37

The 3018g and 3112g materials were prepared by mixing coke particles, TiB_2 powder and pitch. The mix was moulded into cylinders before baking and graphitisation. As can be seen from Table 4.1 the two materials have approximately the same TiB_2-load, but the particle size differs. 3112g is therefore expected to have a more homogeneous distribution of TiB_2. This is confirmed by the SEM images in Figures 4.3a and 4.3b. Note that 3112g was prepared with a finer quality of TiB_2-particles than the other materials ($<5\,\mu$m vs.$<37\,\mu$m).

The materials 5002g, 5020g and 5036g were prepared by the author during an internship with the external supplier. These were prepared by a different route than 3018g and 3112g. The method is proprietary and can therefore not be disclosed. 6004g was also prepared by the new route, but not by the author. The new method of preparation is designed to produce materials with even more homogeneous distribution of TiB_2 than the mere mixing, by which 3018g and 3112g were prepared.

As these samples contains TiB_2, care had to be taken during cutting. Previous work with the material has shown that if the composite was cut too fast, the hard TiB_2-particles were torn out of the carbon matrix rather than being parted by the blade. Hence, the surface tested was not representative of the bulk composition, nor was the results from the wetting testing. The final dimensions of the samples were typically $1.5 \times 1.5 \times 9$ cm.

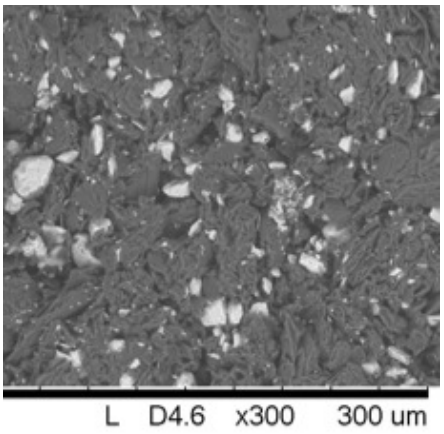

(a) 3018 (34.3%, 37 μm)

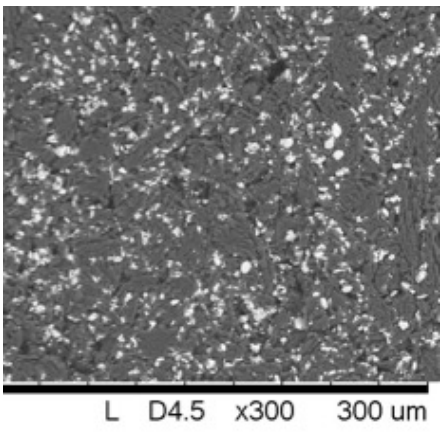

(b) 3112 (33.6%, 37 μm)

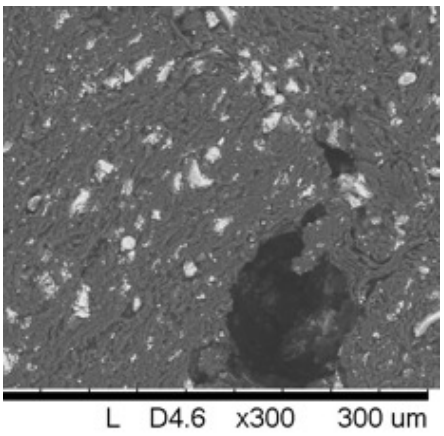

(c) 5002 (28.2%, 37 μm)

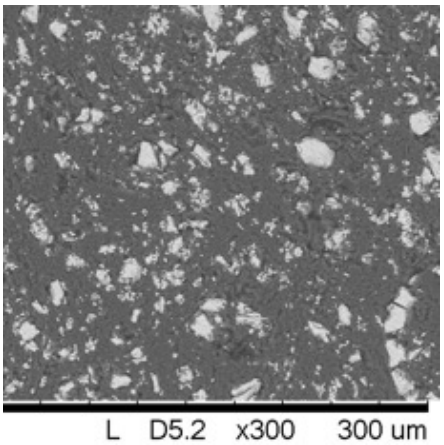

(d) 5020 (41.5%, 37 μm)

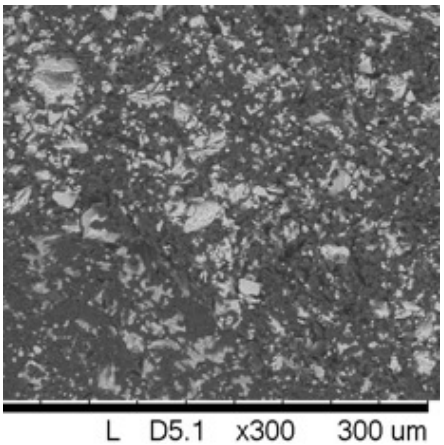

(e) 5036 (55.9%, 37 μm)

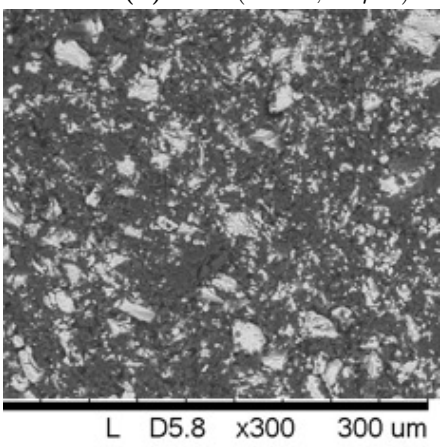

(f) 6004 (55.1%, 37 μm)

Figure 4.3: SEM images of the composite materials tested. Sample name, weight fraction of TiB_2 and TiB_2-particle size are included in captions. The bright areas are TiB_2-particles included in the dark graphite matrix. Images are courtesy of the external manufacturer of the materials.

4.3 Sample Suspension

For fixation of the samples, parallel grooves of approximately 2 mm width were made on opposite sides of the rod. These grooves were used to fixate a stainless-steel clamp to the sample. A steel rod was then screwed into the top of the clamp and suspended from the load cell. The clamp and the steel rod also acted as the current collector towards the cathode sample.

Correct assessment of the buoyancy factor requires a well-defined geometry of the contact between the sample and the liquid. If the sample touches the liquid in a skewed manner, such a defined geometry will not be the case. To minimise this error, the sample is suspended in a rod rather than a wire for better vertical alignment. Additionally, extra weights are added to the sample to keep it vertical during the experiment. The setup is shown in Figure 4.4.

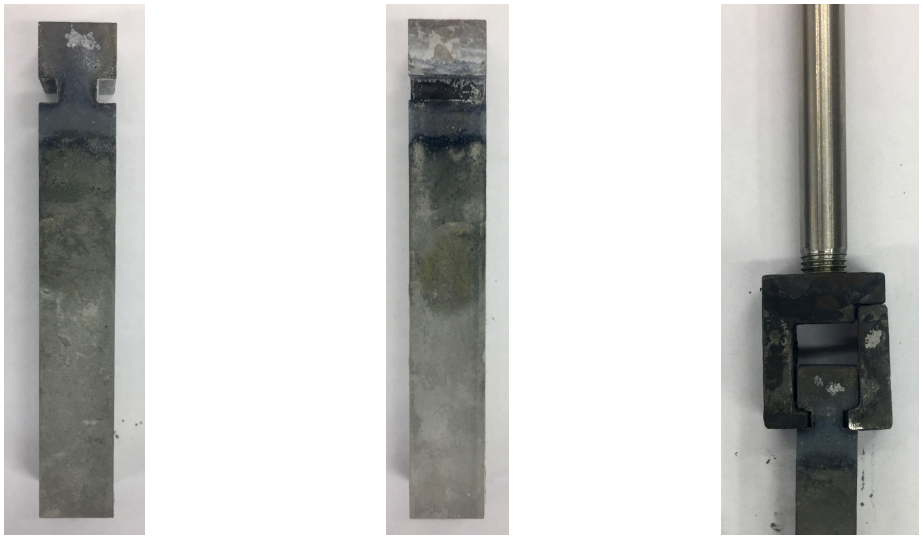

(a) Front **(b)** Side **(c)** With clamp

Figure 4.4: Sample with grooves for fixation with steel clamps and rod.

4.4 Preparation of Metal

As explained in Section 3.1.1, an alloy of aluminium and copper was used for the metal phase in order to reduce surface curvature. The metal bath was prepared from aluminium shots (irregular, 15 mm and up) and cut copper wire. The metal pieces were placed in the graphite crucible and gently mixed by shaking. The typical amounts of metals used in the experiments are summarised in Table 4.2.

Table 4.2: Amounts and composition of metal alloy.

Metal	**Amount [g]**	**Fraction [wt%]**
Aluminium	283	70
Copper	121	30
Total	**404**	**100**

4.5 Preparation of Electrolyte

The electrolyte was prepared from a sample of industrial bath [6]. Additional alumina was added, giving a final composition of the bath as shown in Table 4.3 for the standard experimental procedure. The salts were placed in the graphite crucible on top of the metal. A cross-section of the crucible with solidified metal and bath after a completed experiment is shown in Figure 4.5.

Table 4.3: Electrolyte composition.

Component	Amount [wt%]
Cryolite	80.4
AlF_3 (excess)	12.0
CaF_2	4.6
Al_2O_3	3.0

Figure 4.5: Cross-section of crucible with solidified electrolyte and metal after completed wetting test.

4.6 Experimental Procedure for Immersion-Emersion Tests

4.6.1 Determination of Contact Point

Locating the correct position of both the electrolyte and the metal surface is a prerequisite for the experimental procedure. The contact point between the sample and the cryolite bath is easily determined by the apparatus software, based on the significant change in recorded weight as the sample moves from the gas phase into the liquid phase. The contact point between the sample and the metal on the other hand, is more subtle, and must be determined analytically. The necessary data is collected by lowering the sample by a distance believed to be greater than the bath height, i.e. into the metal. The collected weight is plotted as a function of position, as shown in Figure 4.6. Beware that it is in fact the crucible which moves, not the sample.

However, it is often conceptually easier to explain and understand the mechanisms based on the sample's movement, but in practice this is brought about by moving the crucible.

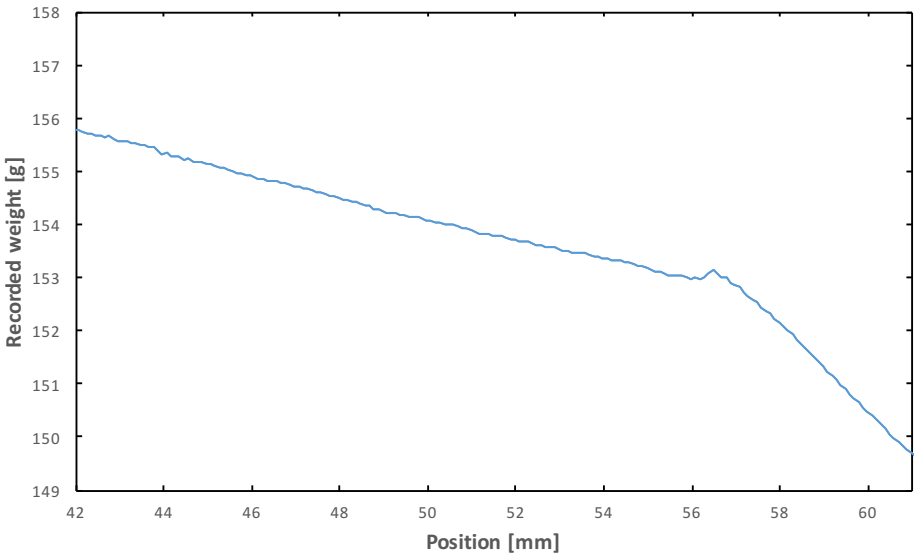

Figure 4.6: Recorded weight (not corrected) as a function of crucible position. The contact point between the sample and the molten metal is indicated by the change in slope in the curve at ∼56 mm.

As can be seen from the graph, there is a sudden change in the slope at ∼56 mm. This change in slope is brought upon by the change in density in the liquid surrounding the sample and indicates the position of the metal surface. At this point the recorded weight drops sharply. It is fairly easy to locate this point, but it cannot be expected to be completely accurate. From experience the margin of error in the measurement is in the order of 1 mm, which is considered to be sufficiently small.

The two positions form the reference points for the standard measuring sequence described in the following section.

4.6.2 Standard Measuring Sequence

To mitigate the effect of the two menisci discussed in Section 3.1.2, a new measuring sequence was designed. The new sequence should allow for accurate determination of the bath meniscus for each individual sample, and thereby isolation of the wetting force of interest, i.e. the wetting of the sample by the metal meniscus.

In the project done earlier [11], a phase of pre-treatment of the sample was introduced. The pre-treatment consisted of immersion of the sample in the electrolyte for approximately 10 minutes, in order to remove any oxides and other surface contaminations. This was shown to have a beneficial effect on the validity of the results [11]. Whether polarisation of the sample is beneficial during this phase will be investigated. The required duration of the pre-treatment is not yet explored.

The current applied corresponds to a current density of $\sim 1\ \mathrm{A/cm^2}$ when 30 mm of the sample is immersed. The absolute value of the current applied will therefore vary with the cross section of the sample. The actual current density will not be constant during the experiment, but vary with sample position. The standard procedure used is described below:

1. Preheat oven to ∼970 °C
2. Locate the bath surface using the software.
3. Immerse the sample ∼5 mm into the bath, and set this position as rest position.
4. **Electrolyte 1:** From the rest position, repeat the following steps five times:
   a) Immerse sample 2 cm into the bath at a speed of 0.2 mm/s.
   b) Pause at bottom position for 30 sek.
   c) Return to rest position at 0.2 mm/s.
   d) Pause at rest position for 30 sek.
5. Locate the position of the metal surface as described in Section 4.6.1. Set this position as the new rest position.
6. **Pre-treatment:** Let the sample sit at the new rest position for 10 minutes.
7. **Metal 1:** Repeat step 4 from the metal surface.
8. **Electrolyte 2, polarised:** Return to the electrolyte surface. From here, repeat step 4 *with* current applied.
9. **Metal 2, polarised:** Return to the metal surface and from here, repeat step 4 *with* current applied.
10. **Electrolyte 3:** Return to the electrolyte surface. From here, repeat step 4 *without* current applied.
11. **Metal 3:** Return to the metal surface and from here, repeat step 4 one final time, *without* polarisation.
12. Finally, lift the entire sample out of the bath before the oven is turned off.

Step 4, 7, 8, and 9 allows for the comparison of wetting with and without polarisation. Step 10 and 11 are included to investigate whether any effect of polarisation remains after the polarisation is turned off. The different steps of the sequence are illustrated in Figure 4.7. For simplicity, each step in **bold** will be referred to as a series, and each of these series consists of five cycles, namely the five repetitions of dipping.

4.7 Processing of Data From Immersion-Emersion Method

For this method, the post-processing of the data is an essential and time consuming component. To extract the degree of wetting from the raw-data the recorded weight must be converted into a corrected weight, w_{corr}. This corrected weight is the residual after the effect of buoyancy and the apparatus weight has been accounted for. See Section 3.1 and Equation 3.1 for further explanation. The buoyancy factor, f_b, has a mathematical expression which can be calculated. Likewise, the apparatus weight, w_0, can be measured prior to the experiment. However, both parameters will vary over the course of the experiment as the sample collects some electrolyte and the density of the surrounding liquid changes. Therefore, both parameters are in practice found by fitting the data to the function given in Equation 4.1.

$$w_{corr} = w - w_{th} = w + f_b \times x - w_0 \tag{4.1}$$

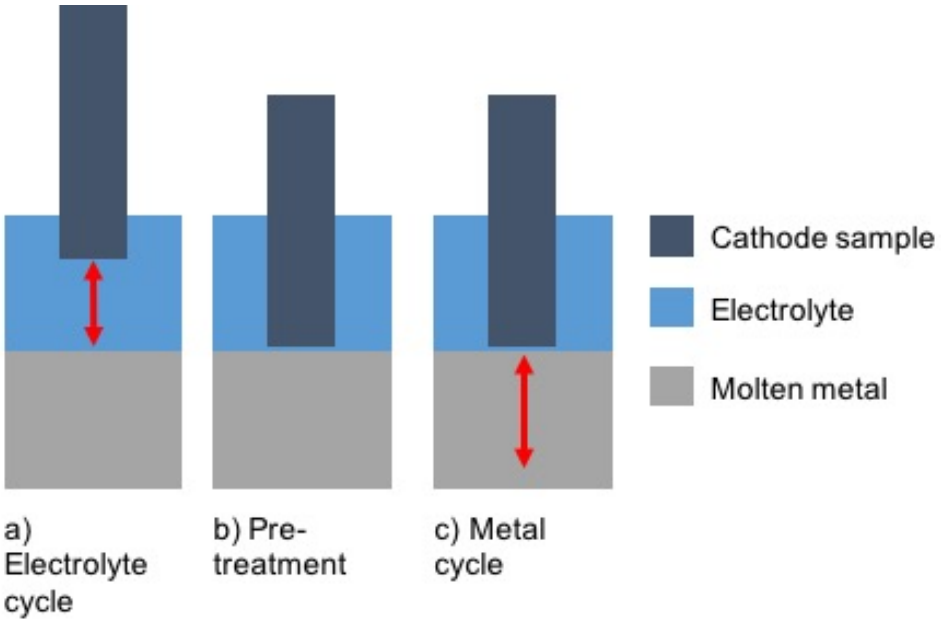

Figure 4.7: Illustration of the three different cycles described in the standard measuring sequence: a) Step 4, 8 and 10. b) Step 6. c) Step 7, 9 and 11. Here shown for neutral wetting of sample.

In this expression w is the recorded weight, x is the recorded position and w_{th} is the theoretical weight, i.e. what the recorded weight would have been in the absence of any wetting forces. The term $f_b \times x$ represents the correction for the buoyancy in the system and w_0 is the apparatus weight.

A theoretical sketch of the corrected weight as a function of position is illustrated in Figure 4.8. When the sample begins to move through the molten metal, there will be an initial buildup of meniscus. This reaches a maximum after which a dynamic steady-state is established. It is the degree of wetting during this period of steady-state which reflects the wettability of the sample material.

The buoyancy factor is determined by minimising the standard deviation of the data in the averaging area of the graph using Solver in Excel. The optimisation problem is expressed in Equation 4.2.

$$\begin{aligned} &\text{Minimise} && \sum_i \left[w_{corr,i}(f_b, w_0) - \bar{w}_{corr}(f_b, w_0)\right]^2 \quad \forall \quad i : x_{start} < x_i < x_{end} \\ &\text{By varying} && f_b \\ &\text{Subject to} && f_b > 0 \end{aligned} \tag{4.2}$$

$\bar{w}_{corr}$ is the average corrected weight for the entire averaging area. x_{start} and x_{end} designates the start and the end position of this area, respectively. The start and endpoint for every cycle are given to the Solver model manually. Solver is also used to determine the constant w_0 so that the peak resulting from the meniscus build-up corresponds to $w_{corr} = 0$. This is merely a convention to ensure consistent processing of data across parallels. The optimisation problem is expressed in Equation 4.3. Both optimisation problems are solved for each cycle individually, allowing for the parameters to be adjusted. Normally the optimisation problems are solved for the immersion and emersion part of the cycle simultaneously, but in cases where the two greatly differ in shape, only the immersion part is used. In these cases, the behaviour of the liquid is fundamentally different during immersion and emersion, so there is no theoretical foundation for

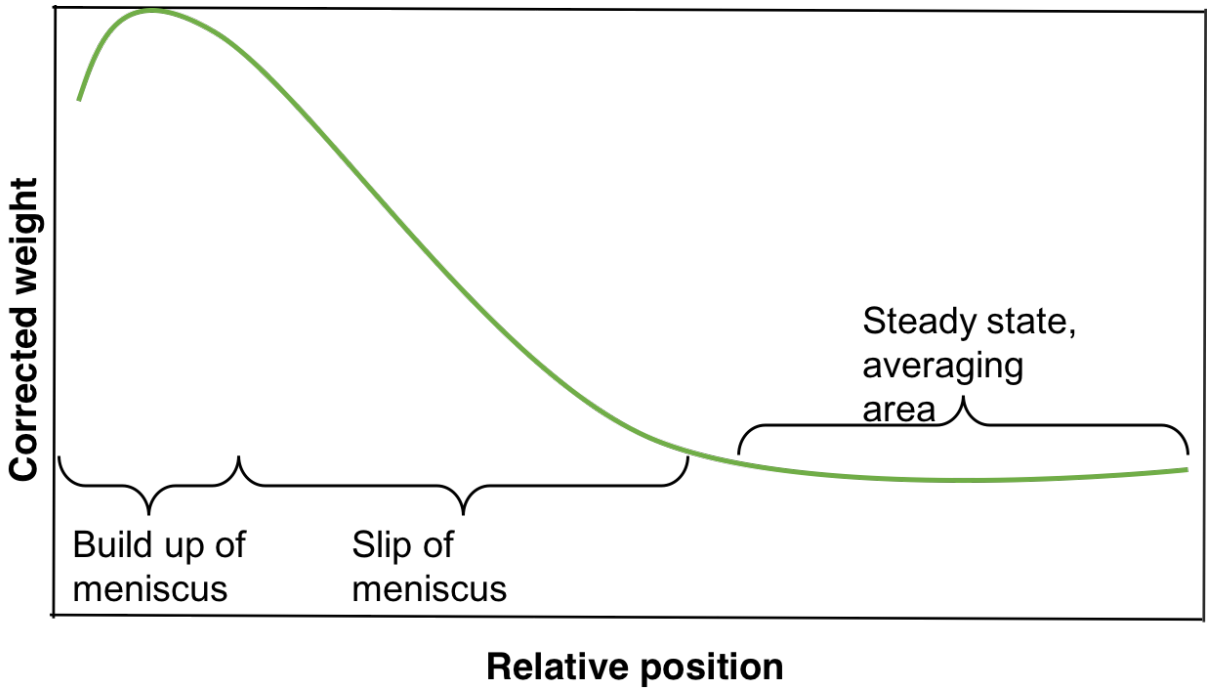

Figure 4.8: Sketch of corrected weight as a function of position for a non-wetting system. Note that this not an actual experimental curve, merely an illustration.

force fitting them to the same type of curve. Previous work has shown that the emersion signal varies the most, and therefore the immersion signal is chosen as the standard [11].

$$\begin{array}{ll} \text{Minimise} & max\left(\left[w_{corr,i}(f_b, w_0)\right]^2\right) \quad \forall \quad i : x_{start} < x_i < x_{end} \\ \text{By varying} & w_0 \\ \text{Subject to} & w_0 > 0 \end{array} \tag{4.3}$$

Figure 4.9 shows plots of the corrected weight before and after buoyancy correction as a function of the relative position, i.e. position indexed to the starting position of the cycle.

4.7.1 Final Output

Each cycle gives two numbers for average corrected weight - one from the immersion part and one from the emersion part of the cycle. As previously mentioned, each series consists of five cycles. From these cycles an overall average corrected weight for the entire series is calculated. The mathematical expression for this is given in Equation 4.4 (bars indicate average values). The first of the five cycles is not included in this overall average; The first dip is fundamentally different from all of the successive ones, as the material is now clean. In the subsequent dips the sample has previously been exposed to the liquid [11] and will likely be partly covered in electrolyte. In the earlier phase of this work, each series only included three cycles of which all were included in the average [11]. Since one is now to be disregarded, the number of cycles has been increased to five, in order to have a sufficient amount of observations to make up an average.

$$\bar{w}_{series} = \bar{w}_{cycle,i} \quad 2 \leq i \leq 5 \tag{4.4}$$

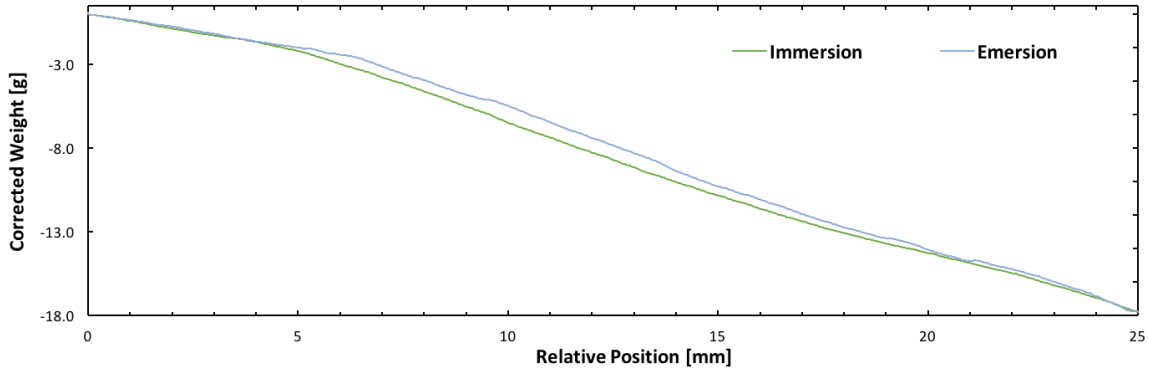

(a) Before buoyancy correction ($w_{corr} = w - w_0$)

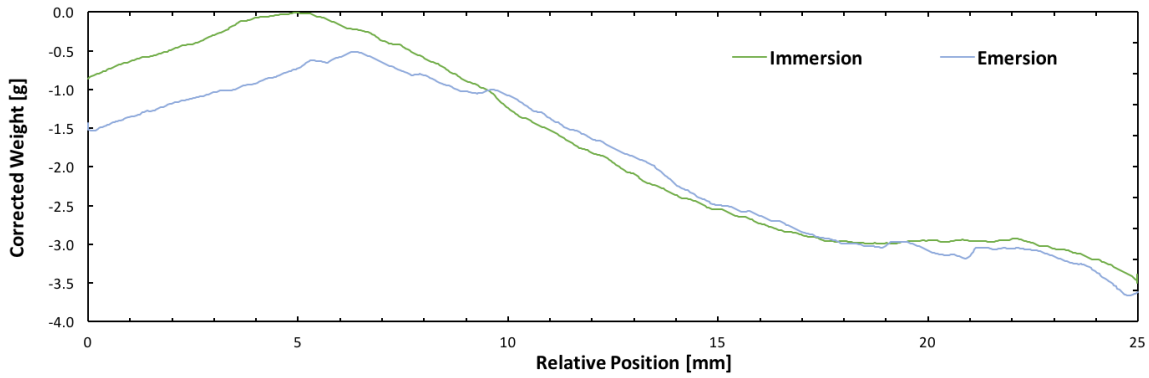

(b) After buoyancy correction

Figure 4.9: Plots of corrected weight a) before and b) after buoyancy correction. Both plots are adjusted for apparatus weight, w_0. Data for both graphs are collected for this work and are fully presented and discussed in Section 6

As mentioned in Section 3.1.2 the effect of the electrolyte meniscus is an unwanted disturbance. With the new measuring sequence the magnitude of this effect can be accurately determined for every series, and hence the result can be adjusted. This is done by subtracting the average for the electrolyte series from the average of the metal series, resulting in what will be referred to as the adjusted average. The mathematical expression is given in Equation 4.5. It is this final adjusted average that will summarise the material's wetting properties.

$$\bar{w}_{adjusted} = \bar{w}_{metal} - \bar{w}_{electrolyte} \tag{4.5}$$

For the final plotting of the data, the results are smoothed by a five-point moving average. The formula is given in Equation 4.6. The position coordinates (x-coordinates) are indexed to the starting point of the immersion, meaning that x = 0 corresponds to the position of the metal surface. This is just a matter of visual representation, and does not affect the numerical results.

$$\tilde{w}_i = \frac{w_{i-2} + w_{i-1} + w_i + w_{i+1} + w_{i+2}}{5} \tag{4.6}$$

4.7.2 Interpretation of Results

The final output from the data processing, i.e. the adjusted average corrected weight, requires some interpretation in order to be connected to the material's wetting property. If no surface forces were present, the corrected weight would be zero [6]. However, this is practically never the case. In the case of a non-wetting system a convex meniscus will form at the interface and push the sample *upwards*, giving it a *negative* corrected weight (i.e. the sample appears lighter than it is). For a wetting system, the opposite is true; a concave meniscus pulls the sample *downwards*, resulting in a *positive* corrected weight. The two cases are illustrated in Figure 4.10

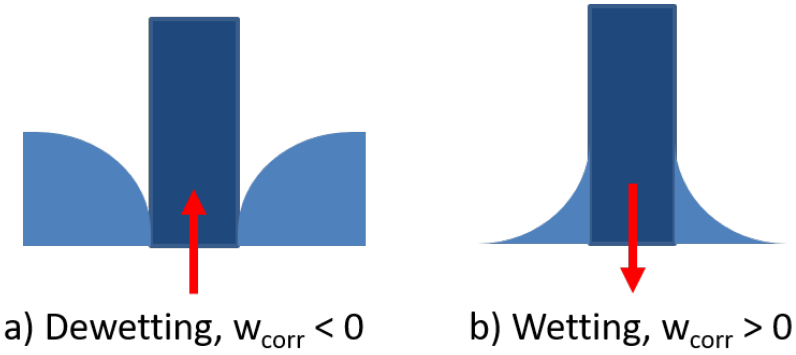

Figure 4.10: The forces exerted on the sample by the meniscus in case of a) dewetting and b) wetting.

It should be noted that the value of w_0 will have a significant impact on the absolute value of the final average corrected weight. This is an inherent weakness of the method - a wrong choice of w_0 could put the numerical result for a wetted material in the category of non-wetted and vice versa. One should therefore also sanity-check the numerical results with their graphical representation. The resulting curve for a wetted sample will show a sharp increase in corrected weight at a certain position when the metal suddenly adsorbs on the surface. A material which is wetted by the metal will also exhibit greater, positive hysteresis between the immersion and the emersion part of the cycle. As the cathode is pulled out, the adsorbed metal will stick for some time before abruptly letting go. Figure 4.11 illustrates the general curves for both cases.

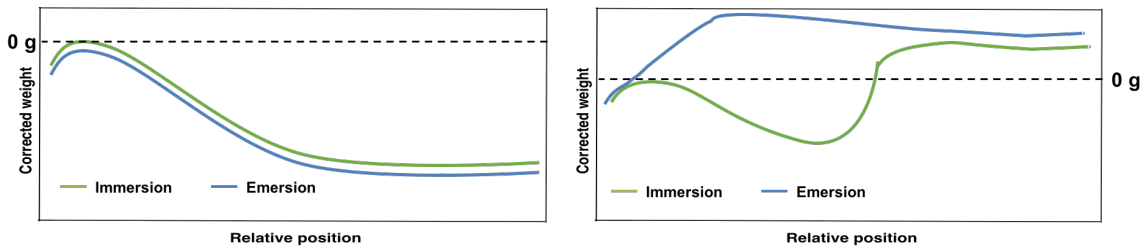

(a) Non-wetting system **(b)** Wetting system

Figure 4.11: Sketched, theoretical curves for a) non-wetting and b) wetting system, showing the qualitative differences in the graphical representation of the two.

4.8 Experimental Procedure for Sessile Drop Tests

The samples to be tested with the sessile drop test had to be cut into squares with sides of 10 mm and an approximate height of 4 mm. This was done using a high-precision saw with a diamond blade. The saw was set to cut at 0.02 mm min^{-1} and rotation speed 3500 rpm. The slow cutting speed was necessary to preserve the TiB_2-inclusions and have a representive surface. No other surface treatment was done to the samples.

The aluminium pieces for the test, or "probe liquid", were prepared from the same aluminium shots as used in the immersion-emersion method. These were cut with a pair of cutting pliers, polished with 500 SiC-paper and immediately placed in a glass of ethanol to prevent the formation of aluminium oxide.

The cathode sample with probe liquid was placed on a sample holder. The holder was then placed in the apparatus chamber. After evacuation, the chamber was heated at a rate of 713°C min^{-1} to 950°C. After this temperature was reached, the heating was continued at 50 °C min^{-1} until the final temperature of 1100°C was achieved. This final temperature was then maintained for one hour. A schematic illustration of the apparatus is included in Figure 4.12.

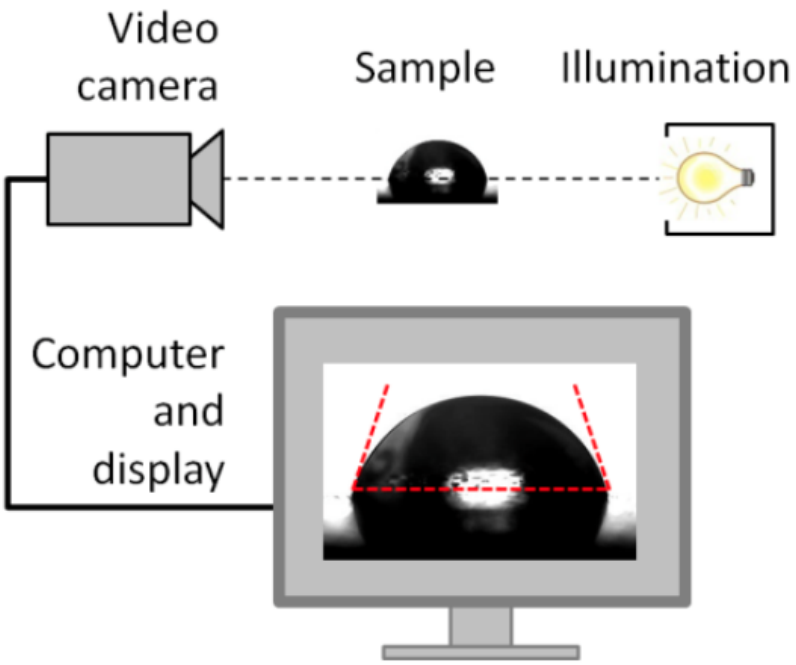

Figure 4.12: Sketch of the apparatus used for sessile drop tests. The figure is extracted from [17].

The entire apparatus is constructed in graphite and designed to accommodate rapid heating and cooling. The rapid heating is necessary in order to perform the experiments without the formation of oxides on the surface of the probe metal. The sample inside the chamber is observed by a digital camera, producing a high resolution image every second [18].

4.9 Surface Characterisation with Scanning Electron Microscope

One pure, untreated sample of TiB_2 and one which had undergone polarisation in electrolyte were fixated on a sample holder using conducting copper tape. Excess solidified electrolyte was gently removed from the polarised sample using a soft brush. No other surface preparation was done to the samples, as the aim was to investigate a surface as similar as possible to the one tested in the wetting experiments.

The sample holder with samples was placed on the stage of the microscope and inserted into the chamber before evacuation. The final pressure inside the chamber was below 1 Pa. Accelerating voltage of the electron gun was set to 20 kV and working distance to 6.1 mm. Both samples were imaged at identical conditions at magnification x250, x500, x1000, x2000 and finally x5000 using secondary electrons. After the imaging, the samples were analysed with EDS. Three spectra were collected at each site.

Chapter 5

Investigation of Immersion-Emersion Method

5.1 Effect of Polarisation During Pre-Treatment

As mentioned in Section 4.6.2, a period of pre-treatment was included in the measurement sequence. The rationale for doing so was to have a representative surface without any contamination. This was initially believed to require a period of cathodic polarisation of the sample while it was immersed in the electrolyte, but previous results suggested that the mere immersion was sufficient [11]. The effect of polarisation during this stage was therefore further investigated.

5.1.1 Experimental

The sequence described in Section 4.6.2 was performed on two samples of pure graphite and two samples of pure TiB_2. One sample of each material was pre-treated without any current applied, whereas the other was polarised with a current equivalent to $1\,A/cm^2$. Other than this, the experimental procedure was identical for all the samples. Again, the necessary duration of the pre-treatment has not been investigated. Note that all samples were polarised during the third and fourth measuring series (electrolyte2 and metal2) - it was merely the polarisation during the pre-treatment which differed.

5.1.2 Results

The average corrected weights for the samples of pure graphite and pure TiB_2 are shown in Figure 5.1 and 5.3 respectively. Normal pre-treatment means that the sample was immersed in electrolyte for 10 minutes. For polarised pre-treatment, the holding period was the same, but with current applied ($1\,A/cm^2$). The numerical details underlying the graphs are given in Tables 5.1 and 5.2 respectively. Typical wetting curves, i.e. corrected weights as a function of position, for both samples of graphite are included in Figure 5.2, and for both samples of TiB_2 in Figure 5.4. Optimisation parameters and more detailed numerical results are shown in Appendices A.1 and A.2.

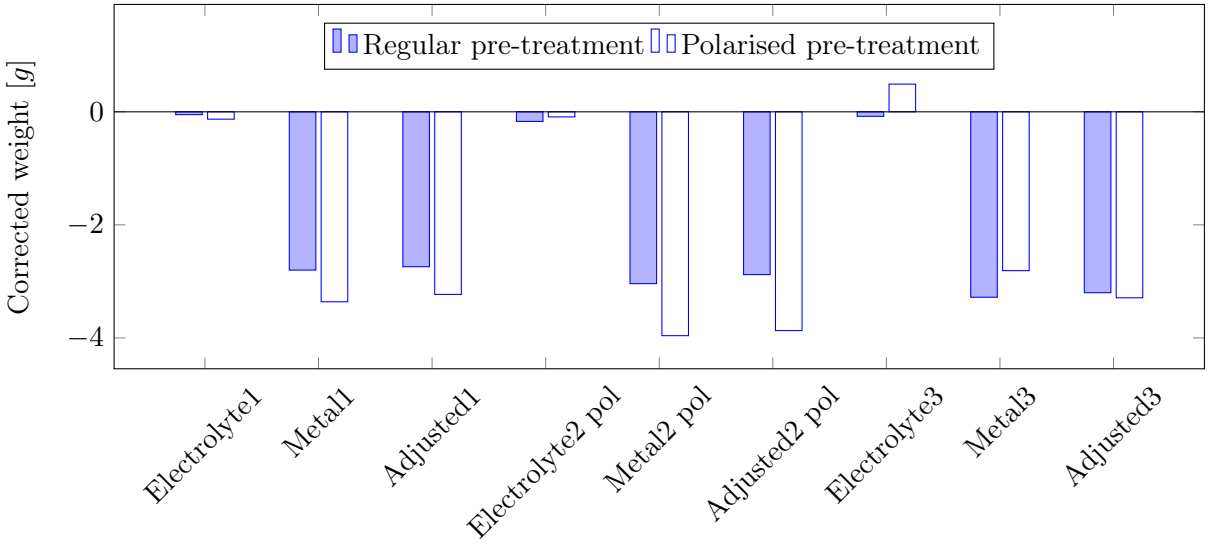

Figure 5.1: Average corrected weight for pure graphite with and without polarisation during pre-treatment. Values are from the immersion part of the series.

Table 5.1: Adjusted average corrected weight for pure graphite with non-polarised and polarised pre-treatment. Values are given for both immersion and emersion, and hysteresis is the difference between the two (emersion minus immersion value).

Graphite	**Non-polarised pre-treatment**			**Polarised pre-treatment**		
Series	Immersion $\bar{w}_{corr}[g]$	Emersion $\bar{w}_{corr}[g]$	Hysteresis $[g]$	Immersion $\bar{w}_{corr}[g]$	Emersion $\bar{w}_{corr}[g]$	Hysteresis $[g]$
Adjusted1	-3.23	-3.33	-0.09	-2.74	-2.93	-0.19
Adjusted2 pol	-3.87	-3.83	0.04	-2.88	-3.00	-0.12
Adjusted3	-3.29	-3.64	-0.35	-3.20	-3.41	-0.21

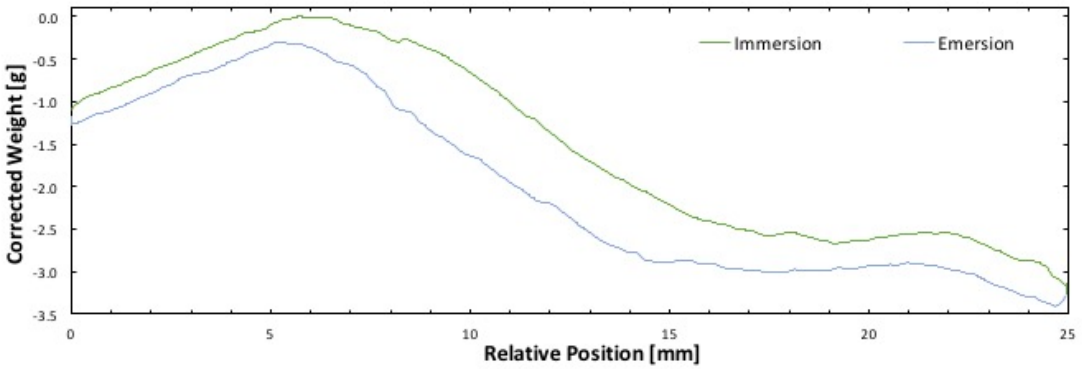

(a) Non-polarised pre-treatment

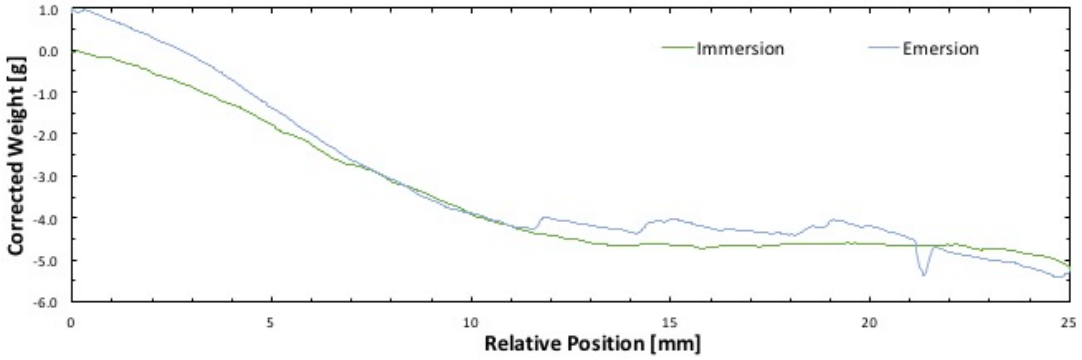

(b) Polarised pre-treatment

Figure 5.2: Resulting wetting curves for pure graphite with a) non-polarised and b) polarised pre-treatment.

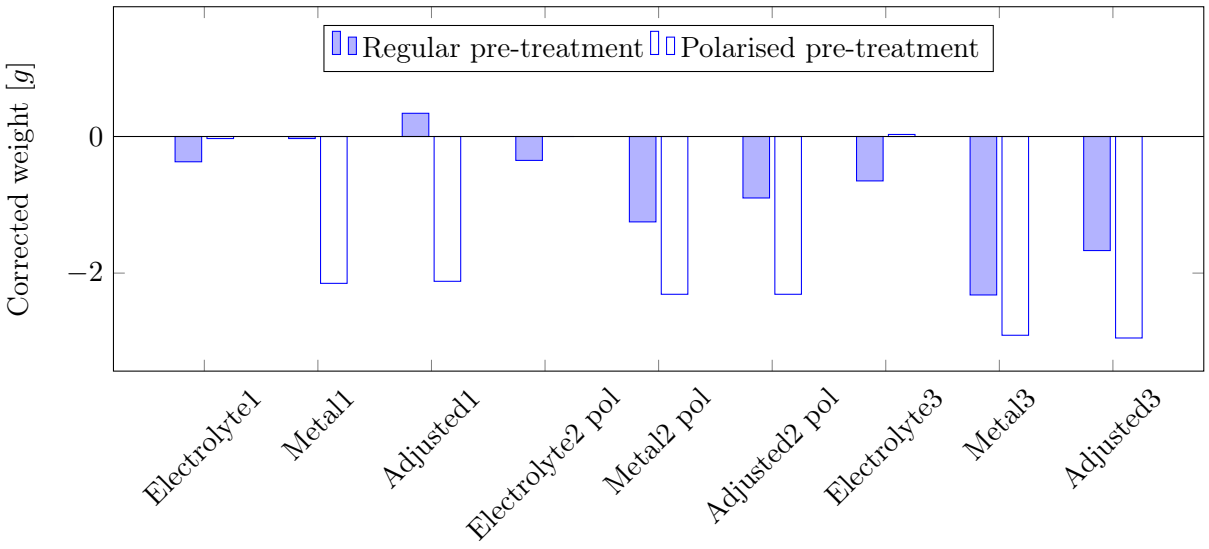

Figure 5.3: Average corrected weight for pure TiB_2 with and without polarisation during pre-treatment. Values are from the immersion part of the series.

Table 5.2: Adjusted average corrected weight for pure TiB_2 with non-polarised and polarised pre-treatment. Values are given for both immersion and emersion, and hysteresis is the difference between the two (emersion minus immersion value).

TiB_2	Non-polarised pre-treatment			Polarised pre-treatment		
Series	Immersion $\bar{w}_{corr}[g]$	Emersion $\bar{w}_{corr}[g]$	Hysteresis $[g]$	Immersion $\bar{w}_{corr}[g]$	Emersion $\bar{w}_{corr}[g]$	Hysteresis $[g]$
Adjusted1	0.34	0.43	0.09	-2.12	-1.61	0.51
Adjusted2 pol	-0.90	-0.36	0.54	-2.31	-2.39	-0.08
Adjusted3	-1.67	-1.21	0.46	-2.95	-3.02	-0.07

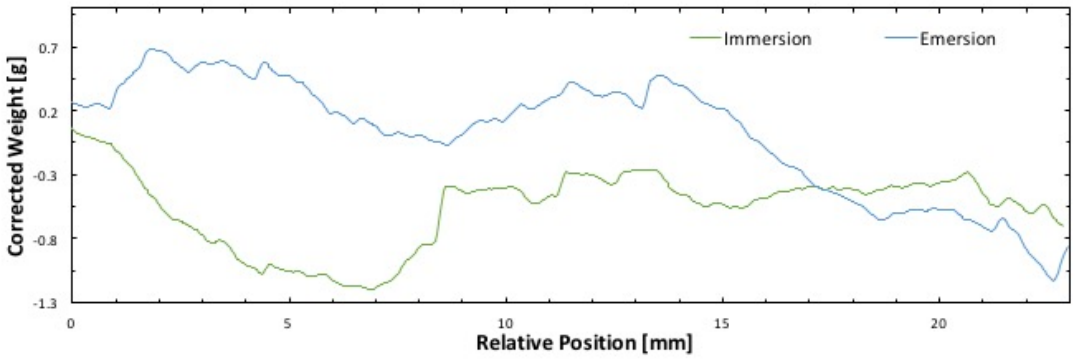

(a) Non-polarised pre-treatment

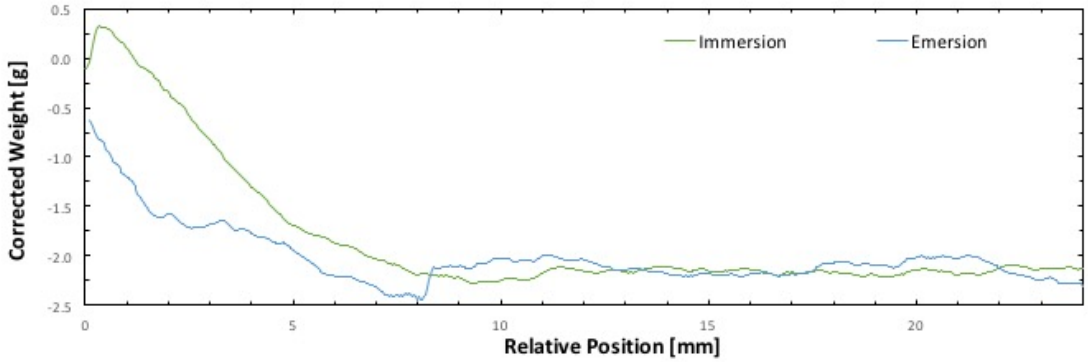

(b) Polarised pre-treatment

Figure 5.4: Resulting wetting curves for pure TiB_2 with a) non-polarised and b) polarised pre-treatment.

5.1.3 Discussion

As can be seen from Figure 5.1 the sample which was polarised during the pre-treatment seems more dewetted than the one which was not. The two samples follow the same trend for the first two experimental series, but after the polarised series there is a change in behaviour - the previously polarised sample is now slightly wetted by the electrolyte, contrary to what was observed in the earlier stage of this work [11]. The effect of the electrolyte meniscus is also much stronger than for the first two series.

For TiB_2 on the other hand, the difference between polarising during pre-treatment and not seems to have a more drastic effect. The TiB_2-aluminium system is industry-wide recognised as an extremely well wetting system [2], but in this case only the non-polarised sample exhibit this behaviour. The polarised one shows dewetting in same order of magnitude as pure graphite. After the sample with regular pre-treatment was polarised for the second series, that too becomes non-wetting in terms of corrected weight, although it still shows positive hysteresis.

It should also be noted that for TiB_2 the wetting seems to become poorer within the same series. Figure 5.5 shows a wetting curve from the same series as represented in Figure 5.4a, but from a later cycle. In the time between the two cycles, the wetting has clearly decreased.

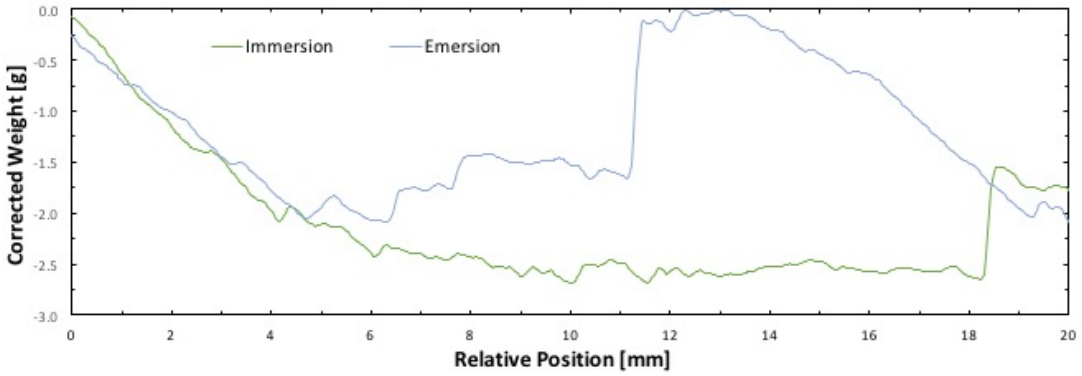

Figure 5.5: Wetting curve from TiB_2 with non-polarised pre-treatment. Curve is taken from the same series as Figure 5.4a, but from a later cycle.

For the sample of regular pre-treatment the effect of the electrolyte meniscus is significant and remains non-negligible for all three series. The polarised sample on the other hand shows negligible electrolyte meniscus. This underlines why it is important to assess this meniscus for every sample, as it is hard to predict the effect of it.

5.1.4 Conclusion

As the polarisation does not appear to have a significant impact on the pure graphite, but drastically alters the behaviour of TiB_2, it was decided that further experimental procedure would include a stage of pre-treatment *without* polarisation.

5.2 Reproducibility of Results

5.2.1 Experimental

Previous experience with the immersion-emersion method has proven it to be rather fickle. It was therefore of interest to establish the reproducibility of the results obtained. The standard measuring sequence described in Section 4.6.2 was repeated once more with a similar sample as tested in Section 5.1 and without polarisation during pre-treatment.

5.2.2 Results

The results for both graphite samples are given graphically for the immersion part of the series in Figure 5.6. Numerical results for both immersion and emersion are shown in Table 5.3. Optimisation parameters and more detailed numerical results are shown in Appendix A.1. The resulting wetting curves for both parallels are shown in Figure 5.7.

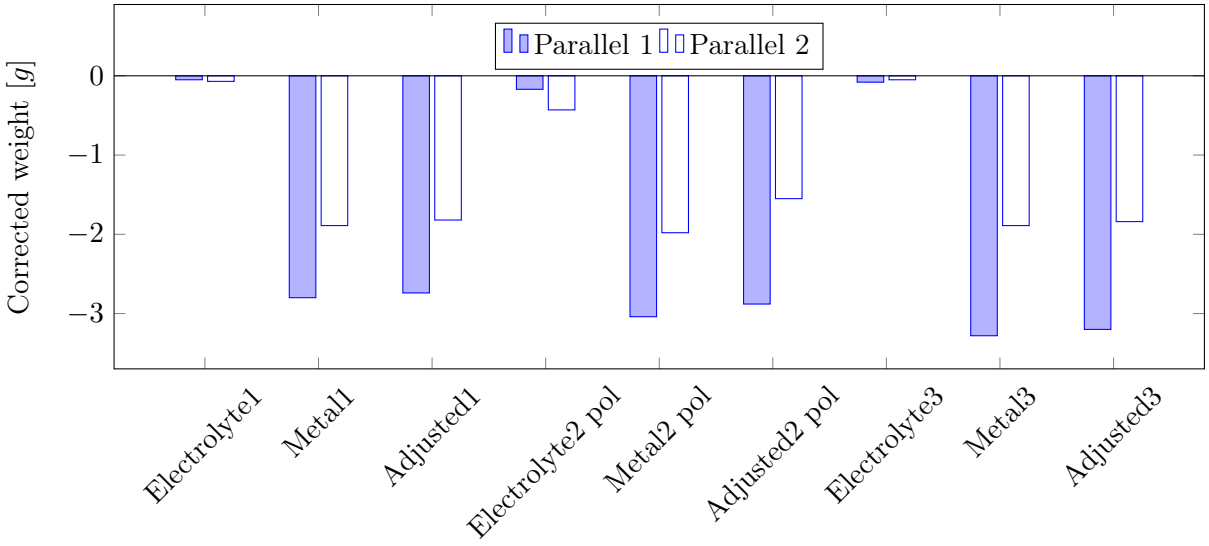

Figure 5.6: Average corrected weight for two identical parallels of pure graphite, both without polarisation during pre-treatment. Values are from the immersion part of the series.

Table 5.3: Adjusted average corrected weight for both parallels of pure graphite with non-polarised pre-treatment. Values are given for both immersion and emersion, and hysteresis is the difference between the two (emersion minus immersion value).

Graphite	**Parallel 1**			**Parallel 2**		
Series	Immersion $\bar{w}_{corr}[g]$	Emersion $\bar{w}_{corr}[g]$	Hysteresis $[g]$	Immersion $\bar{w}_{corr}[g]$	Emersion $\bar{w}_{corr}[g]$	Hysteresis $[g]$
Adjusted1	-2.74	-2.93	-0.19	-1.82	-2.02	-0.20
Adjusted2 pol	-2.88	-3.00	-0.12	-1.55	-1.86	-0.31
Adjusted3	-3.20	-3.41	-0.21	-1.84	-2.17	-0.33

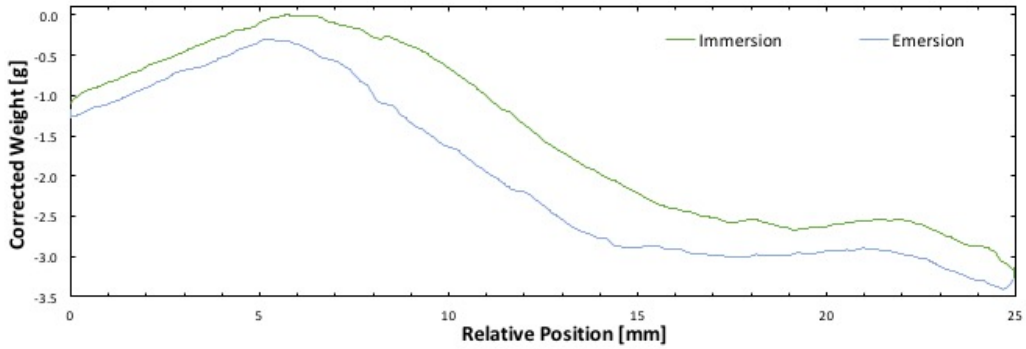

(a) Parallel 1

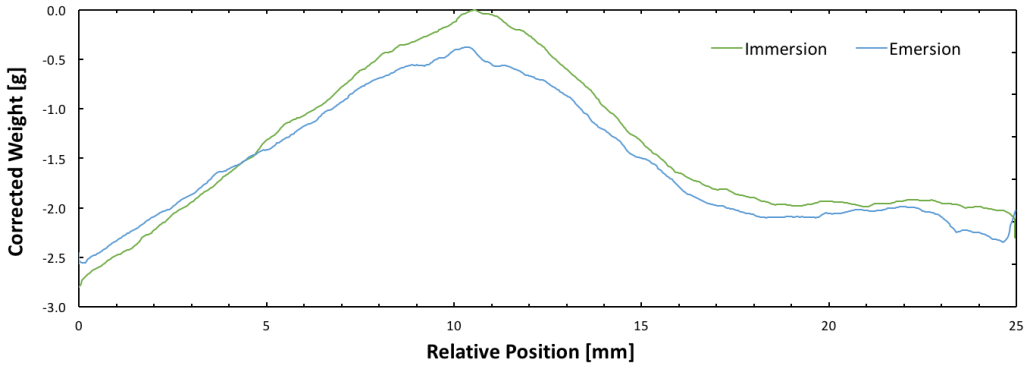

(b) Parallel 2

Figure 5.7: Resulting wetting curves for two identical parallels of graphite, both with non-polarised pre-treatment.

5.2.3 Discussion

As can be seen from Figure 5.6 the two parallels differ quite a lot in the absolute values of corrected weight. However, they do follow the same trend from series to series. Both are clearly non-wetting and exhibit negative hysteresis, as shown in Table 5.3 and the shapes of the graphs in Figure 5.7. As mentioned in Section 4.7 the data processing greatly affects the results and can sometimes be difficult to do correctly. The determination of the apparatus weight may shift the absolute value of the final corrected weight, but would still maintain the overall trends. However, such a large difference as observed for these parallels seems too much to be explained by flaws in data processing alone.

It has previously been shown that the wetting of graphite is dependent on the alumina content in the electrolyte [6]. As the electrolyte is prepared from a crude sample of an industrial bath and a relatively small amount is used, the alumina concentration may well differ from parallel to parallel. This effect may also be an explanation for the variation in the results. Ideally, the procedure should have been carried out for more samples of pure graphite, and for a larger selection of the materials tested. However, due to the limited amount of materials available, this was not carried out for this work.

5.2.4 Conclusion

In conclusion, the variation in the results obtained is larger than what is desirable. It is unlikely that it is only caused by errors in data processing, and other sources of error should be further investigated.

Chapter 6

Wetting Testing with Immersion-Emersion Method

6.1 Wetting of Composites

In this section, the results for a single composite material will be presented and commented on in each subsection. The full description of their composition and preparation is given in Section 4.2.3. A summary of the final results and a comparison across samples will follow in Section 6.1.6. A complete discussion of the results and their implications can be found in Chapter 8 and Chapter 9 respectively.

6.1.1 3018g

The composite 3018g contains 34.3 wt% of TiB_2 and relatively large coke particles. It was prepared by the old synthesis route (see Section 4.2.3 for description of this), using $<37\,\mu$m particles of TiB_2. An image of the sample after completed wetting test is included in Figure 6.1 and the resulting wetting curves are shown in Figure 6.2. Numerical details and curve fitting parameters are given i Appendix A.3.

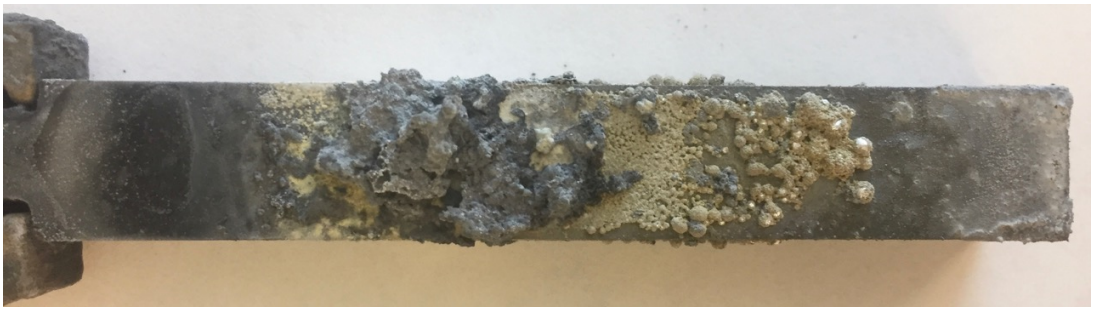

Figure 6.1: Composite sample 3018g after completed wetting test.

Table 6.1: Adjusted average corrected weight for composite sample 3018g. Values are given for both immersion and emersion, and hysteresis is the difference between the two (emersion minus immersion value).

3018g Series	Immersion $\bar{w}_{corr}[g]$	Emersion $\bar{w}_{corr}[g]$	Hysteresis $[g]$
Adjusted1	-1.97	-2.13	-0.16
Adjusted2 pol	-1.50	-1.65	-0.15
Adjusted3	-1.42	-1.76	-0.34

All series for 3018g show negative corrected weight, i.e. non-wetting of the material. The numerical values are generally supported by the qualitative features of the wetting curves, although Figure 6.2a shows a moderate increase in corrected weight after 12 mm, and positive hysteresis. After polarisation, all qualitative features of wetting have disappeared. Bear in mind that only one out of five wetting curves for each series is included here. In general, this selection was made in an effort to give a representative impression of the nature of the results. In cases where results differed substantially between cycles, this will be highlighted.

6.1.2 3112g

Composite 3112g contains 33.6 wt% of TiB_2, i.e. almost the same amount as 3018g, but with smaller coke particles and a finer quality of TiB_2 ($<5\,\mu$m) than the other composites. The tested sample is shown in Figure 6.3. Table 6.2 gives the overall numerical result and a selection of wetting curves are shown in Figure 6.4.

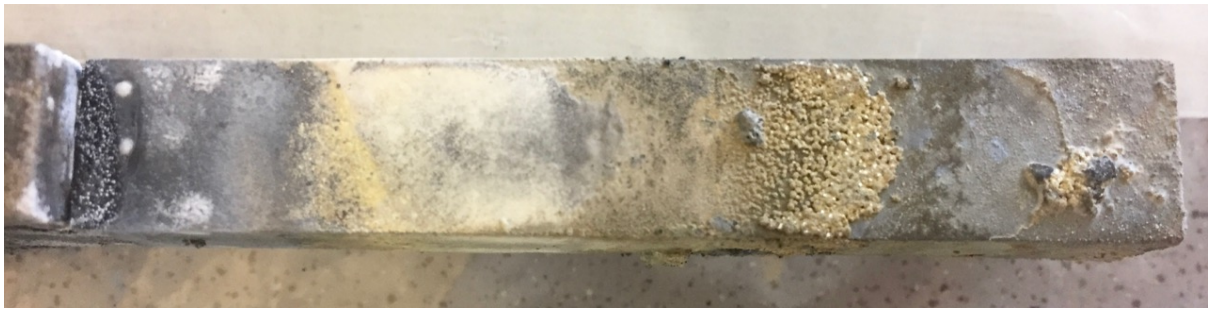

Figure 6.3: Composite sample 3112g after completed wetting test.

After the experiment, the sample showed clear signs of aluminium carbide formation, which can be seen as a yellow film on the material in Figure 6.3. Such a layer may influence the measured wetting. The first series is strongly non-wetting, but during the polarisation this changes drastically; The subsequent, polarised series has a much higher corrected weight. Most of this increase seems to fade when the polarisation is turned off in the final series. The curve in Figure 6.4b does not show much hysteresis, as would have been expected for a well wetting system. This may be due to low surface surface tension, causing the liquid to easily detach from the surface.

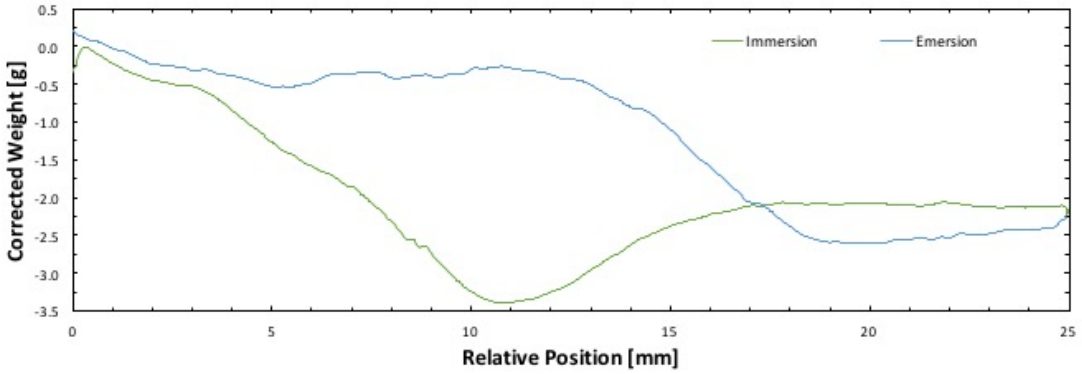

(a) Before polarisation

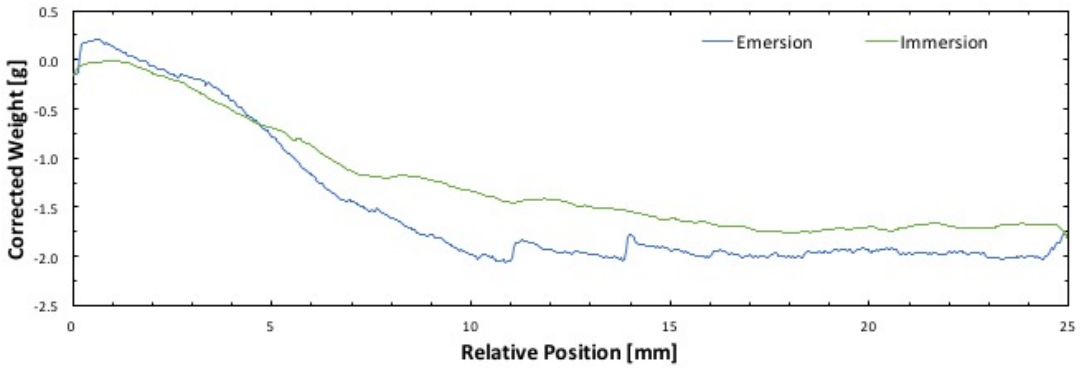

(b) During polarisation

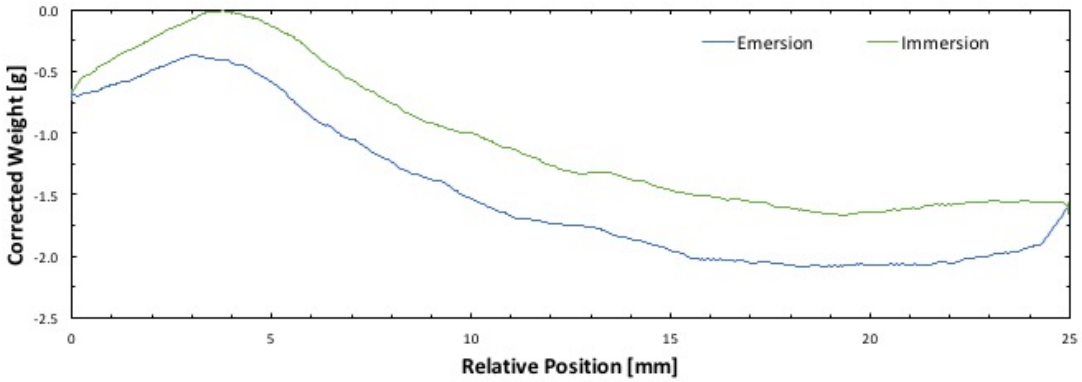

(c) After polarisation

Figure 6.2: Resulting wetting curves for the composite 3018g a) before, b) during and c) after polarisation

Table 6.2: Adjusted average corrected weight for composite sample 3112g. Values are given for both immersion and emersion, and hysteresis is the difference between the two (emersion minus immersion value).

3112g Series	Immersion $\bar{w}_{corr}[g]$	Emersion $\bar{w}_{corr}[g]$	Hysteresis $[g]$
Adjusted1	-4.20	-4.51	-0.31
Adjusted2 pol	-0.26	-0.21	-0.05
Adjusted3	-1.97	-1.94	0.03

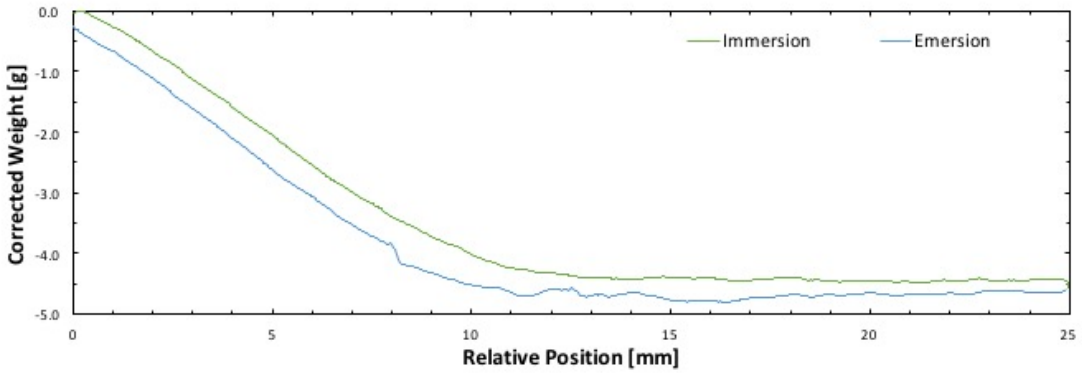

(a) Before polarisation

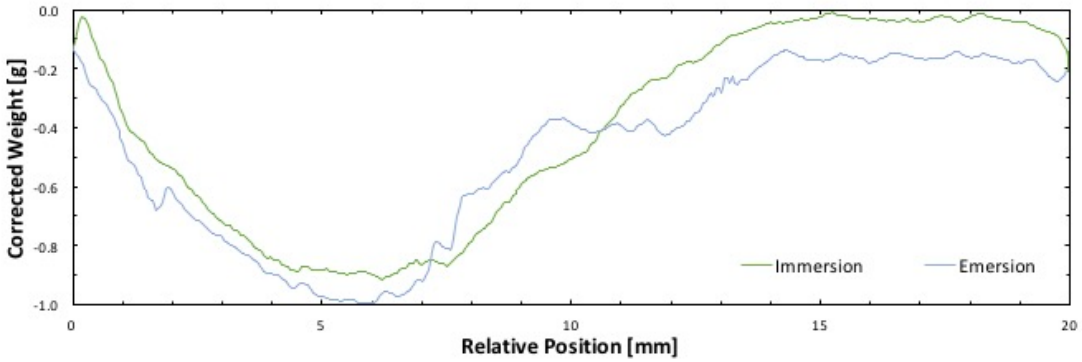

(b) During polarisation

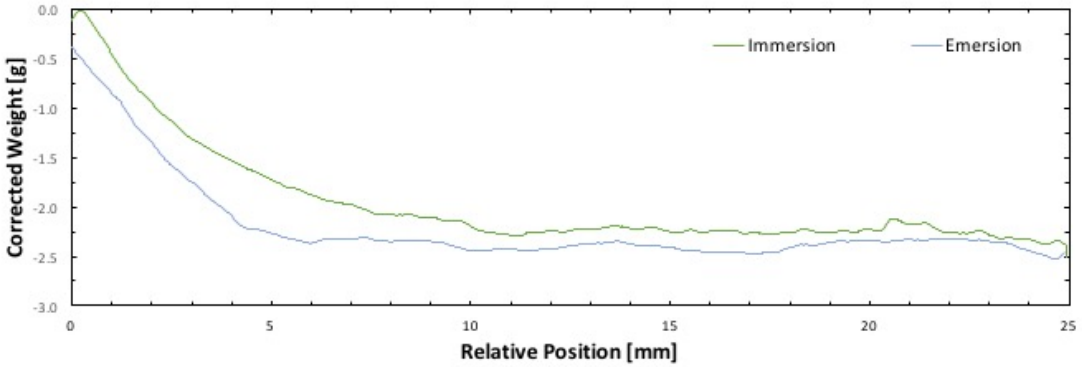

(c) After polarisation

Figure 6.4: Resulting wetting curves for the composite 3112g a) before, b) during and c) after polarisation

6.1.3 5002g

Material 5002g is the first sample prepared by the new and proprietary synthesis route. The TiB_2-load is 28.2 wt%, and the particles are homogeneously distributed. The sample after testing is shown in Figure 6.5 and resulting wetting curves are shown in Figure 6.6, while Table 6.3 gives the numerical overview. Further numerical details and optimisation parameters are given in Appendix A.3.

All series are on the side of non-wetting, although the first one shows surprisingly large hysteresis, see Figure 6.6a. The polarised cycle in Figure 6.6b exhibit the typical slip pattern for a wetted material during emersion and has a less negative value of corrected weight than the

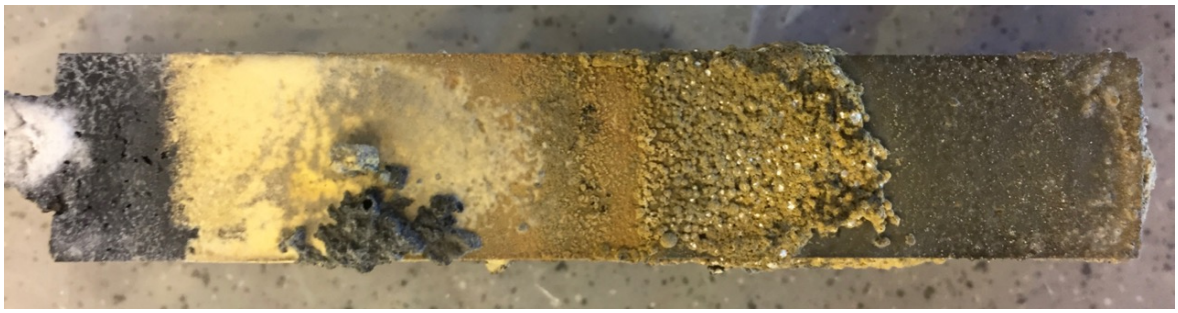

Figure 6.5: Composite sample 5002g after completed wetting test.

non-polarised one - both indications of improved wetting. In the final cycle, no sign of wetting remains.

Table 6.3: Adjusted average corrected weight for composite sample 5002g. Values are given for both immersion and emersion, and hysteresis is the difference between the two (emersion minus immersion value).

5002g Series	Immersion $\bar{w}_{corr}[g]$	Emersion $\bar{w}_{corr}[g]$	Hysteresis $[g]$
Adjusted1	-3.24	-3.22	0.02
Adjusted2 pol	-2.97	-2.34	0.63
Adjusted3	-3.19	-3.35	-0.16

6.1.4 5020g

Material 5020g has a higher fraction of TiB_2 than the materials presented up until now, namely 41.5 wt%. The tested sample can be seen in Figure 6.7 and its wetting curves in Figure 6.8. Adjusted average corrected weights are given in Table 6.3 whereas details from the optimisation procedure can be found in Appendix A.3.

None of the series for 5020g show any sign of wetting, neither in terms of numerical result or qualitative behaviour. However, the wetting does seem to improve over the course of the experiment. The largest increase in corrected weight occurs between the first and the second series, but the improvement continues after the polarisation ceases. Again, much carbide formation can be seen on the tested sample.

Table 6.4: Adjusted average corrected weight for composite sample 5020g. Values are given for both immersion and emersion, and hysteresis is the difference between the two (emersion minus immersion value).

5020g Series	Immersion $\bar{w}_{corr}[g]$	Emersion $\bar{w}_{corr}[g]$	Hysteresis $[g]$
Adjusted1	-4.91	-5.00	-0.09
Adjusted2 pol	-2.70	-2.61	0.09
Adjusted3	-1.49	-1.65	-0.16

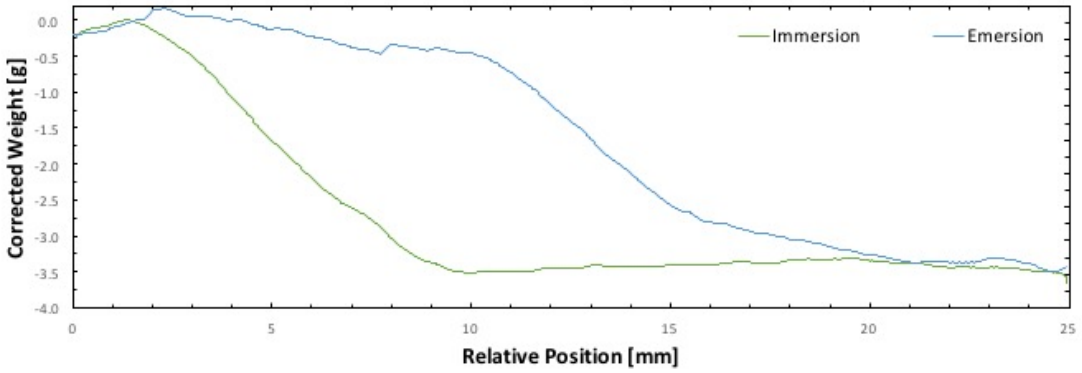

(a) Before polarisation

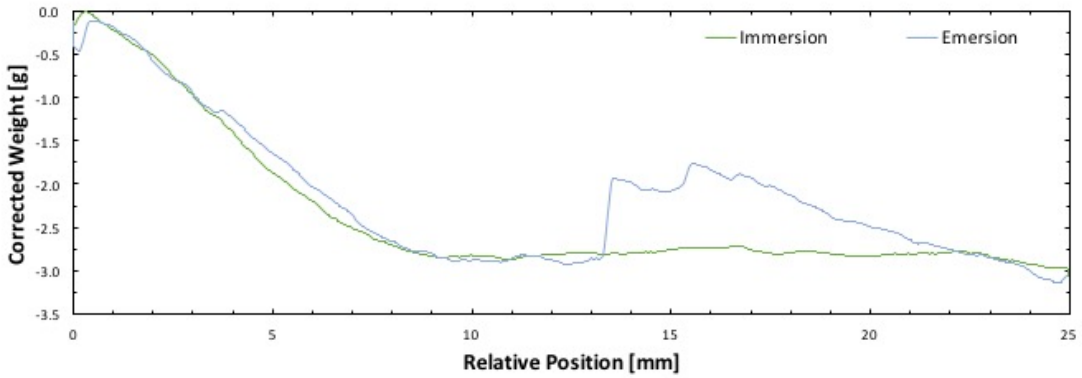

(b) During polarisation

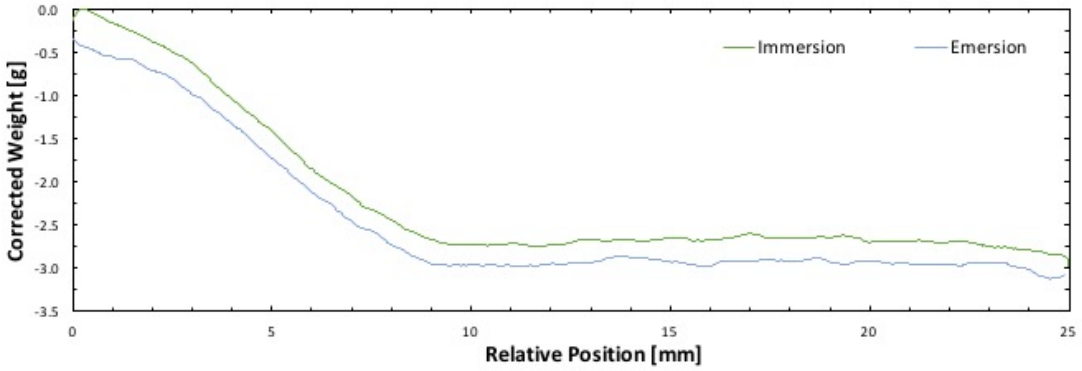

(c) After polarisation

Figure 6.6: Resulting wetting curves for the composite 5002g a) before, b) during and c) after polarisation

6.1.5 6004g

The final tested composite material is the one with the highest TiB_2 content, i.e. 55.1 wt%. The sample is depicted in Figure 6.9 and the wetting curves from the test can be seen in Figure 6.10. The main numerical results are summarised in Table 6.5, while more details can be found in Appendix A.3.

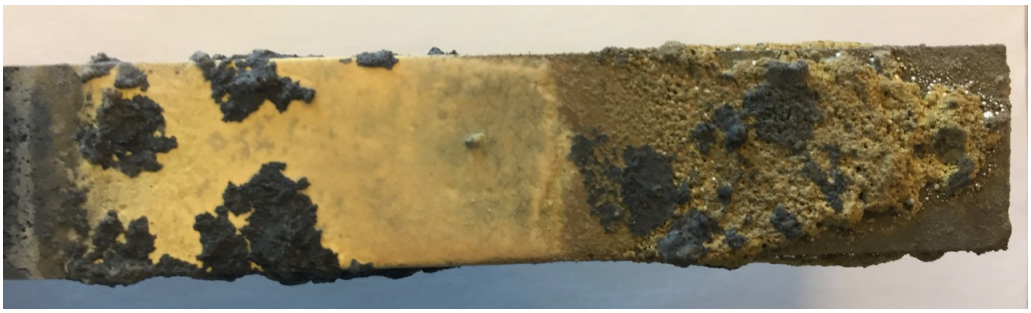

Figure 6.7: Composite sample 5020g after completed wetting test.

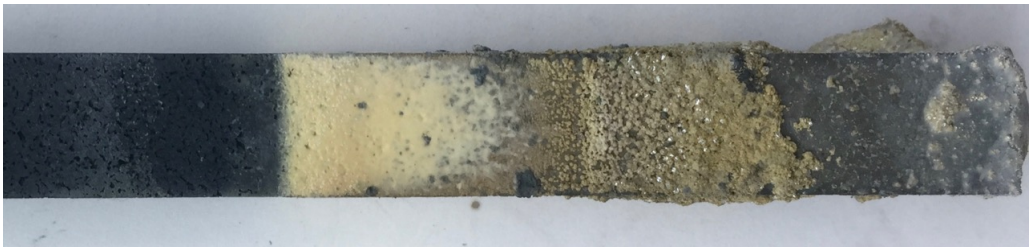

Figure 6.9: Composite sample 6004g after completed wetting test.

In terms of numbers, all of the series obtained for 6004g are non-wetting. However, the polarised one in Figure 6.10b show some hysteresis. The sharp drop in corrected weight in the emersion signal is most likely caused by liquid suddenly letting go of the solid sample. The polarised series appears to be somewhat less dewetting than the other series. This effect was strongest for the earliest cycles in the series, and almost depleted in the later ones. No sign of wetting remains in the final non-polarised series.

Table 6.5: Adjusted average corrected weight for composite sample 6004g. Values are given for both immersion and emersion, and hysteresis is the difference between the two (emersion minus immersion value).

6004g Series	Immersion $\bar{w}_{corr}[g]$	Emersion $\bar{w}_{corr}[g]$	Hysteresis $[g]$
Adjusted1	-3.21	-2.94	0.27
Adjusted2 pol	-3.65	-2.72	0.93
Adjusted3	-3.80	-3.69	0.11

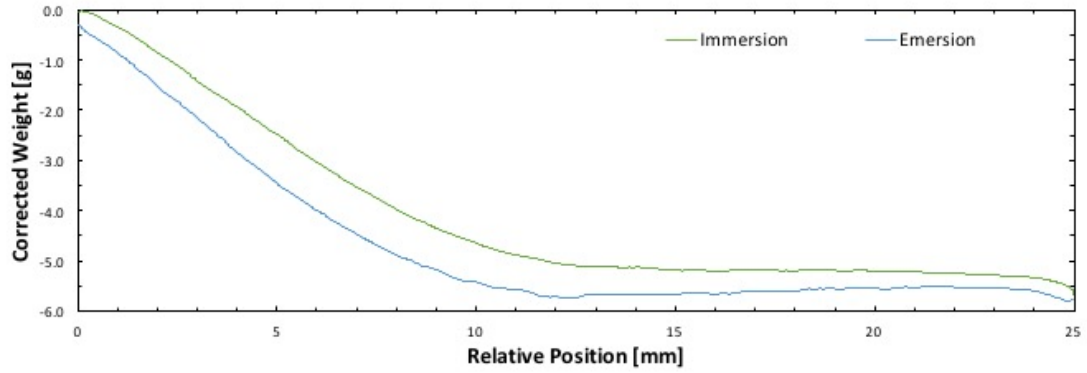

(a) Before polarisation

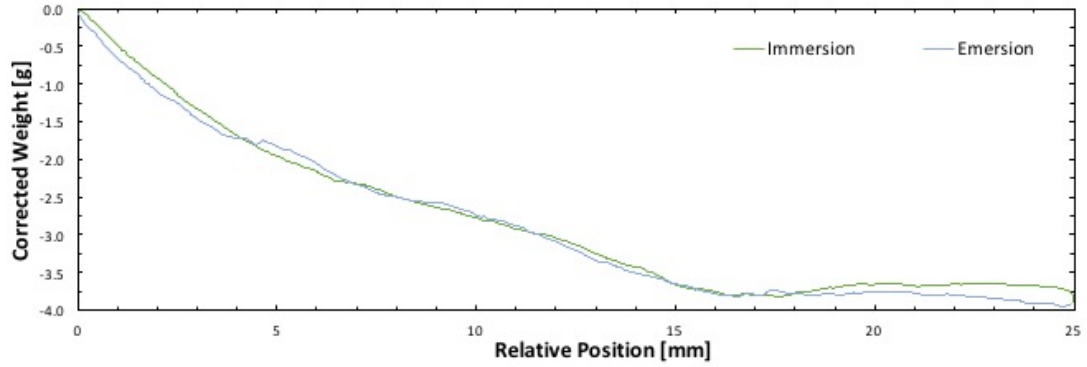

(b) During polarisation

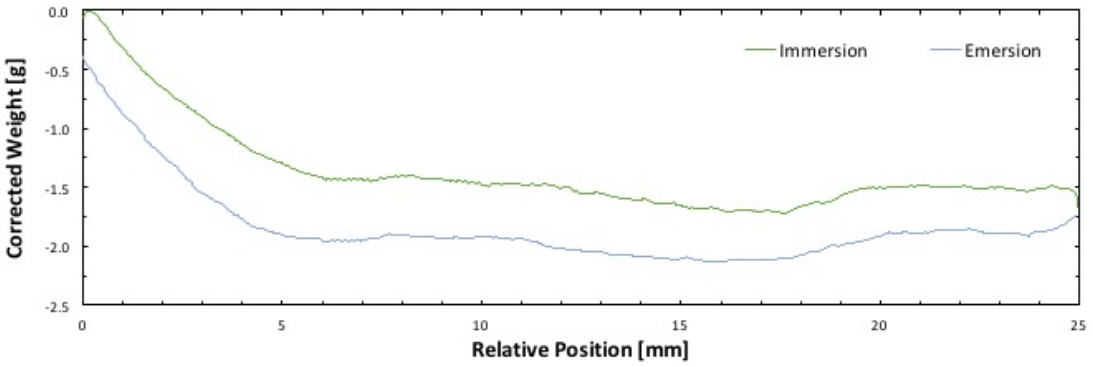

(c) After polarisation

Figure 6.8: Resulting wetting curves for the composite 5020g a) before, b) during and c) after polarisation

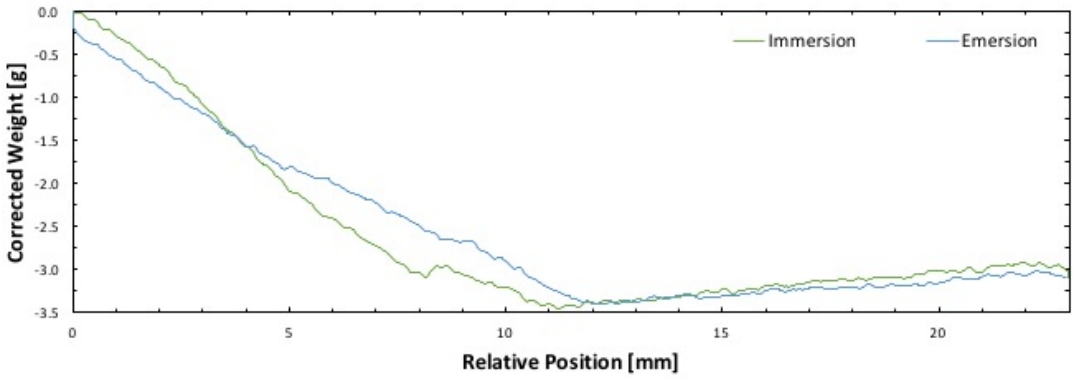

(a) Before polarisation

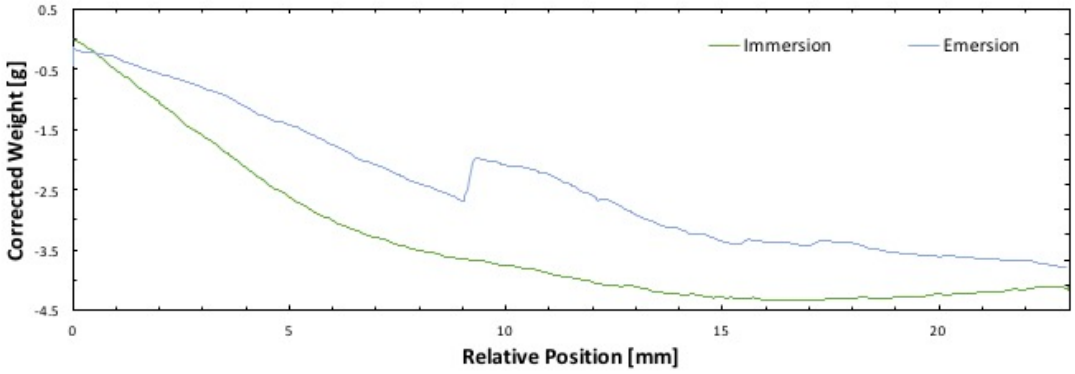

(b) During polarisation

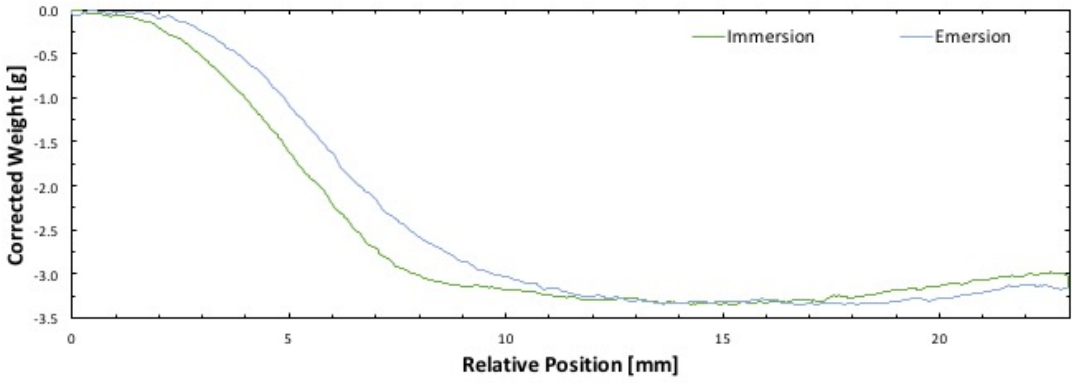

(c) After polarisation

Figure 6.10: Resulting wetting curves for the composite 6004g a) before, b) during and c) after polarisation

6.1.6 Summary

The adjusted average corrected weight for all samples have been plotted against their TiB_2-fraction in Figure 6.11. The boundary result at 0% is pure graphite from Section 5.2. On the other end of the scale is pure TiB_2, which is presented in Section 5.1. Individual plots of each series with sample names are shown in Figure 6.12.

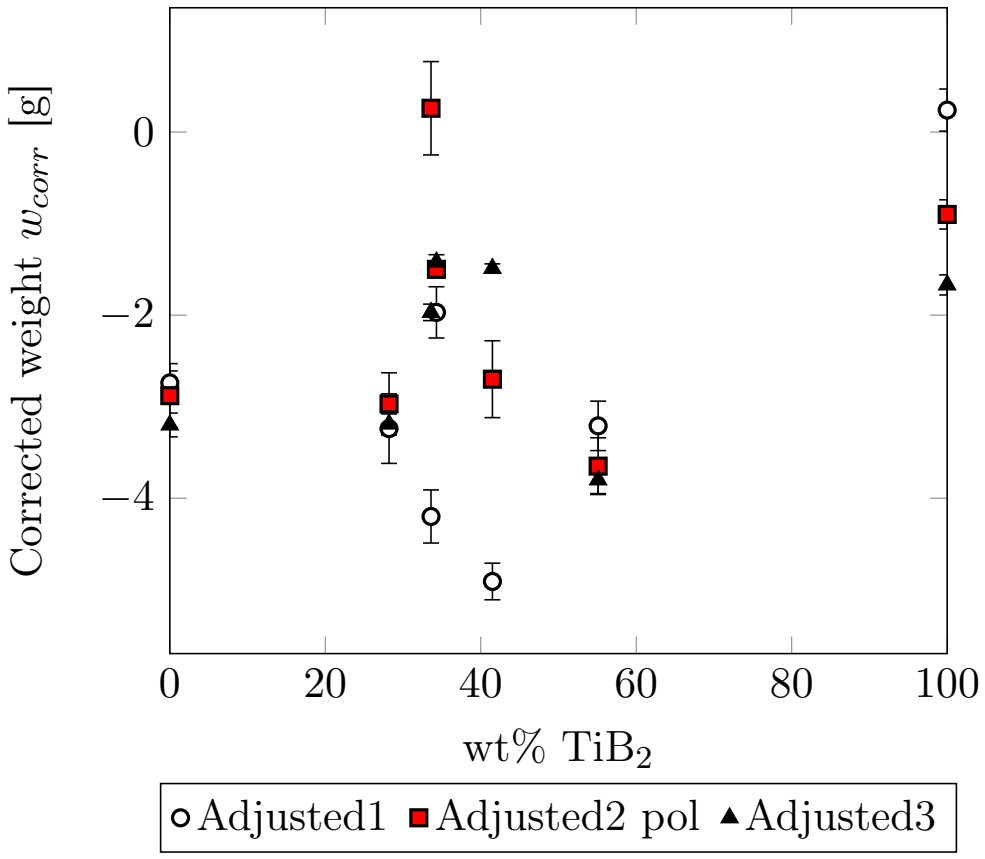

Figure 6.11: Adjusted average corrected weight as a function of TiB_2 weight fraction

Overall there is a weak, positive relation between the fraction of TiB_2 and wetting of the material, but its not a clear trend. The only result that is significantly different from the others is the polarised sample at 33.6 wt% of TiB_2. This data point corresponds to composite 3112g, which is manufactured with a finer quality of TiB_2 than the other materials. For most of the samples the first, unpolarised series is the one with the most negative adjusted average corrected weight, i.e. the strongest dewetted one, with subsequent series slightly better wetted.

6.2 Effect of Alumina Concentration on Wetting

During the experimental work discussed so far, it was observed that samples tended to be increasingly dewetted over the course of a measuring series. This trend seemed particularly strong when the sample was polarised. As mentioned in Section 5.2 there is a known relation between alumina concentration in the electrolyte and wetting of graphite. Earlier work done with the same apparatus found the wetting of graphite by electrolyte to increase significantly at higher alumina concentrations [19]. A similar dependence between wetting and alumina concentration as exist for graphite, has to our knowledge not been investigated for TiB_2. It was therefore of interest to establish whether this existed and if so, if it could explain the decrease in wetting.

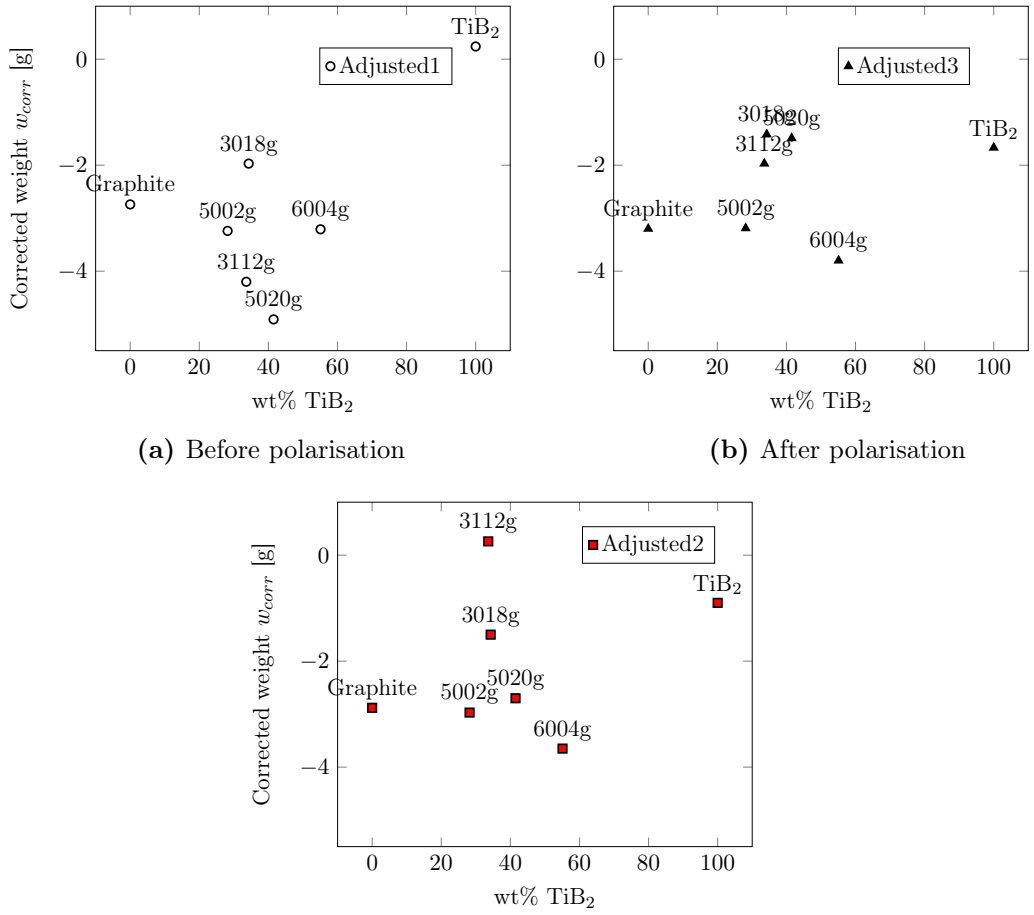

(a) Before polarisation

(b) After polarisation

(c) During polarisation

Figure 6.12: Wetting as a function of TiB_2 content for all three measuring series.

The entire polarisation period in the standard experimental procedure takes approximately one hour. For about half of this time the cell is effectively short circuited as the cathode is in contact with the molten metal. Assuming full current efficiency, this amounts to a consumption of ∼4 grams of Al_2O_3. This corresponds to about 35% reduction in the overall alumina concentration. Hence, if there is any dependency between the alumina concentration and wetting of TiB_2, it may significantly affect the results over the course of the experiment. For details on the calculation of the alumina consumption, see Appendix B.

6.2.1 Experimental

The standard alumina concentration in the ordinary setup is ∼3%. To investigate whether the wetting of TiB_2 was affected by the concentration, two sets of electrolyte with low and high alumina content respectively were prepared, and the first two series of the standard measuring sequence described in Section 4.6.2 were conducted. The alumina concentrations for the parallels are given in Table 6.6.

Table 6.6: Alumina content in the prepared electrolyte baths, for investigation of the effect of alumina concentration on wetting of TiB_2.

Parallel	Alumina concentration[wt%]
Low	1.8
Standard	2.9
High	4.1

6.2.2 Results

The results obtained for all three alumina concentrations are graphically represented in Figure 6.13. The numerical results for the two non-standard concentrations are represented in Table 6.8 and the wetting curves are shown in Figure 6.14. Similar data for the parallel of standard concentration of alumina were presented in Section 5.1, but are repeated here in Table 6.7 for improved readability.

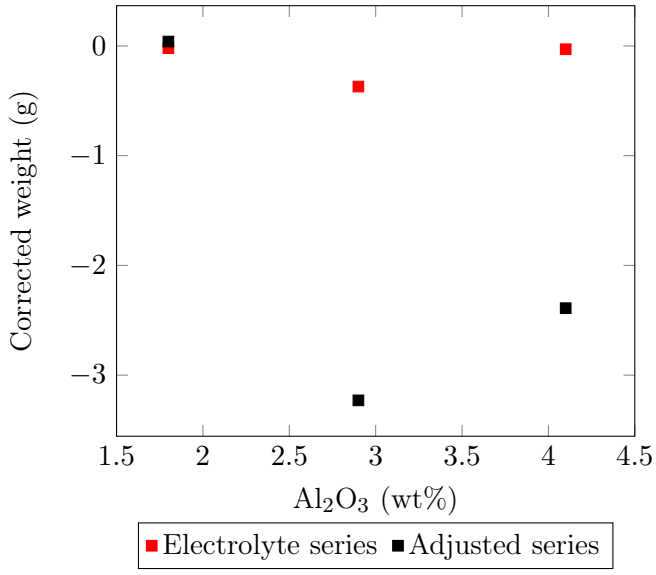

Figure 6.13: Average corrected weights for TiB_2 as a function of alumina concentration in the electrolyte. Values are from the immersion part of the cycles.

Table 6.7: Adjusted average corrected weight pure TiB_2 with standard alumina concentration (2.9 wt%). Values are given for both immersion and emersion, and hysteresis is the difference between the two (emersion minus immersion value).

TiB_2	Standard concentration (2.9 wt%)		
Series	Immersion $\bar{w}_{corr}[g]$	Emersion $\bar{w}_{corr}[g]$	Hysteresis $[g]$
Electrolyte	-0.37	-0.18	0.19
Metal	-0.03	0.25	0.28
Adjusted	0.34	0.43	0.09

Table 6.8: Adjusted average corrected weight for the two parallels of TiB_2 at non-standard alumina concentrations. Values are given for both immersion and emersion, and hysteresis is the difference between the two (emersion minus immersion value).

TiB_2	**Low concentration** (1.8 wt%)			**High concentration** (4.1 wt%)		
Series	Immersion $\bar{w}_{corr}[g]$	Emersion $\bar{w}_{corr}[g]$	Hysteresis $[g]$	Immersion $\bar{w}_{corr}[g]$	Emersion $\bar{w}_{corr}[g]$	Hysteresis $[g]$
Electrolyte	-0.02	-0.12	0.10	-0.03	-0.12	-0.09
Meta	0.01	-0.06	-0.07	-3.03	-2.51	0.52
Adjusted	0.04	0.06	0.04	-2.39	-3.00	0.61

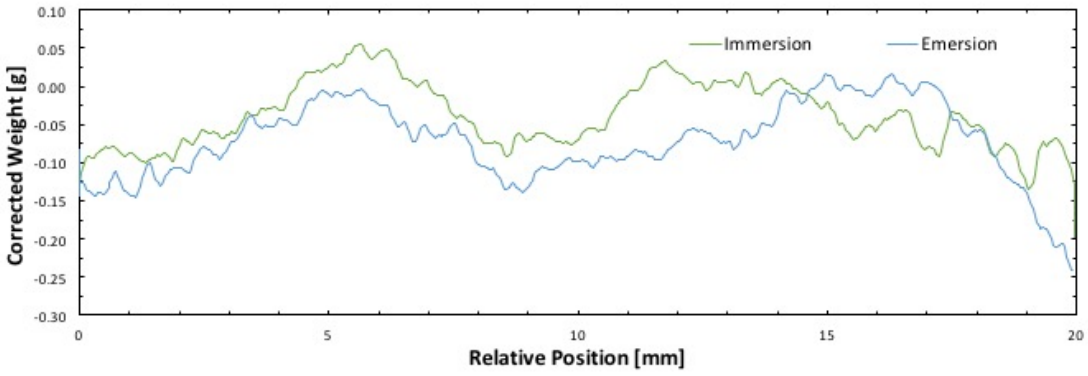

(a) Low alumina concentration, $[Al_2O_3] = 1.8\,\text{wt\%}$

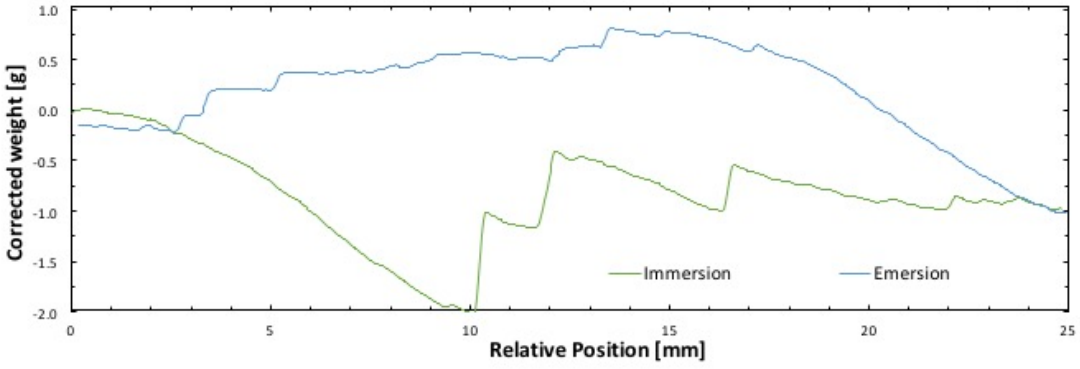

(b) High alumina concentration, $[Al_2O_3] = 4.1\,\text{wt\%}$

Figure 6.14: Resulting wetting curves for TiB_2 at low and high alumina concentration in the electrolyte.

6.2.3 Discussion

The plot in Figure 6.13 suggests that the wetting between TiB_2 and the electrolyte does not depend much on the alumina concentration in the electrolyte. With respect to aluminium on the other hand, the wetting seems to become poorer at higher concentrations of alumina. Note that it is the adjusted average corrected weight that is given in the plot, meaning that the effect of the electrolyte meniscus has been accounted for. It is interesting that a change in the composition of one phase alters the behaviour of a different phase. Why this happens is not known at this point.

This finding is not consistent with the pattern observed in the wetting curves in Figure 6.14. Figure 6.14a shows no qualitative sign of wetting - there is almost no hysteresis and the immersion curve does not have the characteristic jump to higher values as previously seen in wetting systems. The plot for TiB_2 in Figure 6.14b on the other hand exhibit both of these features. Hence, in qualitative terms it seems that TiB_2 is better wetted by aluminium at higher alumina concentrations in the electrolyte, but this is not supported by the numerical results. Again, the heavy reliance on the data processing is problematic. This could have partly have been mitigated by conducting more parallels at a larger range of concentrations.

6.2.4 Conclusion

In conclusion, the alumina concentration in the electrolyte must be considered to affect the wetting of TiB_2 by the metal. Regardless of the exact relation between alumina concentration and wetting, this means that measures should be taken to reduce the variation in alumina content in the electrolyte. Better standardisation can be achieved by preparing the electrolyte from pure salts rather than samples from an industrial bath.

The results, somewhat surprisingly, indicate poorer wetting at higher concentrations. If the negative relationship between alumina concentration and wetting of TiB_2 is correct, this effect cannot explain why the TiB_2 becomes dewetted after polarisation, which causes a decrease in the alumina concentration, and other explanations are required. This is further explored in Chapter 7, in relation to surface characterisation with SEM.

Chapter 7

Wetting Testing with Sessile Drop Method and Surface Characterisation

7.1 Wetting testing with Sessile Drop

A graphite sample and three of the composite materials (3112g, 5002g and 5036g) were selected for sessile drop testing, in order to create a basis for comparison with the results obtained with the immersion-emersion technique. The contact angles between the cathode material and a piece of melted aluminium was measured and are presented in Figure 7.1. A full description of the experimental procedure can be found in Section 4.8.

Resulting images from the sessile drop testing for the four tested samples with contact angles can be seen in Figure 7.2. All images are from the end of the holding period. Due to cost considerations, TiB_2 was not tested. Similar work done by others has found the contact angle of TiB_2 to be approximately 30° [13]. This literature result is plotted together with the experimental results obtained in Figure 7.1

7.2 Discussion of Sessile Drop Results

From the sessile drop technique, contact angles between substrate and the proble liquid, are reported. An acute contact angles, $\theta < 90$ ° is interpreted as a wetting system while $\theta > 90$ ° means poor wetting. I.e. the *smaller* the reported value, the better the wetting. For corrected weight the opposite is true - the *higher* the value, the better the wetting. In other words, the trend observed from the sessile drop tests conducted is the exactly opposite of that observed with the immersion-emersion method.

Unfortunately, stable results from the immersion-emersion method could not be obtained for 5036g, but this material is equivalent to 6004g. The difference in result between 5002g and 5036g is so small that it is considered to be insignificant, given the error in measurement. Composite 3112g stands out as the least wetted material with a contact angle larger than 90°. As previously mentioned, this material is made with a finer quality of TiB_2 than the others. This could explain differences in behaviour between otherwise similar materials. The test result for 3112g is somewhat unreliable though, as it was a plane-polished surface that was tested, and not one that was merely cut. This was simply a mistake, but re-testing of the sample was not

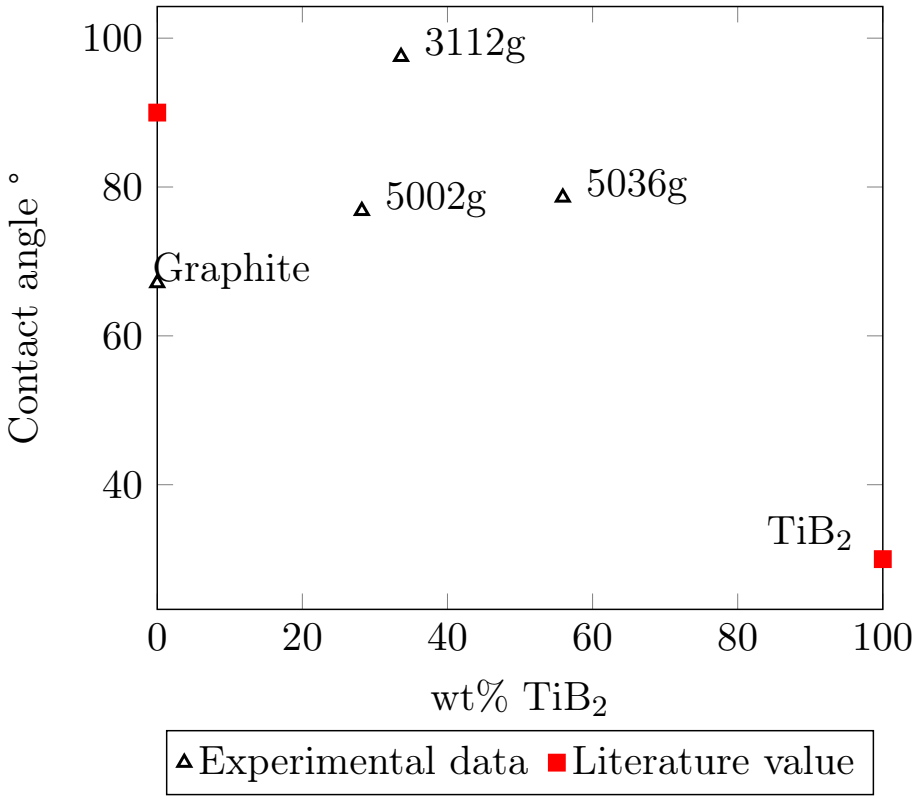

Figure 7.1: Contact angles from sessile drop tests as a function of TiB_2-content, plottet together with literature value for pure TiB_2 [13].

possible due to the limited amount of material available. The obtained results must therefore be considered with care.

It should be noted that the system studied with the two methods, sessile drop and immersion-emersion, differ both in terms of the third phase (vacuum vs. electrolyte) and polarisation. Even so, it is difficult to think of a reasonable, physical explanation for why a composite material is poorer wetted than either of its constituent materials, in this case graphite and TiB_2. The exception would be if the two components reacted to form unexpected chemical phases. However, the SEM images of the composites included in Section 4.2.3 suggest no phase formation.

The experimental results also differ from the literature values plotted in Figure 7.1, a fact that does not speak to their validity. These contact angles were obtained in the presence of hydrogen gas, not vacuum, which would influence the absolute values [13]. For the sake of comparison, it would therefore have been useful to test TiB_2 with the same procedure and apparatus used in this work, to see how it compares to the literature value. Accurate determination of contact angles is inherently difficult, and reported angles tend to vary [13]. Even so, the general trend should be applicable.

7.3 Conclusion

In conclusion, the results obtained with the sessile drop method does not support those obtained with the immersion-emersion method. Again, the composite material with smaller particles of TiB_2 stands out from the overall trend, but in this case, the result is not completely reliable.

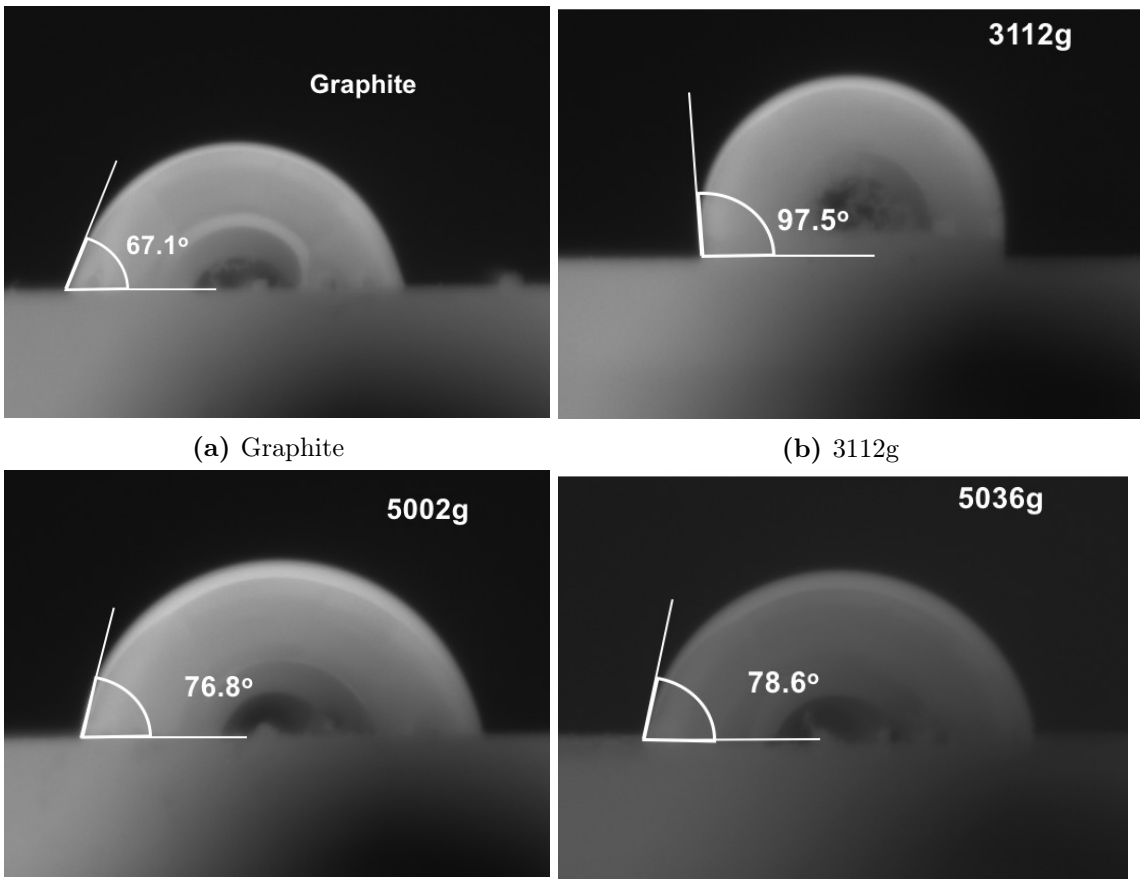

(a) Graphite **(b)** 3112g

(c) 5002g **(d)** 5036g

Figure 7.2: Images from sessile drop testing of pure graphite and three composite materials with measured contact angles. All images are taken after a holding period of one hour.

7.4 Surface Characterisation of TiB_2 Before and After Electrolysis

SEM-images of TiB_2 before and after polarisation are included in Figure 7.3 and 7.6 respectively. Spectra collected from both samples are shown in Figures 7.5 and 7.8, and the numerical results from the elemental characterisation are summarised in Tables 7.1 and 7.2. Additional spectras not presented here can be found in Appendix C.

The SEM images of the pure TiB_2 show a clear and homogeneous microstructure, with no obvious inclusions or other contaminations. The elemental overview shown in Table 7.1 confirms that the atomic ratio between titanium and boron was approximately 1:2. In addition to these elements, non-negligible amounts of carbon and oxygen were present. Both oxygen and carbon traces may stem from contamination from the atmosphere. However, the amounts of carbon observed in this case is far too high to be explained by atmospherical contamination alone. It is possible that some of it comes from the machining of the sample. It should also be noted that EDS analysis of light elements such as carbon is inherently tricky, due to overlap between the elemental peaks [20].

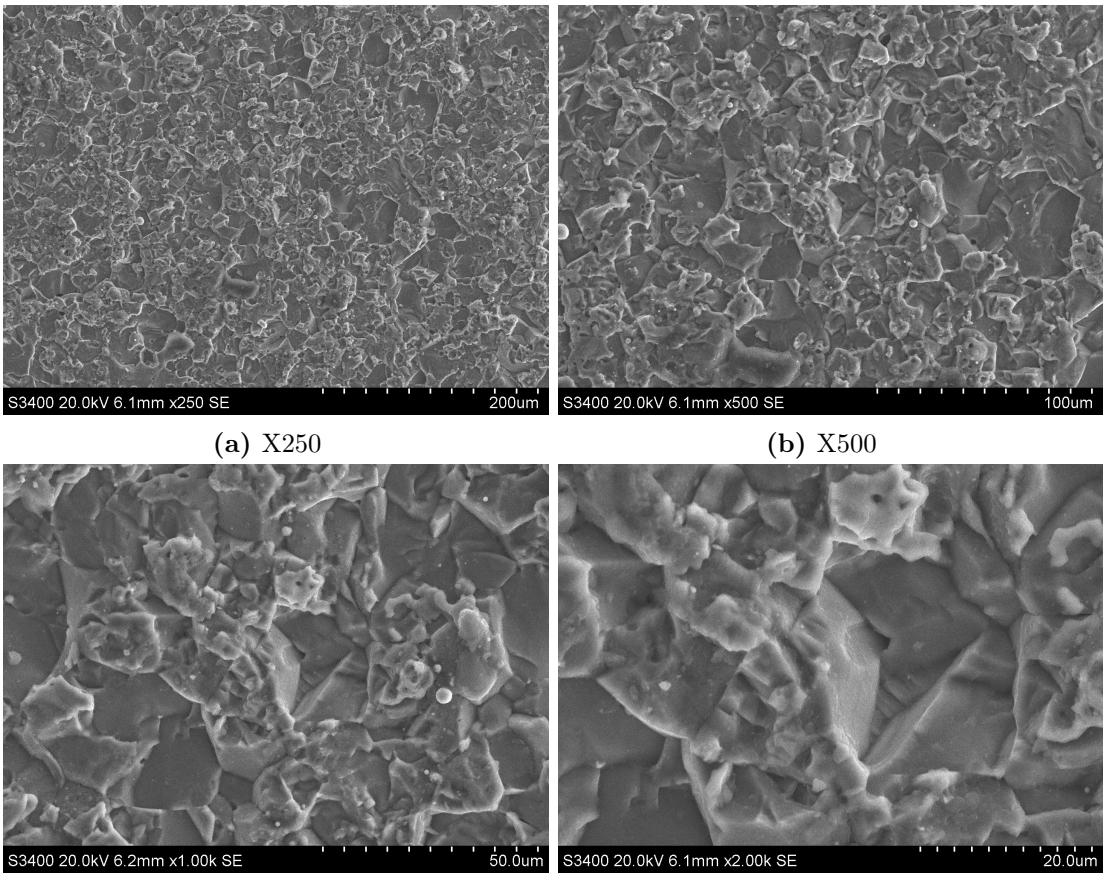

(a) X250 **(b)** X500

(c) X1000 **(d)** X2000

Figure 7.3: SEM images of pure TiB_2 before exposure to electrolyte and polarisation. All images are taken at 20 kV. Magnifications are given in subcaptions.

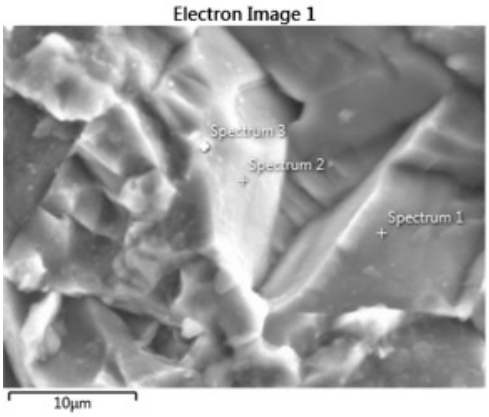

Figure 7.4: Image of sampling site for spectra on pure TiB_2, before exposure to electrolyte and polarisation.

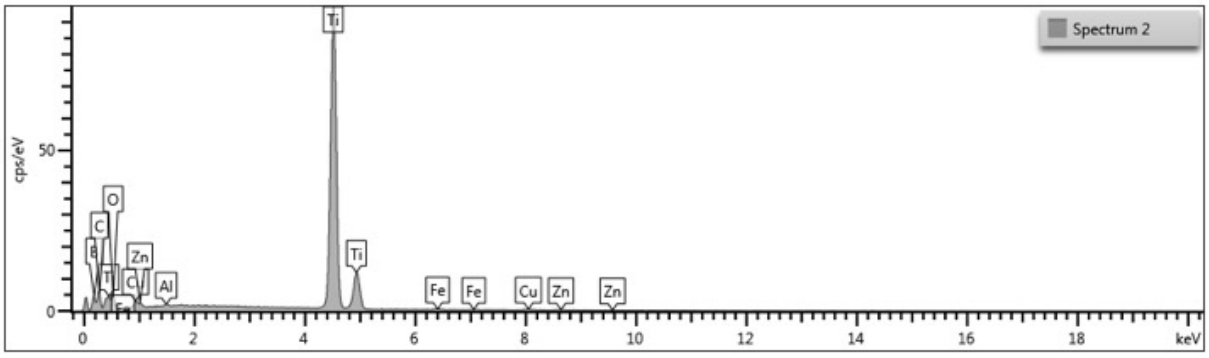

Figure 7.5: Spectrum collected from untreated TiB_2 using EDS. The site for spectrum collection is shown in Figure 7.4.

Table 7.1: The amounts of the elements detected with EDS on untreated TiB_2. Amounts are given in atomic weight percentages. Numbers in *italics* are below the certainty limit.

Site 1	**Spectrum 1**		**Spectrum 2**		**Spectrum 3**		**Average**	
Element	[at%]	[wt%]	[at%]	[wt%]	[at%]	[wt%]	[at%]	[wt%]
B	40.92	22.62	37.98	19.63	29.78	16.99	36.23	19.75
C	29.39	18.05	25.1	14.41	36.14	22.91	30.21	18.46
O	8.38	6.86	12.28	9.39	16.47	13.91	12.38	10.05
Ti	20.93	51.23	24.08	55.12	15.08	38.11	20.03	48.15
Al	*0*	*0.00*	*0.13*	*0.17*	*0.13*	*0.19*	*0.09*	*0.12*
Si	*0*	*0.00*	*0*	*0.00*	*0.06*	*0.09*	*0.02*	*0.03*
Fe	*0.07*	*0.20*	*0.12*	*0.32*	*0.11*	*0.32*	*0.10*	*0.28*
Cu	*0.22*	*0.71*	*0.18*	*0.55*	*1.98*	*6.64*	*0.79*	*2.63*
Zn	*0.1*	*0.33*	*0.13*	*0.41*	*0.24*	*0.83*	*0.16*	*0.52*
Total	100.0	100.0	100	100.0	100.0	100.0	100.0	100.0

After exposure to electrolyte and polarisation, the surface of TiB_2 looks very different - as is to be expected. Some crystals have formed on the surface, and the microstructure observed earlier is no longer visible. However, the layer of electrolyte did not cover the original material completely, and it was thus possible to acquire an elemental analysis. The exact points of collection are shown in Figure 7.7. Spectrum 9 has a very different composition than spectra 7 and 8. It is believed to be sampled from electrolyte traces rather than the cathode material itself, and is therefore not included in the numerical average.

7.5 Discussion of Surface Characterisation

From the results in Table 7.2 it can be seen that most of the carbon has disappeared after polarisation, while the oxygen content is stable. Some of the oxygen may stem from alumina in the electrolyte, but assuming that all of the detected aluminium is in the form of oxide, that still leaves a significant amount of oxygen not accounted for. The atomic ratio of boron to titanium remains more or less the same also decreased.

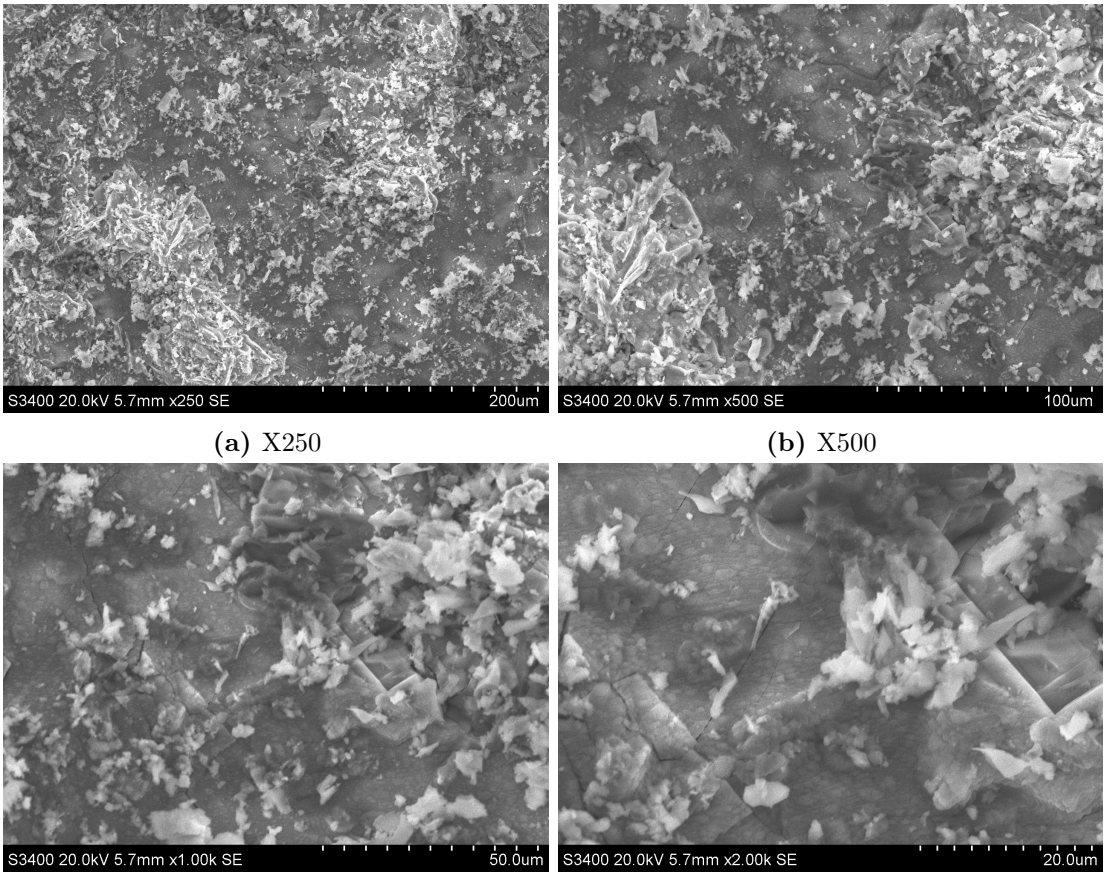

(a) X250 **(b)** X500

(c) X1000 **(d)** X2000

Figure 7.6: SEM images of pure TiB_2 after exposure to electrolyte and polarisation. All images are taken at 20 kV. Magnifications are given in subcaptions.

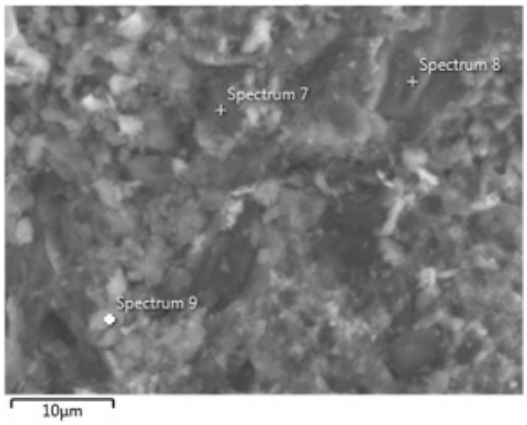

Figure 7.7: Image of sampling site for spectra on TiB_2, after exposure to electrolyte and polarisation.

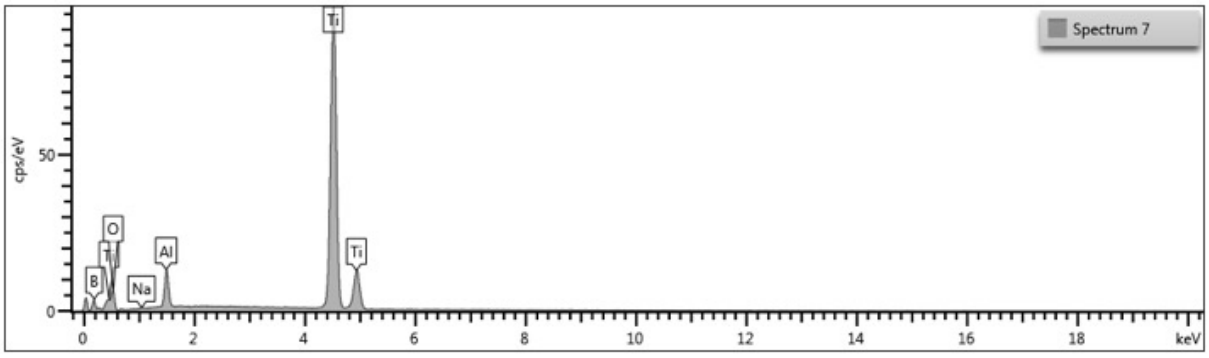

Figure 7.8: Spectrum collected from polarised TiB_2 using EDS. The site for spectrum collection is shown in Figure 7.7.

Table 7.2: The amounts of the elements detected with EDS on polarised TiB_2. Amounts are given in atomic weight percentages. Numbers in *italics* are below the certainty limit. Spectrum 9 is not included in the average

Site 1	**Spectrum 7**		**Spectrum 8**		**Spectrum 9**		**Average***	
Element	[at%]	[wt%]	[at%]	[wt%]	[at%]	[wt%]	[at%]	[wt%]
B	45.66	1.97	54.78	2.19	0	0.00	50.22	22.49
Ti	29.08	1.25	36.76	1.47	6.36	0.32	32.92	65.23
O	22.27	0.96	7.68	0.31	66.88	3.40	14.98	10.13
Al	2.85	0.12	0.78	0.03	16.88	0.86	1.82	2.08
C	*0*	*0.00*	*0*	*0.00*	*7.42*	*0.38*	*0.00*	*0.00*
F	*0*	*0.00*	*0*	*0.00*	*2.24*	*0.11*	*0.00*	*0.00*
Na	*0.13*	*0.01*	*0*	*0.00*	*0.22*	*0.01*	*0.07*	*0.06*
Total	100.0	100.0	100	100.0	100.0	100.0	100.0	100.0

7.6 Conclusion

No changes to the surface during polarisation can be said to have been found with certainty. However, the exact quantity of some of the lighter elements are somewhat unreliable when analysed in EDS and the results obtained are insufficient to draw firm conclusions from [20].

Chapter 8

Discussion

The results from the immersion-emersion method show little wetting of the cathode materials. Some of them exhibit qualitative signs of wetting, but this is rarely reflected in the adjusted average corrected weight, suggesting that the issue of data processing is still not completely resolved. The final corrected weight is particularly sensitive to the determination of the apparatus weight, which is done through optimisation and curve fitting. One suggestion to mitigate this problem is to start the immersion from a position just below the metal surface, rather than above. This should reduce the build-up of meniscus at the beginning of the cycle. The apparatus weight could then be set to the initial weight. Such a modification would influence the polarisation of the sample, as the cell is effectively short-circuited when the cathode comes into contact with the metal. Thus, the sample will never truly be cathodically polarised. With the current procedure, there is at least a brief moment of polarisation. The series measuring the electrolyte meniscus, the movement is in fact started from below the surface, as this closer resembles the actual situation at the electrolyte meniscus during measurement in the metal series. The apparatus weight is still found according to the optimisation criteria described in Section 4.7, but the value of it is usually close to the initial recorded weight.

The lack of wetting of the composites is supported by the sessile drop test presented in Figures 7.1 and 7.2, although the trend observed is not the same for the two methods. The sessile drop test was performed in vacuum rather than in the presence of electrolyte and without polarisation, so the systems are not directly comparable. Polarisation may be the key to explaining the difference in the trend - those composites that show the clearest signs of wetting only do so when polarised, or after having been polarised for some time, almost as if the material becomes 'activated'. This could be related to the removal of oxides on the ceramic particles. Removal of boron oxide from the TiB_2 surface has been shown to lead to increased wetting of TiB_2 [13]. Previous work has also found polarisation to increase wetting of cathode materials [21, 11]. It would therefore be of interest to repeat the sessile drop tests with polarisation, to see how that affects the results.

In fact, such a test was done by the external supplier, which tested a comparable set of materials in a system with electrolyte and polarisation of the samples. The results were presented in Section 2.4. Wetting of the materials was not observed with this method either, but a significant improvement occurred during polarisation of the samples. The TiB_2 particle size does not appear to influence the results to the same extent as observed in the other measurements; material 3112g does not stand out remarkably. The two materials of the highest TiB_2 content on the other hand exhibit a large spread in the measured contact angle in the external sessile drop test (see Figure 2.4). The materials in question are 5036g (55.9 wt% TiB_2, $<37\,\mu$m) and 6004g (55.1 wt% TiB_2, $<37\,\mu$m). These materials were prepared through the same synthesis route and with the same type of TiB_2 particles. In other words, there is no known difference in these materials which

could explain the great difference in wettability. This again raises the question of the whether the method is reliable. To investigate this further, several parallels of identical materials should be tested, to establish the margin of error in measurement. If this proves to be much smaller than the spread observed in the results, the physical properties of the materials should be closer inspected - there may be subtle differences in microstructure or phase formation influencing the wetting properties of the composites. The actual sample area tested in a sessile drop test is only a few square millimetres, and hence a heterogeneous material would be expected to give some variation in the angles observed.

In the cases where some wetting of the sample is measured with the immersion-emersion method, this effect decays over the course of the experimental series, as mentioned in Section 5.1.3. The meniscus does not move as smooth as expected either, but rather seems to slip and stick to the sample. Furthermore, the alumina concentration in the electrolyte affects how well the sample is wetted by the metal. Assuming that the compensation for the electrolyte meniscus is correct, this dependency on alumina concentration is not merely due to a change in the electrolyte's properties, but it also affects the metal meniscus. Together, these observations inspired the idea of a layer forming at the interface between the metal and the electrolyte; it could be that the composition is different here than within the metal. As the sample is dipped into the metal several times at the same position, this layer is introduced into the metal, and forms a barrier between the sample and the aluminium. A sketch of this possible situation is included in Figure 8.1. No such interfacial layer has been identified, nor been sought after, but it is a phenomena potentially worth exploring.

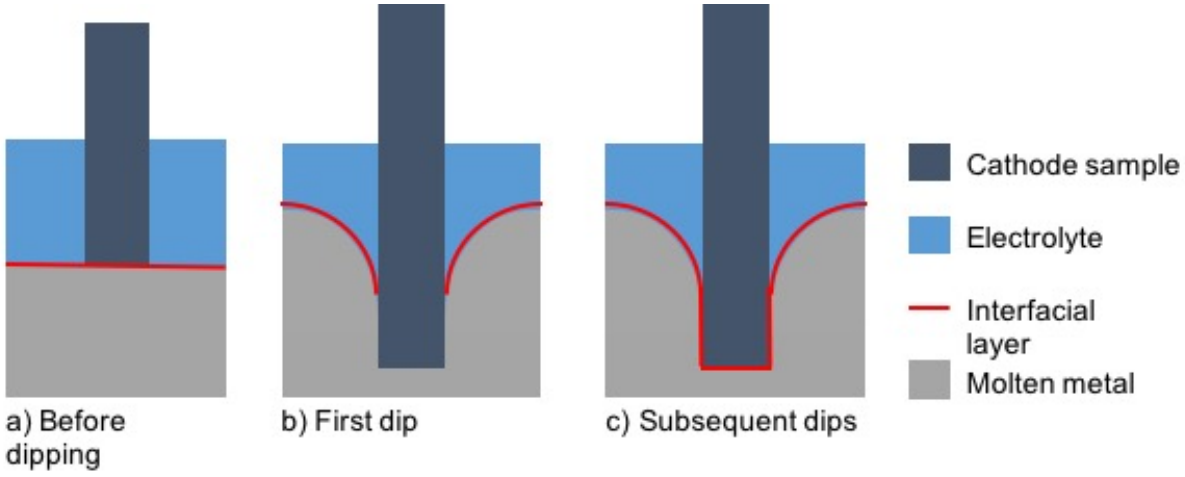

Figure 8.1: Illustration of possible situation during immersion of cathode sample into metal, introducing an interfacial layer.

In an actual aluminium electrolysis cell, the aluminium in the bottom of the cell effectively acts as the cathode and is polarised accordingly. In the experimental setup used here the metal is effectively a part of the anode - hence the polarisation is switched. This is because the apparatus was originally designed to use for anode samples, and it was considered sufficient to merely interchange the electrical poles. In retrospect, this might not be the case. At the very least, it introduces a potential source of error which should be removed in the project's next iteration. One possible work-around is illustrated in Figure 8.2. By placing an electrically insulating crucible, made from silicon nitride or boron nitride, between the metal and the graphite, the metal will no longer be polarised at all. The work-around is not ideal - the aluminium is still not cathodically polarised, but it could potentially eliminate unwanted side effects from an opposite polarisation. Furthermore, it can be implemented without larger modifications to the apparatus.

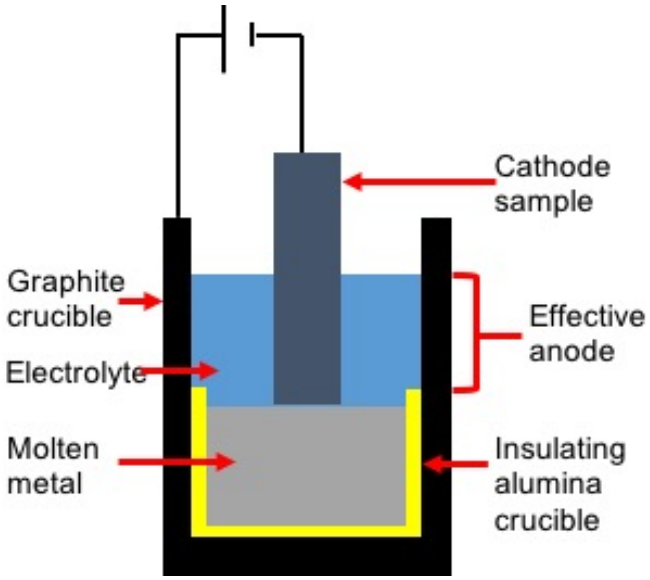

Figure 8.2: Sketch of a suggested modification to the experimental set-up used in the immersion-emersion method. By including an electrically insulating inner crucible, the metal will no longer be anodically polarised.

A chemical component that has been observed on the sample surfaces after immersion-emersion testing, is aluminium carbide. This was not seen to such a large extent in the earlier stages of this work performed by the author [11]. In this most recent part, the duration of the experiment has significantly increased which possibly has affected the carbide formation. If a carbide film is present on the sample during the wetting test, it is effectively the wetting between this film and the metal which is assessed - not the one between the cathode material and the metal. Hence, this will be a major source of error and should be further investigated. It is not yet known at which point in the experiment the carbide is formed. There is no way of observing the surface of the cathode during the experiment with the current setup, without terminating the experiment. Even then, several hours of cooling is necessary before the apparatus can be opened and the sample inspected. The mechanisms for aluminium carbide formation is not fully understood, but both direct reaction between aluminium and carbide and electrochemical mechanisms have been suggested [22]. If the reaction is elecrochemical in nature, a prolonged duration of polarisation is likely to increase the amount of carbide formed.

The reason for the extended duration of the experimental procedure is the modification of the measuring sequence. The new sequence allows for the wetting by the electrolyte meniscus to be measured for every sample and series. In coherence with previous work, the effect of the electrolyte meniscus is found to be negligible in absence of polarisation of the sample. However, when the sample is polarised, the effect is both significant and unpredictable, and it should therefore be measured. If the experiment does not require polarisation, this extra measurement is not necessary and the time required for the experiment can be greatly reduced.

Chapter 9

Conclusion and Further Work

In conclusion the newly developed composite materials are not as well wetted by aluminium as expected, even at more than 50 wt% TiB_2. This finding is consistent across all results obtained; with the immersion-emersion method, with the sessil drop method with vacuum and with electrolyte. Some of the composites exhibit better wetting than graphite. One composite in particular, 3112g, was measured to have comparable wetting properties to pure TiB_2, but only during polarisation and only with the immersion-emersion method. A clear relationship between the TiB_2 content in the material and its wettability was not found. Economically, there is still room for increasing the load of TiB_2 given the potential that lies in improved operational efficiency. However, before that, a better proof of concept is necessary. Since the immersion-emersion technique is not yet fully understood, it is of interest to see if the obtained results can be reproduced.

The immersion-emersion experimental procedure has been further developed in this work, yet some work on the method remains. The processes occurring during polarisation is not yet fully understood nor controlled. As such, the results obtained are not always consistent. The suggested modification of the set-up with an inner, insulating crucible should be included in the next round of testing, in attempt to have better control of the experimental conditions.

Minor improvements in the data processing for better standardisation of the method has been suggested, such as choosing the initial weight as the apparatus weight. Furthermore, one should consider preparing the electrolyte from 'scratch', using pure salts rather than an industrial bath. It has been shown that the wetting of both graphite and TiB_2 is affected by the alumina concentration in the electrolyte. This dependency remains even after the electrolyte meniscus has been accounted for. To ensure an equal concentration of alumina across parallels may therefore be important. One should also further investigate this relation at a wider range of concentrations than what has been done so far.

Polarisation of samples during pre-treatment was not found to be necessary nor advisable, but it does seem to improve the wetting of the samples during the actual testing. In certain cases, it is only after current is applied that any sign of wetting can be observed, as if the material becomes activated. This may be attributed to the removal of boron oxide. The problem with polarisation is that it introduces a range of different processes, which are not yet fully understood, hence complicating the situation to be analysed. Among these are the formation of aluminium carbide on the graphitic samples and changes to the surface of TiB_2. Particularly the carbide formation has been problematic in this work. It is therefore advised to further investigate this process and how it can be eliminated.

In terms of further development of the composites themselves, it was found that the material prepared with smaller particles of TiB_2 behaved differently than materials with a comparable

load of coarser particles. During testing with the immersion-emersion method this composite was found to be significantly better wetted, although only during polarisation. In unpolarised sessile drop testing on the other hand, this material was the only one which was dewetted. Nevertheless, it seems that the particle size of TiB_2 is an important factor which is worth further pursuing. From a cost perspective, it is desirable to achieve the best wettability at the lowest amount of TiB_2. That may entail using smaller particles of the expensive ceramic material. This aspect will be important for the potential commercial application of composite cathode materials.

Bibliography

[1] Morten Sundheim Jensen. *Hot Pressing and Degradation of TiB_2 Inert Cathodes*. NTNU, Trondheim, Norway, 2009. PhD Dissertation.

[2] L. Xi, I. Kaban, R. Nowak, B. Korpała, G. Bruzda, N. Sobczak, N. Mattern, and J. Eckert. High-temperature wetting and interfacial interaction between liquid Al and TiB_2 ceramic. *Journal of Materials Science*, 50:2682 – 2690, 2015.

[3] Samuel Senanu, Tor Grande, and Arne Petter Ratvik. Role of pitting in the formation of potholes in carbon cathodes - a review. *The International Committee for Study of Bauxite, Alumina Aluminium*, AL31.

[4] Johannes Aalbu. Presentation: Karmøy site visit: Technology update. `http://www.hydro.com/upload/Documents/Presentations/Investor/Hydro%20Technology%20Update.pdf`. Accessed: 11.11.2016.

[5] Ji Lie, Jing Fang, Qingju Li, and Yarrking Lai. Effect of TiB_2 content on resistance to sodium penetration of TiB_2/C cathode composites for aluminium electrolysis. *Journal of Central South University of Technology*, 11(4):400–403, 2004.

[6] Ana Maria Martinez, Ove Paulsen, Asbjørn Solheim, Henrik Gudbrandsen, and Ingo Eick. Wetting between carbon and cryolitic melts. Part I: Theory and equipment. *Light Metals*, pages 665–670, 2015.

[7] Asbjørn Solheim and Henrik Gudbrandsen. Wetting between cathode materials and molten aluminium. (Project number F27577):4–11, 2015. Internal report from SINTEF, describing the wetting testing of various cathode samples using the immersion-emersion technique.

[8] Vincent Makala. Substrate Wetting: Wetting Agents Selection. `http://coatings.specialchem.com/selection-guide/wetting-agents-selection-for-coatings`. Accessed: 09.11.2016.

[9] Asbjørn Solheim. Wetting test in an aluminium-copper alloy, 2016.

[10] J. Schmitz, J. Brillo, I. Egry, and R. Schmid-Fetzer. Surface tension of liquid Al-Cu binary alloys. *International Journal of Materials Research*, 100(11):1529–1535, 2009.

[11] Vilde S. Haslund. Wetting testing of cathodes for aluminium production. pages 13–35, 2016. Project thesis.

[12] B. Schwarz, C. Eisenmenger-Sittner, and H. Steiner. Construction of a high-temperature sessile drop device. *Vacuum*, 82(2):186–188, 2007.

[13] D. A. Weirauch Jr, W. J. Krafick, G. Ackart, and P. D. Ownby. The wettability of titanium diboride by molten aluminium drops. *Journal of materials science*, pages 2301–2306, 2005.

[14] Susan Swapp. Scanning electron microscopy (SEM). `http://serc.carleton.edu/research_education/geochemsheets/techniques/SEM.html`. University of Wyoming. Accessed: 19.04.2017.

[15] Purdue University. Scanning electron microscope. `https://www.purdue.edu/ehps/rem/rs/sem.htm`. Accessed: 19.04.2017.

[16] John Goodge. Energy-dispersive x-ray spectroscopy (EDS). `http://serc.carleton.edu/research_education/geochemsheets/eds.html`. University of Minnesota-Duluth Accessed: 19.04.2017.

[17] Antoniu Moldovan and Marius Enachescu. *Wetting and Wettability*. 2015. Mahmood Aliofkhazraei (Ed.), Available by `https://www.intechopen.com/books/wetting-and-wettability/wetting-properties-at-nanometer-scale`.

[18] Tone Anzjøn. Sessile drop apparatus. Description of apparatus used for Sessile drop testing, used internally at NTNU, provided by Tone Anzjøn.

[19] Asbjørn Solheim, Henrik Gudbrandsen, Ana Maria Martinez, Kristian Etienne Einardsrud, and Ingo Eick. Wetting between carbon and cryolytic melts. Part II: Effect of bath properties and polarisation. *Light Metals*, pages 671–676, 2015.

[20] Australian Microscopy Microanalysis Research Facility. Quantitative eds x-ray microanalysis using sem. `http://www.ammrf.org.au/myscope/analysis/eds/quantitative/`. Accessed: 16.05.2017.

[21] Camilla Sommerseth. *The effect of production parameters on the performance of carbon anodes for aluminium production*. NTNU, Trondheim, Norway, 2016. PhD Dissertation.

[22] Kristin Vasshaug, Trygve Foosnæs, Geir Martin Haarberg, Arne Petter Ratvik, and Egil Skybakmoen. Formation and dissolution of aluminium carbide in cathode blocks. *TMS Light Metals*, 2009.

Appendix A

Detailed Results From Wetting Tests with Immersion-Emersion Method

A.1 Pure Graphite

Table A.1: Average corrected weights, optimisation parameters and standard deviations for pure graphite, parallel 1 without polarisation during pre-treatment.

Series	$\mathbf{w}_{corr}$ [g]	**Std.dev**	$\mathbf{f}_b$ [g cm^{-1}]	**Std.dev**	$\mathbf{w}_0$ [g]	**Std.dev**
Immersion						
Electrolyte1	-0.05	0.04	3.58	0.00	160.09	0.04
Electrolyte2 pol	-0.17	0.04	4.35	0.27	164.24	1.36
Electrolyte3	-0.08	0.02	3.63	0.04	161.40	0.20
Metal1	-2.80	0.13	5.51	0.07	171.7	0.52
Metal2 pol	-3.96	1.17	5.48	0.14	163.7	1.20
Metal3	-2.81	0.23	5.68	0.12	165.8	0.90
Emersion						
Electrolyte1	-0.18	0.01	3.58	0.00	160.09	0.04
Electrolyte2 pol	-0.14	0.09	4.35	0.27	164.24	1.36
Electrolyte3	-0.24	0.04	3.63	0.04	161.40	0.20
Metal1	-3.11	0.11	5.51	0.07	171.7	0.52
Metal2 pol	-3.14	0.38	5.90	0.22	174.8	1.28
Metal3	-3.64	0.16	5.75	0.13	174.7	0.92

Table A.2: Average corrected weights, optimisation parameters and standard deviations for pure graphite, parallel 2 without polarisation during pre-treatment.

Series	$\mathbf{w}_{corr}$ [g]	**Std.dev**	$\mathbf{f}_b$ [g cm^{-1}]	**Std.dev**	$\mathbf{w}_0$ [g]	**Std.dev**
Immersion						
Electrolyte1	-0.07	0.16	3.97	0.31	145.65	1.29
Electrolyte2 pol	-0.43	0.17	4.60	0.20	149.40	1.37
Electrolyte3	-0.05	0.07	4.05	0.05	148.23	0.18
Metal1	-1.89	0.29	7.05	0.31	166.2	2.16
Metal2 pol	-1.98	0.31	7.18	0.25	168.5	1.40
Metal3	-1.89	0.10	7.52	0.13	172.6	0.98
Emersion						
Electrolyte1	-0.30	0.26	3.97	0.31	145.65	1.29
Electrolyte2 pol	-0.36	0.20	4.60	0.20	149.40	1.37
Electrolyte3	-0.25	0.09	4.05	0.05	148.23	0.18
Metal1	-2.32	0.34	7.05	0.31	166.2	2.16
Metal2 pol	-2.21	0.40	7.18	0.25	168.5	1.40
Metal3	-2.42	0.11	7.52	0.13	172.6	0.98

Table A.3: Average corrected weights, optimisation parameters and standard deviations for pure graphite with polarised pre-treatment.

Series	$\mathbf{w}_{corr}$ [g]	**Std.dev**	$\mathbf{f}_b$ [g cm^{-1}]	**Std.dev**	$\mathbf{w}_0$ [g]	**Std.dev**
Immersion						
Electrolyte1	-0.13	0.15	3.41	0.19	144.04	0.81
Electrolyte2 pol	-0.09	0.06	4.19	0.24	152.14	1.58
Electrolyte3	0.49	0.12	4.03	0.16	152.30	0.59
Metal1	-3.36	0.52	5.53	0.17	161.1	1.03
Metal2 pol	-3.96	1.17	5.48	0.14	163.7	1.20
Metal3	-2.81	0.23	5.68	0.12	165.8	0.90
Emersion						
Electrolyte1	-0.06	0.20	3.41	0.19	144.04	0.81
Electrolyte2 pol	-0.03	0.15	4.19	0.24	152.14	1.58
Electrolyte3	0.36	0.09	4.03	0.16	152.30	0.59
Metal1	-3.39	1.06	5.53	0.17	161.1	1.03
Metal2 pol	-3.86	0.93	5.48	0.14	163.7	1.20
Metal3	-3.28	0.17	5.68	0.12	165.8	0.90

A.2 Pure TiB_2

Table A.4: Average corrected weights, optimisation parameters and standard deviations for pure TiB_2 without polarisation during pre-treatment.

Series	$\mathbf{w}_{corr}$ [g]	**Std.dev**	$\mathbf{f}_b$ [g cm^{-1}]	**Std.dev**	$\mathbf{w}_0$ [g]	**Std.dev**
Immersion						
Electrolyte1	-0.37	0.12	1.65	0.09	149.30	0.62
Electrolyte2 pol	-0.35	0.14	1.91	0.08	151.98	0.63
Electrolyte3	-0.65	0.27	1.82	0.10	151.74	0.58
Metal1	-0.03	0.23	4.19	0.23	172.2	2.46
Metal2 pol	-1.25	0.16	3.24	0.03	162.5	0.53
Metal3	-2.32	0.11	2.64	0.05	158.0	0.47
Emersion						
Electrolyte1	-0.18	0.10	1.65	0.09	149.30	0.62
Electrolyte2 pol	-0.32	0.11	1.91	0.08	151.98	0.63
Electrolyte3	-0.23	0.15	1.82	0.10	151.74	0.58
Metal1	0.25	0.11	4.19	0.23	172.2	2.46
Metal2 pol	-0.68	0.30	3.24	0.03	162.5	0.53
Metal3	-1.44	0.11	2.64	0.05	158.0	0.47

Table A.5: Average corrected weights, optimisation parameters and standard deviations for pure TiB_2 with polarised pre-treatment.

Series	$\mathbf{w}_{corr}$ [g]	**Std.dev**	$\mathbf{f}_b$ [g cm^{-1}]	**Std.dev**	$\mathbf{w}_0$ [g]	**Std.dev**
Immersion						
Electrolyte1	-0.03	0.08	2.05	0.09	144.69	0.57
Electrolyte2 pol	0.00	0.08	2.22	0.08	145.95	0.48
Electrolyte3	0.03	0.05	1.98	0.05	144.75	0.26
Metal1	-2.15	0.23	2.92	0.12	151.7	1.03
Metal2 pol	-2.31	0.08	2.80	0.04	150.5	0.52
Metal3	-2.91	0.14	2.92	0.04	152.9	0.37
Emersion						
Electrolyte1	-0.09	0.09	2.05	0.09	144.69	0.57
Electrolyte2 pol	-0.07	0.06	2.22	0.08	145.95	0.48
Electrolyte3	-0.02	0.11	1.98	0.05	144.75	0.26
Metal1	-1.70	0.70	2.92	0.12	151.7	1.03
Metal2 pol	-2.46	0.09	2.80	0.04	150.5	0.52
Metal3	-3.04	0.15	2.92	0.04	152.9	0.37

A.2.1 Pure TiB_2 with Different Alumina Concentrations

Table A.6: Average corrected weights, optimisation parameters and standard deviations for pure TiB_2 with low alumina concentration (1.9 wt%).

Series	$\mathbf{w}_{corr}$ [g]	**Std.dev**	$\mathbf{f}_b$ [g cm^{-1}]	**Std.dev**	$\mathbf{w}_0$ [g]	**Std.dev**
Immersion						
Electrolyte1	-0.02	0.05	1.98	0.04	195.99	0.40
Metal1	0.01	0.03	2.87	0.05	208.0	0.59
Emersion						
Electrolyte1	-0.12	0.03	1.98	0.04	195.99	0.40
Metal1	-0.06	0.03	2.87	0.05	208.0	0.59

Table A.7: Average corrected weights, optimisation parameters and standard deviations for pure TiB_2 with high alumina concentration (4.1 wt%).

Series	$\mathbf{w}_{corr}$ [g]	**Std.dev**	$\mathbf{f}_b$ [g cm^{-1}]	**Std.dev**	$\mathbf{w}_0$ [g]	**Std.dev**
Immersion						
Electrolyte1	-0.03	0.03	1.97	0.03	193.35	0.21
Metal1	-3.03	1.37	3.26	0.41	207.3	3.77
Emersion						
Electrolyte1	-0.12	0.04	1.97	0.03	193.35	0.21
Metal1	-2.51	1.27	3.26	0.41	207.3	3.77

A.3 Composites

A.3.1 3018g

Table A.8: Average corrected weights, optimisation parameters and standard deviations for composite sample 3018g.

Series	w_{corr} [g]	Std.dev	f_b [g cm^{-1}]	Std.dev	w_0 [g]	Std.dev
Immersion						
Electrolyte1	0.02	0.09	2.78	0.02	111.48	0.05
Electrolyte2 pol	-0.15	0.07	3.08	0.12	114.12	0.89
Electrolyte3	-0.11	0.04	2.73	0.04	115.20	0.21
Metal1	-1.95	0.28	4.11	0.06	121.8	0.31
Metal2 pol	-1.65	0.04	4.53	0.07	126.7	0.24
Metal3	-1.53	0.08	4.52	0.05	128.3	0.34
Emersion						
Electrolyte1	-0.20	0.04	2.78	0.02	111.48	0.05
Electrolyte2 pol	-0.15	0.04	3.08	0.12	114.12	0.89
Electrolyte3	-0.23	0.02	2.73	0.04	115.20	0.21
Metal1	-2.32	0.29	4.11	0.06	121.8	0.31
Metal2 pol	-1.80	0.10	4.53	0.07	126.7	0.24
Metal3	-1.99	0.07	4.52	0.05	128.3	0.34

A.3.2 3112g

Table A.9: Average corrected weights, optimisation parameters and standard deviations for composite sample 3112g.

Series	w_{corr} [g]	Std.dev	f_b [g cm^{-1}]	Std.dev	w_0 [g]	Std.dev
Immersion						
Electrolyte1	-0.03	0.02	3.02	0.02	127.97	0.14
Electrolyte2 pol	-0.34	0.12	3.43	0.15	130.58	1.26
Electrolyte3	-0.34	0.06	3.85	0.04	136.67	0.29
Metal1	-4.23	0.29	4.08	0.16	138.2	1.78
Metal2 pol	-0.08	0.51	5.83	0.07	151.7	0.66
Metal3	-2.31	0.09	4.39	0.04	140.6	0.36
Emersion						
Electrolyte1	-0.20	0.01	3.02	0.02	127.97	0.14
Electrolyte2 pol	-0.36	0.20	3.43	0.15	130.58	1.26
Electrolyte3	-0.51	0.10	3.85	0.04	136.67	0.29
Metal1	-4.71	0.30	4.08	0.16	138.2	1.78
Metal2 pol	-0.15	0.36	5.83	0.07	151.7	0.66
Metal3	-2.45	0.10	4.39	0.04	140.6	0.36

A.3.3 5002g

Table A.10: Average corrected weights, optimisation parameters and standard deviations for composite sample 5002g.

Series	$\mathbf{w}_{corr}$ [g]	**Std.dev**	$\mathbf{f}_b$ [g cm^{-1}]	**Std.dev**	$\mathbf{w}_0$ [g]	**Std.dev**
Immersion						
Electrolyte1	-0.02	0.05	3.14	0.01	156.26	0.12
Electrolyte2 pol	-0.17	0.14	3.43	0.19	159.39	1.68
Electrolyte3	0.39	0.09	3.81	0.04	164.43	0.17
Metal1	-3.26	0.38	4.59	0.11	170.6	0.88
Metal2 pol	-3.14	0.34	5.28	0.13	177.7	1.13
Metal3	-2.81	0.11	4.91	0.05	175.3	0.57
Emersion						
Electrolyte1	-0.15	0.09	3.14	0.01	156.26	0.12
Electrolyte2 pol	-0.37	0.12	3.43	0.19	159.39	1.68
Electrolyte3	0.29	0.20	3.81	0.04	164.43	0.17
Metal1	-3.37	0.43	4.59	0.11	170.6	0.88
Metal2 pol	-2.71	0.73	5.28	0.13	177.7	1.13
Metal3	-3.06	0.14	4.91	0.05	175.3	0.57

A.3.4 5020g

Table A.11: Average corrected weights, optimisation parameters and standard deviations for composite sample 5020g.

Series	$\mathbf{w}_{corr}$ [g]	**Std.dev**	$\mathbf{f}_b$ [g cm^{-1}]	**Std.dev**	$\mathbf{w}_0$ [g]	**Std.dev**
Immersion						
Electrolyte1	0.01	0.01	3.77	0.01	167.51	0.10
Electrolyte2 pol	-0.36	0.15	4.21	0.12	171.19	1.29
Electrolyte3	-0.10	0.04	4.56	0.02	176.26	0.17
Metal1	-4.89	0.20	5.72	0.14	185.6	1.18
Metal2 pol	-3.06	0.42	6.22	0.29	187.8	2.89
Metal3	-1.59	0.05	6.60	0.04	191.8	0.39
Emersion						
Electrolyte1	-0.25	0.02	3.77	0.01	167.51	0.10
Electrolyte2 pol	-0.53	0.18	4.21	0.12	171.19	1.29
Electrolyte3	-0.37	0.04	4.56	0.02	176.26	0.17
Metal1	-5.25	0.29	5.72	0.14	185.6	1.18
Metal2 pol	-3.14	0.41	6.22	0.29	187.8	2.89
Metal3	-2.02	0.04	6.60	0.04	191.8	0.39

A.3.5 6004g

Table A.12: Average corrected weights, optimisation parameters and standard deviations for composite sample 6004g.

Series	$\mathbf{w}_{corr}$ [g]	**Std.dev**	$\mathbf{f}_b$ [g cm^{-1}]	**Std.dev**	$\mathbf{w}_0$ [g]	**Std.dev**
Immersion						
Electrolyte1	-0.03	0.03	2.54	0.02	228.40	0.10
Electrolyte2 pol	-0.30	0.07	2.90	0.18	233.12	1.42
Electrolyte3	0.35	0.02	3.38	0.05	235.64	0.40
Metal1	-3.24	0.27	4.03	0.20	241.0	1.70
Metal2 pol	-3.94	0.31	3.82	0.10	240.2	0.63
Metal3	-3.45	0.15	3.99	0.09	240.8	0.63
Emersion						
Electrolyte1	-0.15	0.05	2.54	0.02	228.40	0.10
Electrolyte2 pol	-0.30	0.18	2.90	0.18	233.12	1.42
Electrolyte3	0.18	0.04	3.38	0.05	235.64	0.40
Metal1	-3.09	0.35	4.03	0.20	241.0	1.70
Metal2 pol	-3.02	0.55	3.82	0.10	240.2	0.63
Metal3	-3.51	0.16	3.99	0.09	240.8	0.63

Appendix B

Calculation of Alumina Consumption During Experimental Procedure

The current is switched on for approximately one hour for the experimental wetting procedure. The total consumption of alumina can be calculated as below, given the following reduction reaction:

$$\text{Cathode:} \quad \mathrm{Al^{3+}} + 3\,\mathrm{e^-} \quad = \quad \mathrm{Al(l)} \tag{B.1}$$

$$\mathrm{O^{2-}} + \mathrm{C} \quad = \quad \mathrm{CO_2} + 2\,\mathrm{e^-} \tag{B.2}$$

$$\mathrm{Al_2O_3(dissolved)} + \frac{3}{2}\,\mathrm{C(s)} \quad = \quad 2\,\mathrm{Al(l)} + \frac{3}{2}\,\mathrm{CO_2(g)} \tag{B.3}$$

$$I = 13\,\mathrm{A}, \quad t = 1\,\mathrm{h} = 3600\,\mathrm{s} \tag{B.4}$$

$$Q = 3600\,\mathrm{s} \times 13\,\mathrm{Cs^{-1}} = 46.800\,\mathrm{C} \tag{B.5}$$

$$n_e = \frac{Q}{Q_e \times N_A} = \frac{46\,800\,\mathrm{C}}{1.602 \times 10^{-19} C \times 6.022 \times 10^{23} mol^{-1}} = 0.49\,\mathrm{mol} \tag{B.6}$$

$$n_{Al_2O_3} = \frac{1}{6} \times n_e = 0.08\,\mathrm{mol} \tag{B.7}$$

$$m_{Al_2O_3} = n_{Al_2O_3} \times M_{Al_2O_3} = 0.08\,\mathrm{mol} \times 101.96\,\mathrm{gmol^{-1}} = 8.2\,\mathrm{g} \tag{B.8}$$

For half of the time period one can assume that the sample is in contact with the molten metal and that the cell therefore is short circuited. During this period there will be no electrolysis nor consumption of alumina. Therefore, the total consumption is estimated to be $8.2\,\mathrm{g} \times 0.5 = 4.1\,\mathrm{g}$

Appendix C

Details From Surface Characterisation (EDS)

C.1 Untreated TiB_2

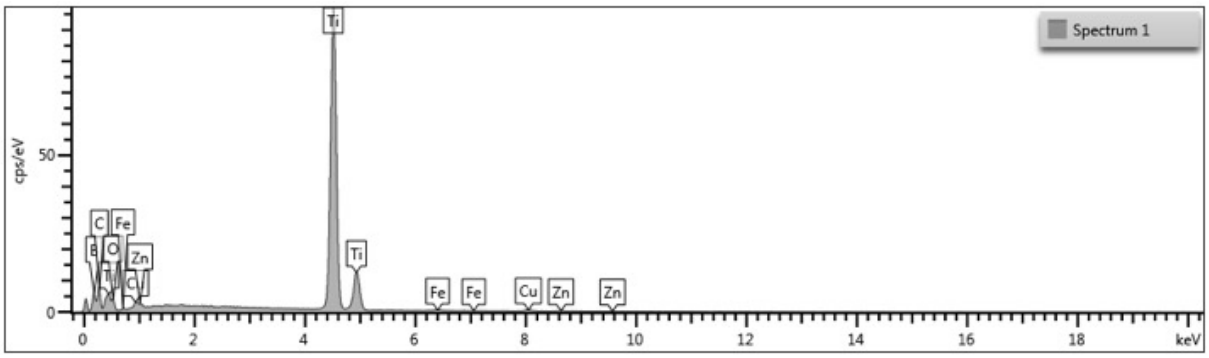

(a) Spectrum 1

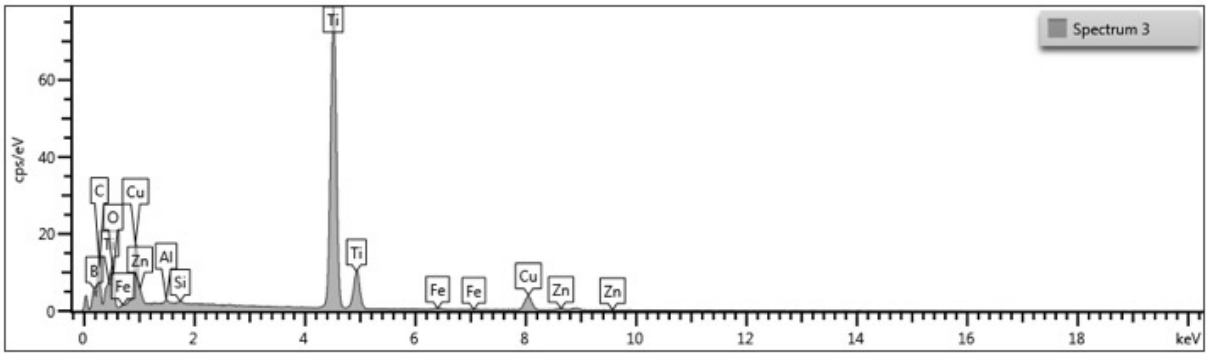

(b) Spectrum 3

Figure C.1: Spectras collected from untreated TiB_2 in EDS characterisation.

C.2 TiB_2 After Polarisation and Electrolyte Exposure

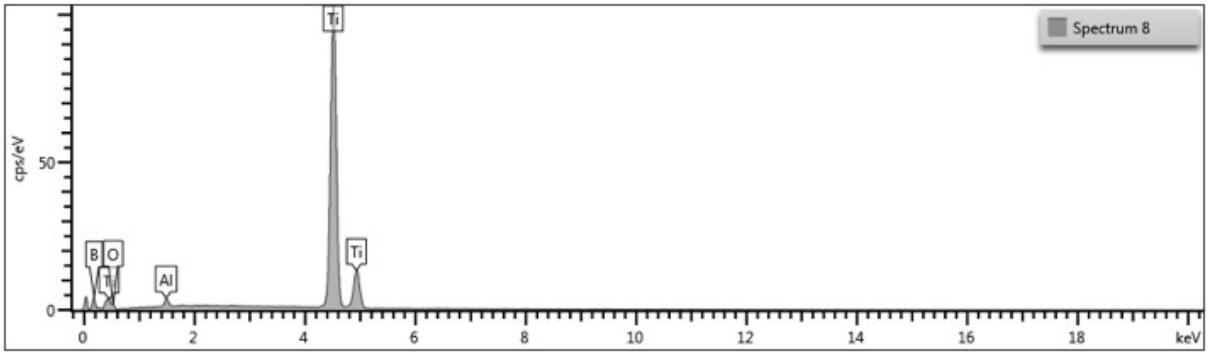

(a) Spectrum 8

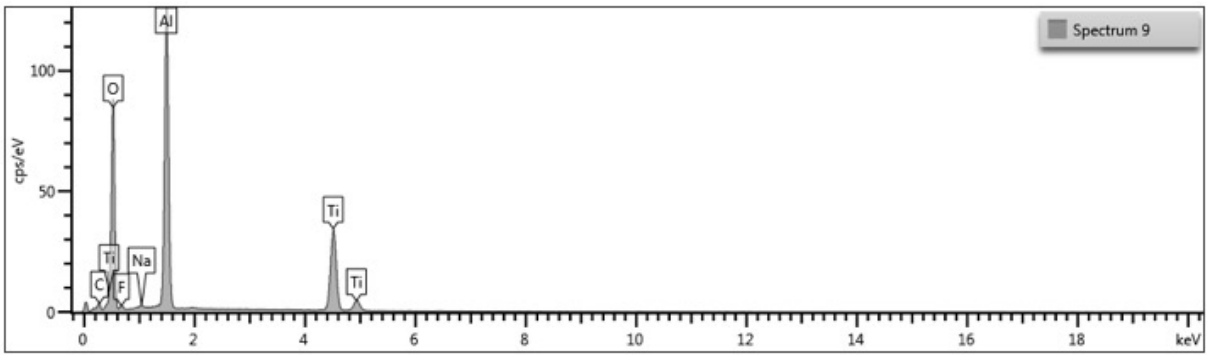

(b) Spectrum 9

Figure C.2: Spectras collected from TiB_2 which has been polarised and exposed to electrolyte, with EDS.